Ministry of Higher Education and Scientific Research

Hassiba Benbouali University of Chlef

Faculty of Exact Sciences and Informatics

Department of Physics

THESIS

Submitted in partial fulfillement of the award of a

Ph.D. degree in physical sciences

By

ABBAS Karima

TITLE

Quantum droplets in random potentials

2023-2024

Thesis committee :

Prof. Mohamed Belabbas	UHB Chlef	President
Prof. Kamel Bencheikh	Univ Setif	Examiner
Prof. Smain Balaska	Univ Oran 1	Examiner
Dr. Rachid Traiche	UHB Chlef	Examiner
Prof. Abdelâali Boudjemâa	UHB Chlef	Supervisor

Dedicated to,

My beloved family, without whose endless love and support, I could not achieve this.

Acknowledgement

I would like to express my heartfelt gratitude to the many individuals and institutions that have played a pivotal role in the completion of this thesis. Without their support, guidance, and encouragement, this work would not have been possible.

First and foremost, I extend my deepest appreciation to my thesis advisor, ***Prof. Abdelâali Boudjemâa****. Your unwavering support, invaluable insights, and dedication to my academic growth have been instrumental throughout this journey. Your mentorship has not only enriched my research but also broadened my horizons as a scholar.*

I am especially indebted to my thesis committee members : ***Prof. Mohamed Belabbas****,* ***Prof. Kamel Bencheikh****,* ***Prof. Smain Balaska****, and* ***Dr. Rachid Traiche****, for their insightful comments, constructive criticism, and thoughtful suggestions that greatly enhanced the depth and breadth of this research. Each committee member brought a unique perspective, contributing to a more robust and well-rounded thesis.*

I would like to extend my thanks to the ***Hassiba Benbouali University of Chlef*** *faculty of Exact Sciences and Informatics, and staff, whose resources and facilities were essential in conducting my research.*

My deepest appreciation goes to my family and friends for their unwavering support and understanding throughout this demanding endeavor. Your patience, encouragement, and belief in me sustained my motivation during challenging times.

I must also express my gratitude to my fellow classmates and colleagues who provided valuable insights and shared their experiences, enriching my academic journey.

This thesis represents the culmination of years of dedication and hard work, and I am acutely aware that I stand on the shoulders of giants. To everyone who has contributed, directly or indirectly, to this endeavor, I extend my deepest appreciation.

Thank you all for being an integral part of this academic voyage.

Karima Abbas*.*

March, 2024

Abstract

One of the important achievements in the field of ultracold atoms is the recent prediction and observation of ultradilute quantum liquid droplets, a new quantum state of matter. Quantum droplet originates due to the subtle balance between the attractive mean-field force and the repulsive force provided by the Lee-Huang-Yang quantum fluctuations.

This thesis aims first to study large bulk properties of self-bound quantum droplets of Bose mixtures in weak disorder potentials, and second introduces finite size effects within a generalized disorder-dependent Gross-Pitaevskii equation. Our investigation encompassed the examination of both uncorrelated and correlated disorders in three dimensions at zero and finite temperatures.

We look in particular at how the intriguing interplay of the disorder, interspecies interaction and the Lee-Huang-Yang quantum fluctuations affect the formation and the stability of such a novel state of matter. New useful analytic expressions for the equation of state, equilibrium density, glassy fraction, depletion, and the anomalous density of the droplet are obtained in terms of the disorder parameters using the Bogoliubov-Huang-Meng theory. Our results reveal the significant role played by the strength and correlations of disorder in the stability and in self-evaporation phenomenon of the droplet state. At finite temperature, we analyze the free energy and the critical temperature above which the droplet evaporates. It is found that the competition between the thermal fluctuations and disorder may strongly destabilize the droplet and completely destroy it above a certain critical temperature. We discuss the validity conditions of the present Bogoliubov theory. Furthermore, the structure and dynamics of the finite size quantum droplet in a three-dimensional random potential are explored by numerically solving the corresponding disorder-dependent Gross-Pitaevskii equation. We also investigate the lowest-lying excitations of self-bound droplets employing a variational method. Our predictions point out that the peculiar interplay of the disorder and the repulsive Lee-Huang-Yang corrections leads to deform the atomic density in the flat-top plateau region and to modify the collective modes of the self-bound droplet.

Finally, our study is extended to one-dimensional geometry. We describe the bulk properties of disordered droplets using the aforementioned Bogoliubov method. We then conduct a numerical study in the purpose of revealing the impacts of weak random external potentials in two physically different regimes are identified, namely: small droplets of an approximately Gaussian shape and large droplets with a broad flat-top plateau.

Contents

List of Figures

General introduction

New opportunities have arisen following the successful achievement of Bose-Einstein condensation (BEC) [1, 2] and Fermi degeneracy [3] in ultracold atomic vapors. These advancements have led to the emergence of novel experimental platforms, enabling the investigation of quantum phenomena and unique states of matter previously unexplored. Weakly-interacting single-component Bose gases received significant attention after first experiments [4].

The high tunability of interactions in ultracold Bose gases using Feshbach resonances open promising avenues for the exploration of novel regimes and phases of matter not encountered in other condensed-matter systems. Thanks to these techniques, both experimental and theoretical efforts have shifted towards more sophisticated systems such as quantum Bose mixtures [5, 6]. Experimentally, Bose–Bose mixtures can be realized using atoms in two different spin states [7, 8, 9, 10, 11, 12], different isotopes of the same species [13, 14], and of two different atom species [15, 16, 17, 18, 19, 20, 21]. In particular, the observation of binary BECs with atoms of the same element in different hyperfine states [7, 8, 9, 10, 11, 12] has received much attention because of its simplicity, yet, reveals essential kinetics related to the transition [22, 23]. Recently, such multi-component quantum gases have become one of several focuses of current interest in the ongoing exploration of the ultralow temperature physics due to their rich phase diagram non-present in their one-component counterparts. One of the most striking feature of Bose mixtures is their miscibility-immiscibility transition which depends on the ratio of the intra-

and interspecies interactions [13, 24, 25], on the condensate numbers [26], and on thermal fluctuations [27, 28, 29, 30]. The dynamics of Bose mixtures sparks a variety of physical effects, including quantum phase transitions, topological defects [31, 32], spin drag [33, 34], spin-orbit coupling [35], temperature effects [28, 29, 30], superfluidity [36, 37, 38, 39, 40, 41, 42], localization in disordered two-component BECs [43, 44, 45], and mixture droplet states (see e.g [46, 47, 48, 49, 50, 51] and references therein).

More recently, the addition of quantum fluctuations to the mean-field approximation was found to explain the stabilization of binary BECs and single-component dipolar BEC against collapse [46, 52, 53, 54], sparking new research concerning the liquefaction of Bose gases into self-bound droplets [46, 47, 48, 49, 50, 55, 56, 57]. D.S. Petrov, a researcher from Paris-Saclay University in his seminal work in October 2015, made a noteworthy prediction stating that, contrary to collapsing, an attractive Bose-Bose mixture can undergo phase transitions into a liquid-like droplet state due to the stabilizing effects of quantum fluctuations stemming from the Lee-Huang-Yang (LHY) corrections [58]. Soon after Petrov's prediction, the existence of quantum droplets was discovered in entirely different systems [59]. Specifically, these droplets were observed in ultracold Dysprosium (^{164}Dy) atoms, which possess the highest dipolar magnetic moment among all atomic species [55]. Subsequent experiments followed [56, 60], and before long, droplets consisting of ^{166}Er atoms, where dipole-dipole interactions play a crucial role, were successfully generated [57]. Observation of droplets emerged in both homonuclear Bose mixtures of ^{39}K and heteronuclear mixtures of ^{41}K-^{87}Rb have been reported in [47, 50]. These two categories of self-bound quantum droplets exhibit notable distinctions. While attractive mixtures give rise to spherical droplets, dipolar gases form elongated droplets aligned along the dipole direction [49]. The differing geometric properties and the distinct interactions responsible for their stabilization contribute to significant disparities in their characteristics, thereby expanding the range of phenomena that

can be explored. Despite their dissimilarities, both quantum liquids rely on the same mechanism for stabilization: quantum fluctuations. Dipolar droplets consist of a single-component dipolar BEC, where the interplay between dipole-dipole interactions and contact interactions reduces the mean-field energy. Furthermore, Bose-Bose mixture droplets solely rely on contact interactions, and the mean-field energy reduction arises from the competition between inter- and intra-component interactions.

From the theoretical side, quantum liquid droplets in weakly-interacting Bose–Bose mixtures have been intensively studied in the past few years with a variety of approaches. The Bogoliubov theory and the generalized Gross-Pitaevskii equation (GPE) can give a good description of self-bound droplets at zero temperature [46, 61]. Nonperturbative calculations including higher-order quantum corrections for both zero- and finite-temperature mixture liquid droplets have been provided by means of the time-dependent (independent) Hartree-Fock-Bogoluibov theory [62, 63, 64, 65, 66]. Other employed approaches include Beliaev theory [67], perturbative approach [68], pairing theory [69], and quantum Monte Carlo simulations [70, 71, 72].

On the other hand, disorder plays a crucial role in both the microscopic and macroscopic realms, as it is inherent in realistic physical systems due to environmental factors or randomly distributed imperfections. Even a minor degree of disorder can give rise to intriguing phenomena that lack a straightforward counterpart, such as the Anderson localization [73]. Over the past decade, there has been a substantial theoretical and experimental endeavor to unveil the impact of disorder on samples of cold atoms (see e.g.[74, 75, 76, 77, 78, 79]). In the realm of quantum physics, disorder pertains to the presence of randomness or irregularity in the characteristics of a physical system. It manifests as a form of potential energy that exhibits random spatial variation, resulting in a disordered arrangement of interacting particles. The sources of disorder in a quantum mechanical system can encompass impurities,

defects, thermal fluctuations, or external disturbances.

The creation of disorder using speckle lasers [80, 81] or incommensurate laser beams [82, 83] opens promising new avenues in ultracold quantum gases. Investigating the impact of disorder effects on a BEC holds immense significance in the domains of quantum physics and condensed matter physics. The competition between disorder and interactions plays a nontrivial role in developing a fundamental understanding of many aspects of ultracold gases namely: the Bose glass (a gapless compressible insulating state) [84, 85, 86, 87, 88] or Griffiths-McCoy phases [86], characterized by the presence of localized particles, Anderson localization [74, 75, 80, 81, 82, 83, 89, 90, 91, 92], disordered BEC in optical lattices [93, 94, 95, 96], Bose-Fermi mixtures [97, 98], and dipolar BEC in random potentials [54, 76, 77, 78, 99, 100, 101, 102].

However, until now, there has been little work dealing with equilibrium states and non-equilibrium dynamics of ultracold Bose-Bose mixtures subjected to weak disorder potentials. Disordered binay BECs present rich physics not encountered in a single component condensate due the intriguing interplay of quantum fluctuations induced by intra- and interspecies interactions and disorder effects (see e.g [103, 104, 105, 106]). Such disordered Bose mixtures could be regarded as a feasible simulator to analyze a plethora of novel quantum phenomena. Furthermore, less is known on the behavior of the quantum droplet in the presence of disordered potentials [107]. Untradilute quantum droplets subjected to an external disorder potential can exhibit quantum phase transitions due to quantum fluctuations. Exploring such disordered droplets is crucial for advancing our understanding of many-body quantum systems and for practical applications in quantum computing, quantum sensing, and materials science.

This thesis

The aim of this thesis is twofold: (i) To investigate the impacts of a weak disorder potential on equilibrium and non-equilibrium properties of dilute Bose-Bose mixtures using a perturbative theory. Therefore, a number of questions arise naturally: How does the interplay of the disorder and interactions alter the miscibility-immiscibility condition and the localization process? Do such Bose mixtures in the presence of Gaussian disorder potentials with time-periodic driving support a steady state that periodically changes during its time propagation? Can the dynamical corrections induced by disorder drive the system into a stationary out-of-equilibrium state? This study not only bridges the gap between superfluidity, interactions and disorder but it also is important from the viewpoint of elucidating the localization phenomenon of two bosonic species. Non-equilibrium evolution of binary BEC offers the unique opportunity to explore strongly correlated systems and transport in realistic physical systems. Understanding the time evolution of Bose mixtures is pivotal for the realization of Floquet condensates.

(ii) To present a comprehensive understanding of the properties of self-bound liquid droplets with weak correlated and uncorrelated disorder potentials for various geometries ranging from spherically symmetric three-dimensional configuration (3D) to 1D case. We look in particular at how the peculiar competition between the interspecies interactions, the LHY quantum fluctuations, and the disorder potential affect the formation and the stability of the self-bound droplet. Herein, the focus is laid on a microscopic description based on the Bogoliubov theory of the disordered self-bound droplet and on the role played by the correlations of the external random potential.

Throughout our study we neglect the surface effects.

Outline of the thesis

This thesis is organized as follows.

Chapter 1 offers a succinct introduction of the ground-state properties of BEC mixtures including the GPE and the Bogoliubov theory which serve as fundamental theoretical frameworks for understanding these mixtures. We present the Bogoliubov-de Gennes (BdG) equations that enable us to calculate the elementary excitations and the noncondensate and anomalous densities. Quantum and thermal fluctuation corrections to the equation of state are accurately calculated. Additionally, we provide a comprehensive overview for the theory of quantum droplets of bosonic mixtures, emphasizing the essential conditions required for their formation and elucidating their equilibrium properties.

Chapter 2 is devoted to an introductory presentation of the fundamental principles and basic concepts of disordered systems. We delve into an in-depth examination of the statistical properties exhibited by random potentials, shedding light on various approaches employed to generate disordered potentials for ultracold neutral atoms. We then turn to dilute Bose gases, and point out the main ideas related to disorder in interacting systems. Moreover, we introduce the main theoretical tools essential for analyzing Bose gases with disorder potentials.

Chapter 3 is dedicated to the impact of weak disorder potentials on homogeneous binary BECs at zero temperature. Using a perturbative theory, we derive analytical expressions for the relevant physical properties of the system, such as the glassy fraction, the equation of state (EoS), the compressibility, and the superfluid density. We look at how each species is influenced by the disorder and how the interaction between disordered bosons influences the coupling and the phase transition between the two components. We explored on the other hand, the non-equilibrium dynamics of binary BECs subjected to a time-dependent random potential with a Gaussian correlation function. To this end, we employ the time-dependent perturbative theory, enabling us to uncover the fascinating interplay between disorder and

interspecies interactions in the non-equilibrium regime.

Chapter 4 discusses the main features of the self-bound droplet of symmetric Bose mixtures in correlated and uncorrelated random potentials, focusing on 3D and 1D geometries. The present analysis encompasses various disorder models namely: δ-correlated white noise, Gaussian-correlated disorder and speckle potentials. Our primary focus is to unveil the fundamental properties exhibited by these disordered droplets on a bulk scale (an infinitely large droplet). This analysis is carried out within the framework of the Huang-Meng (HM) approach, allowing us to obtain useful expressions for the ground-state energy, the equilibrium density, the disorder fraction inside the droplet, the depletion and the anomalous correlation in terms of the system parameters. Furthermore, we consider effects of thermal fluctuations in addition to already present quantum fluctuations on the disordered droplet by examining other quantities of much interest, such as the free energy, the thermal equilibrium density and the critical temperature. Our study is extended to the finite size droplet by numerically solving the disorder-dependent generalized GPE which we derive self-consistently using the local density approximation. The collective modes of the droplet are also analyzed through the application of a variational Gaussian ansatz.

Chapter 5 focuses on the behavior of self-bound liquid droplets in 1D optical speckle potentials. We apply the developed HM theory and derive useful formulas for the equation of state, fluctuations induced by disorder, the equilibrium density, and free energy. In particular, we show that the peculiar competition between the disorder, the interactions and the LHY quantum fluctuations may strongly affect the stability and the occurrence of the self-bound droplet. We address also the static and dynamical properties of such a disordered droplet by numerically solving the finite-temperature generalized GPE.

Finally we conclude the thesis and suggest directions for future works.

List of publications

- **Karima Abbas** and Abdelâali Boudjemâa, Self-bound liquid droplets in one-dimensional optical speckle potentials, New J. Phys. **26**, 033037 (2024).
- **Karima Abbas** and Abdelâali Boudjemâa, Self-bound droplets with uncorrelated disordered potentials, J. Phys. B: At. Mol. Opt. Phys. **97**, 39 (2024).
- **Karima Abbas** and Abdelâali Boudjemâa, Quantum liquid droplets in Bose mixtures with weak disorder, Phys. Rev. A **107**, 033306 (2023).
- Abdelâali Boudjemâa and **Karima Abbas**, Quantum droplets in one-dimensional Bose-Bose mixtures: Beyond the Lee-Huang-Yang description, New J. Phys. **25**, 093052 (2023).
- **Karima Abbas** and Abdelâali Boudjemâa, Binary Bose-Einstein condensates in a disordered time-dependent potential, J. Phys.: Condens. Matter, **34**, 125102 (2022).
- Abdelâali Boudjemâa and **Karima Abbas**, Bose-Bose mixtures in a weak disorder potential: Fluctuations and Superfluidity, Phys. Rev. A **102**, 023325 (2020).

Chapter 1

Quantum self-bound droplets in Bose-Bose mixtures

The peculiar control of parameters in ultracold quantum gases, culminated with the observation of a single component BEC in alkali atoms, boosted a tremendous experimental effort to create multi-component BECs [7, 8]. These systems have been broadly studied over the last years, thus many interesting effects, not achievable in a single component BEC, have been predicted theoretically and determined experimentally. A key property of these systems is that they manifest miscible and immiscible behavior allowing a large variety of interesting physical phenomena.

Since the spectacular prediction of self-bound droplets in ultracold quantum gases in 2015 by Petrov [46], intensive investigations have been carried out in the past years, both to explain the initial observations and to predict new phenomena (see for review [108, 109, 110] and references therein). Such ultradilute quantum liquids originate from a delicate balance between mean-field attraction (collapse) and beyond-mean-field repulsive LHY quantum fluctuations. These new state of matter are quite different from the well-known van der Waals liquids, since they show unusually low densities that are eight orders of magnitude lower than that of liquid helium droplets, and they exist at temperatures that are about nine orders

of magnitude lower than the freezing points of classical liquids. Generally droplets forming in Bose mixtures could be a useful tool to explore complex quantum systems beyond the mean-field paradigm.

This chapter is devoted to the theoretical background on quantum droplets emerging from binary BECs. In the first part, after reporting a brief overview of degenerate 3D Bose-Bose mixtures, we discuss the mechanism leading to the formation of a quantum droplet, in the case of two-component Bose gases. We report the formalism used to describe the properties of a self-bound droplet at both zero and finite temperatures. In the second part of this chapter we plan to summarize recent developments in the theory of quantum droplet in the lower dimension. We will mainly focus on analytical results related to a 1D self-bound phase.

1.1 Mean-field approach for Bose-Bose mixtures

We consider weakly interacting two-component BECs with the atomic mass m_j $(j = 1, 2)$ confined in external traps $U_j(\mathbf{r})$. The many-body Hamiltonian describing this system can be written as:

$$\hat{H} = \sum_{j=1}^{2} \int d\mathbf{r} \hat{\psi}_j^\dagger(\mathbf{r}) \left[h_j^{sp} + \frac{g_j}{2} \hat{\psi}_j^\dagger(\mathbf{r}) \hat{\psi}_j(\mathbf{r}) \right] \hat{\psi}_j(\mathbf{r}) + g_{12} \int d\mathbf{r} \hat{\psi}_2^\dagger(\mathbf{r}) \hat{\psi}_2(\mathbf{r}) \hat{\psi}_1^\dagger(\mathbf{r}) \hat{\psi}_1(\mathbf{r}), \tag{1.1}$$

where $h_j^{sp} = -(\hbar^2/2m_j)\nabla^2 + U_j(\mathbf{r})$ is the single particle Hamiltonian of each component, $g_j = 4\pi\hbar^2 a_j/m_j$ and $g_{12} = g_{21} = 4\pi\hbar^2 a_{12}(m_1^{-1} + m_2^{-1})$ are the coupling constants with a_j and a_{12} being the intraspecies and the interspecies s-wave scattering lengths, respectively, and $\hat{\psi}_j$ and $\hat{\psi}_j^\dagger$ are the boson annihilation and creation field operators, respectively, satisfying the usual canonical commutation rules

$$\begin{aligned} \left[\hat{\psi}_j(\mathbf{r}), \hat{\psi}_j^\dagger(\mathbf{r}') \right] &= \delta(\mathbf{r} - \mathbf{r}'), \\ \left[\hat{\psi}_j(\mathbf{r}), \hat{\psi}_j(\mathbf{r}') \right] &= \left[\hat{\psi}_j^\dagger(\mathbf{r}), \hat{\psi}_j^\dagger(\mathbf{r}') \right] = 0. \end{aligned} \tag{1.2}$$

The equations of motion for the binary BECs follow directly from the Heisenberg equation and reads:

$$i\hbar\frac{d\hat{\psi}_j}{dt} = [\hat{\psi}_j, \hat{H}]. \tag{1.3}$$

At very low temperature it is convenient to decompose the field operator into a condensate and a noncondensate component which remains small in the BEC regime:

$$\hat{\psi}_j(\mathbf{r}) = \Phi_j(\mathbf{r}) + \hat{\tilde{\psi}}_j(\mathbf{r}), \tag{1.4}$$

where $\Phi_j(\mathbf{r}) = \langle\hat{\psi}_j(\mathbf{r})\rangle$ stand for the condensate wavefunctions, $\hat{\tilde{\psi}}_j(\mathbf{r})$ represent the noncondensed field operators. At zero temperature, large majority of the particles are Bose condensed, so that the noncondensate operators can be neglected and $\hat{\psi}_j(\mathbf{r})$ can be replaced by the condensate wavefunction $\Phi_j(\mathbf{r})$. By using this prescription one gets the following the famous coupled GPEs

$$i\hbar\frac{d\Phi_j(\mathbf{r},t)}{dt} = \left(-\frac{\hbar^2}{2m_j}\nabla^2 + U_j(\mathbf{r}) + g_j|\Phi_j(\mathbf{r},t)|^2 + g_{12}|\Phi_{\bar{j}}(\mathbf{r},t)|^2\right)\Phi_j(\mathbf{r},t), \tag{1.5}$$

where $\bar{j} = 3-j$. Equations (1.5) are coupled nonlinear Schrödinger equations for the two condensate wavefunctions. For $g_{12} = 0$, equations (1.5) reduce to the standard GPE for a single component BEC which was derived by E. P. Gross and L. P. Pitaevskii in 1961 [111, 112]. These coupled equations are particularly important since they describe complicated many-body problems and appropriately govern the static and the dynamics of binary BECs at zero temperature.

The wavefunctions are normalized using the condition:

$$N_j = \int d\mathbf{r}|\Phi_j(\mathbf{r})|^2. \tag{1.6}$$

In order to describe the different ground states of the mixture we have to write

the energy functional associated to equations (1.5):

$$E[\Phi_j, \Phi_j^*] = \int d\mathbf{r} \left(\frac{\hbar^2}{2m_j} |\nabla \Phi_j(\mathbf{r})|^2 + U_j(\mathbf{r}) |\Phi_j(\mathbf{r})|^2 + \frac{1}{2} g_j |\Phi_j(\mathbf{r})|^4 + g_{12} |\Phi_j(\mathbf{r})|^2 |\Phi_{\bar{j}}(\mathbf{r})|^2 \right). \tag{1.7}$$

Interatomic interactions between the different components (g_j and g_{12}) determine the structure of the ground-state of the two-component Hamiltonian.

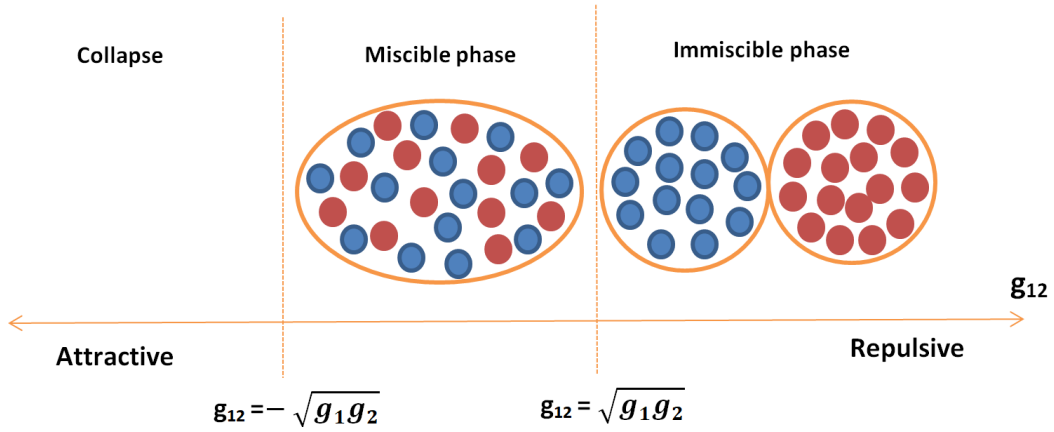

Figure 1.1: Phase diagram of a Bose-Bose mixture

In the regime where all interactions are repulsive (g_j,$g_{12} > 0$), two phases are expected with a possibility of transition between them [24] namely: the miscible regime in which the wavefunctions of the two species are overlapped, and the immiscible regime where they are separated (see figure 1.1). Both regimes have been experimentally observed (see e.g. [13, 113]). The transition between these two regimes was largely studied theoretically and experimentally[13, 114, 115]. When the interspecies interaction is negative enough, the system will collapse even if each component has repulsive intraspecies interactions (see figure 1.1).

The condition that explains the appearance of these three phases in the homogeneous case ($U_j(\mathbf{r}) = 0$) is reported in [117]:

$$|g_{12}| = \sqrt{g_j g_{\bar{j}}}. \tag{1.8}$$

For $g_{12} > \sqrt{g_j g_{\bar{j}}}$, the repulsive interspecies energy is large enough to spatialy separate the two condensates (immiscible regime). On the other side, when $g_{12} < -\sqrt{g_j g_{\bar{j}}}$ the attractive interspecies interactions dominate the repulsive ones and the system collapses. In between, for $-\sqrt{g_j g_{\bar{j}}} < g_{12} < \sqrt{g_j g_{\bar{j}}}$, the system is in the miscible regime, and the two condensates overlap.

1.2 Beyond mean-field quantum fluctuations : the Lee-Huang-Yang correction

In this section we calculate the mean-field energy and its beyond mean-field corrections. Let us then consider a weakly interacting homogeneous binary mixture of bosons with equal masses ($m_1 = m_2 = m$), occupying a volume V. The plane waves expansion appropriate for describing a homogeneous system is

$$\hat{\psi}_j(\mathbf{r}) = \sum_{\mathbf{k}} \frac{1}{V} e^{i\mathbf{k}\mathbf{r}} \hat{a}_{j,\mathbf{k}}, \qquad \text{and} \qquad \hat{\psi}_j^\dagger(\mathbf{r}) = \sum_{\mathbf{k}} \frac{1}{V} e^{-i\mathbf{k},\mathbf{r}} \hat{a}_{j,\mathbf{k}}^\dagger, \tag{1.9}$$

where single-particle creation and annihilation operators in each component are respectively, $\hat{a}_{j,\mathbf{k}}^\dagger$, and $\hat{a}_{j,\mathbf{k}}$ ($j = 1, 2$), then bring the Hamiltonian (1.1) to its second-quantized form:

$$\hat{H} = \sum_{j,\mathbf{k}} E_{\mathbf{k}} \hat{a}_{j,\mathbf{k}}^\dagger \hat{a}_{j,\mathbf{k}} + \frac{1}{2V} \sum_{j,\mathbf{k},\mathbf{k}',\mathbf{q}} g_j \hat{a}_{j,\mathbf{k}}^\dagger \hat{a}_{j,\mathbf{k}'+\mathbf{q}}^\dagger \hat{a}_{j,\mathbf{k}'} \hat{a}_{j,\mathbf{k}+\mathbf{q}} + \frac{g_{12}}{V} \sum_{\mathbf{k},\mathbf{k}',\mathbf{q}} \hat{a}_{1,\mathbf{k}}^\dagger \hat{a}_{1,\mathbf{k}+\mathbf{q}} \hat{a}_{2,\mathbf{k}'+\mathbf{q}}^\dagger \hat{a}_{2,\mathbf{k}'} \tag{1.10}$$

where $E_{\mathbf{k}} = \hbar^2 \mathbf{k}^2/(2m)$ is the energy of free particle.

The elementary excitations and the ground-state energy of the mixture are obtained by applying the Bogoliubov prescription which consists in replacing the operators $\hat{a}_{j,0}$ and $\hat{a}_{j,0}^\dagger$ by a c-number, i.e., $\hat{a}_{j,0} = \hat{a}_{j,0}^\dagger = \sqrt{N_{jc}}$, where N_{jc} is the number of condensed particles. In the resulting equation, we ignore higher-order fluctuations and keep only terms in $\hat{a}_{j,\mathbf{k}\neq 0}$, $\hat{a}_{j,\mathbf{k}\neq 0}^\dagger$ up to second-order in the coupling constants.

Therefore, the Hamiltonian (1.10) can be rewritten as :

$$\hat{H}=\sum_j \frac{g_j}{2V}N_{jc}^2+\frac{g_{12}}{V}N_{1c}N_{2c}+\sum_{j,\mathbf{k}}(E_k+2g_jn_{cj}+g_{12}n_{c3-j})\,\hat{a}_{j,\mathbf{k}}^\dagger\hat{a}_{j,\mathbf{k}} \tag{1.11}$$
$$+\frac{g_j}{2V}N_{cj}\sum_{j,\mathbf{k}}\left(\hat{a}_{j,\mathbf{k}}^\dagger\hat{a}_{j,-\mathbf{k}}^\dagger+\hat{a}_{j,\mathbf{k}}\hat{a}_{j,-\mathbf{k}}\right)+\frac{g_{12}}{V}\sqrt{N_{1c}N_{2c}}\sum_{\mathbf{k}}\left(\hat{a}_{1,\mathbf{k}}^\dagger+\hat{a}_{1,-\mathbf{k}}\right)\left(\hat{a}_{2,-\mathbf{k}}^\dagger+\hat{a}_{2,\mathbf{k}}\right),$$

where $n_{jc}=N_{jc}/V$.

Hamiltonian (4.3) can be diagonalized making the following canonical Bogoliubov transformation [51, 118]

$$\hat{a}_{1k}=(u_{+,k}\hat{b}_{1k}+v_{+,k}\hat{b}_{1,-k}^\dagger)\cos\gamma-(u_{-,k}\hat{b}_{2k}+v_{-,k}\hat{b}_{2,-k}^\dagger)\sin\gamma, \tag{1.12a}$$
$$\hat{a}_{2k}=(u_{+,k}\hat{b}_{1k}+v_{+,k}\hat{b}_{1,-k}^\dagger)\sin\gamma+(u_{-,k}\hat{b}_{2k}+v_{-,k}\hat{b}_{2,-k}^\dagger)\cos\gamma, \tag{1.12b}$$

where

$$\cos\gamma,\sin\gamma=\frac{1}{\sqrt{2}}\sqrt{1\pm\frac{1-\alpha}{\sqrt{(1-\alpha)^2+4\Delta^{-1}\alpha}}}, \tag{1.13}$$

and $\alpha=n_{c2}g_2/n_{c1}g_1$, $\Delta=g_1g_2/g_{12}^2$ is the miscibility parameter of Bose mixtures, $\hat{b_{j_\mathbf{k}}}$ and $\hat{b_{j_\mathbf{k}}}^\dagger$ are the quasi-particle annihilation and creation operators obeying the usual Bose commutation relations:

$$\left[\hat{b_{j_\mathbf{k}}},\hat{b_{j_{\mathbf{k}'}}}^\dagger\right]=\delta_{\mathbf{k},\mathbf{k}'},\quad\text{and}\quad\left[\hat{b_{j_\mathbf{k}}},\hat{b_{j_{\mathbf{k}'}}}\right]=\left[\hat{b_{j_\mathbf{k}}}^\dagger,\hat{b_{j_{\mathbf{k}'}}}^\dagger\right]=0. \tag{1.14}$$

The Bogoliubov quasiparticle amplitudes are given by:

$$\begin{aligned}u_{\pm,k}&=\frac{1}{2}\left(\sqrt{\frac{\varepsilon_{\pm,k}}{E_k}}+\sqrt{\frac{E_k}{\varepsilon_{\pm,k}}}\right),\\ v_{\pm,k}&=u_{\pm,k}-\sqrt{\frac{E_k}{\varepsilon_{\pm,k}}},\end{aligned} \tag{1.15}$$

which are chosen to be real without loss of generality. They must obey the constraint

$$u_{\pm k}^2 - v_{\pm k}^2 = 1. \tag{1.16}$$

The Bogoliubov spectra are expressed as [29, 119]

$$\varepsilon_{\pm,k} = \sqrt{E_k^2 + 2E_k\mu_\pm}, \tag{1.17}$$

where

$$\mu_\pm = \frac{1}{2}\left(g_1 n_1 + g_2 n_2 \pm \sqrt{(g_1 n_1 - g_2 n_2)^2 + 4g_{12}^2 n_1 n_2}\right), \tag{1.18}$$

and $n_j = N_j/V$ is the density of the j-th component. In equation (1.17) the highest energy branch $\varepsilon_{+,k}$, known as the hard mode, corresponds to the spin excitations while the lowest energy branch $\varepsilon_{-,k}$ is known as the soft branch and corresponds to the density excitations [6].

Hence, the Hamiltonian (4.3) in the diagonalized form is written as:

$$\hat{H} = E + \sum_{\mathbf{k}\neq 0}\left(\varepsilon_{+,k}\hat{b_{1\mathbf{k}}}^\dagger \hat{b_{1\mathbf{k}}} + \varepsilon_{-,k}\hat{b_{2\mathbf{k}}}^\dagger \hat{b_{2\mathbf{k}}}\right), \tag{1.19}$$

which describes binary Bose gas of noninteracting quasi-particles.

The ground-state energy of the system reads [29, 119]

$$\frac{E}{V} = \sum_j \frac{g_j}{2} n_j^2 + g_{12} n_1 n_2 + \frac{E_{\mathrm{LHY}}}{V}. \tag{1.20}$$

The leading term is the mean-field energy, and the subleading term, E_{LHY}, is the first beyond mean-field correction to the ground-state energy, the so-called LHY energy (i.e. the zero-point energy corresponding to the Bogoliubov modes):

$$\frac{E_{\mathrm{LHY}}}{V} = \frac{1}{2V}\sum_{\mathbf{k}}\left[\varepsilon_{+,k} + \varepsilon_{-,k} - 2E_k - \mu_\pm\right]. \tag{1.21}$$

The task now is to find the LHY corrected energy. If one uses this integral directly by summing over all states, we find that the energy (1.21) suffers from the ultraviolet divergence from large k contributions. This difficulty comes from the use of short-range contact potential which is valid only for small momenta. To cure this issue, we renormalize the coupling constants and introduce the Beliaev-type second-order corrections [46, 119, 29]

$$g_j(\mathbf{k}) = g_j + \frac{g_j^2}{V}\sum_{\mathbf{k}}\frac{1}{2E_k}, \quad \text{and} \quad g_{12}(\mathbf{k}) = g_{12} + \frac{g_{12}^2}{V}\sum_{\mathbf{k}}\frac{1}{2E_k}. \tag{1.22}$$

After the subtraction of the ultraviolet divergent part, the renormalized energy takes the form:

$$E_{\mathrm{LHY}} = \frac{1}{2}\sum_{\mathbf{k}}\left[\varepsilon_{+k} + \varepsilon_{-k} - \sum_{j=1}^{2}\left(E_{jk} + g_j n_{cj} - \frac{n_{cj}^2 g_j^2}{2E_{jk}}\right) + n_{c1}n_{c2}g_{12}^2\sum_{j=1}^{2}\frac{2}{E_{jk}}\right]. \tag{1.23}$$

Working in the thermodynamic limit where the atoms number $N \to \infty$ and the volume $V \to \infty$, the sums over k transform to integrals, $\sum_{\mathbf{k}} \longrightarrow V\int d^3k/(2\pi)^3$. With this we obtain for the LHY corrected energy

$$\frac{E_{\mathrm{LHY}}}{V} = \frac{8}{15\pi^2}m^{3/2}(g_1 n_1)^{5/2} f\left(1, \frac{g_{12}^2}{g_1 g_2}, \frac{g_2 n_2}{g_1 n_1}\right), \tag{1.24}$$

where the dimensionless function f is defined as:

$$f\left(1, x, y\right) = \sum_{\pm}\left(1 + y \pm \sqrt{(1-y)^2 + 4xy}\right)^{5/2}/4\sqrt{2}. \tag{1.25}$$

Its behavior is displayed in figure 1.2.

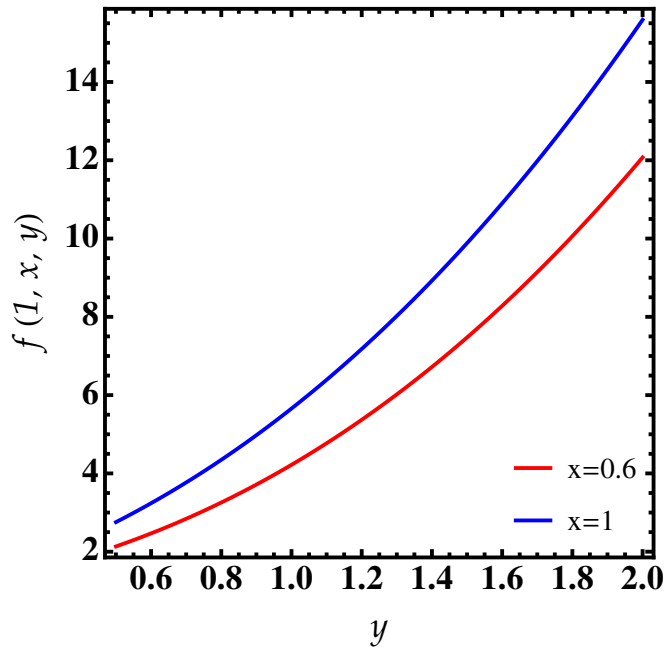

Figure 1.2: The function $f(1, x, y)$ from equation 1.25 as a function of y.

1.2.1 Free energy

At finite temperatures, thermal fluctuations become significant, and the condensate coexists with a thermal cloud of non-condensed particles. Hence, to understand Bose mixtures at constant temperature and volume, we need to calculate the Helmholtz free energy F which is defined as [29, 62]

$$F = E + T\int_0^\infty \frac{d^3k}{(2\pi)^3}\left[\ln\left(\frac{2}{\sqrt{I_{k+}}+1}\right)+\ln\left(\frac{2}{\sqrt{I_{k-}}+1}\right)\right], \tag{1.26}$$

where $I_{k\pm} = \coth^2(\varepsilon_{k\pm}/2T)$, with T being the temperature, the ground-state energy E is given by equation (1.20). The Boltzmann constant set $k_B = 1$ throughout the manuscript.

At low temperatures, $T \ll n_1 g_1$, where the main contribution to equation (1.26) comes from the phonon region, the evaluation of the thermal contribution of the free

energy yields the famous T^4-law [29]

$$\frac{F}{V} = \frac{E}{V} - \frac{16g_1\sqrt{a_1^3/\pi}}{15\sqrt{2}} n_1^{5/2} \sum_{\pm} \left[\frac{1}{2\sqrt{2}} f\left(1, \frac{g_{12}^2}{g_1 g_2}, \frac{g_2 n_2}{g_1 n_1}\right)^{-3/2} \left(\frac{\pi T}{g_1 n_1}\right)^4 \right], \tag{1.27}$$

here we employed the identity $\int_0^\infty dx x^2 \ln[2/(\coth(x/2)+1)] = -\pi^4/45$. In the limit of lower density $n \to 0$, the thermal corrections to the free energy (1.27) diverge as $n^{-3/2}$ and vanish at zero temperature. The free energy is important for studying the behavior of a self-bound droplet at finite temperatures.

1.2.2 Noncondensed and anomalous densities

The microscopic origin of interaction-driven quantum depletion, $\tilde{n}$, of a BEC can be explained according to the Bogoliubov theory [122]. The condensate depletion which represents the fraction of particles that coherently expelled from the condensate due to interaction effects must be very small compared to the total density [122]. Recently the experimental measure of the quantum depletion of an interacting homogeneous single BEC has been reported in [123]. Another important quantity that arises from the Bogoliubov theory is the anomalous density, $\tilde{m}$. This latter quantifies the correlations of pairs of noncondensate atoms with pairs of condensate atoms due to the Bogoliubov pair promotion process in which two condensate atoms scatter each other out of the condensate which is responsible for the well-known Bogoliubov particle-hole structure of excitations in the system [120, 121]. Certainly, the presence of these quantities add new features to the well-known problems and play a key role in understanding the equilibrium properties and the dynamics of Bose mixtures.

The noncondensed and the anomalous densities are defined, respectively as

$$\tilde{n} = \frac{1}{V} \sum_{j,\mathbf{k}\neq 0} \langle \hat{a}_{j,\mathbf{k}}^\dagger \hat{a}_{j,\mathbf{k}} \rangle. \tag{1.28}$$

and

$$\tilde{m} = -\frac{1}{V}\sum_{j,\mathbf{k}\neq 0}\langle \hat{a}_{j,\mathbf{k}}\hat{a}_{j,-\mathbf{k}}\rangle, \tag{1.29}$$

Using the transformation (4.4), we find for the noncondensed and anomalous densities associated with the spin and density channels:

$$\begin{aligned}\tilde{n}_{\pm} = \frac{1}{V}\sum_{\mathbf{k}\neq 0}\Bigg\{ &\left[v_{\pm k}^2 + \left(u_{\pm k}^2 + v_{\pm k}^2\right) N_{\pm k}\right]\cos^2\gamma \\ &+ \left[v_{\mp k}^2 + \left(u_{\mp k}^2 + v_{\mp k}^2\right) N_{\mp k}\right]\sin^2\gamma\Bigg\},\end{aligned} \tag{1.30}$$

$$\begin{aligned}\tilde{m}_{\pm} = -\frac{1}{V}\sum_{\mathbf{k}\neq 0}\Bigg\{ &\left[u_{\pm k}v_{\pm k}(1+2N_{\pm k})\right]\cos^2\gamma \\ &+ \left[u_{\mp k}v_{\mp k}(1+2N_{\mp k})\right]\sin^2\gamma\Bigg\},\end{aligned} \tag{1.31}$$

where $N_{\pm,k} = \langle \hat{b}_{\pm,\mathbf{k}}^{\dagger}\hat{b}_{\pm,\mathbf{k}}\rangle = [\exp(\varepsilon_{k,\pm}/T) - 1]^{-1}$ are occupation numbers for the excitations.

After a straightforward calculation, we obtain for the total noncondensed, $\tilde{n}$, and anomalous, $\tilde{m}$, densities

$$\tilde{n} = \sum_{\pm}\tilde{n}_{\pm} = \frac{1}{V}\sum_{\pm,\mathbf{k}} v_{\pm,\mathbf{k}}^2 + \sum_{\pm,\mathbf{k}}(v_{\pm,\mathbf{k}}^2 + u_{\pm,\mathbf{k}}^2)N_{\pm,k}, \tag{1.32}$$

and

$$\tilde{m} = \sum_{\pm}\tilde{m}_{\pm} = -\frac{1}{V}\sum_{\pm,\mathbf{k}} v_{\pm,\mathbf{k}}u_{\pm,\mathbf{k}} - \frac{2}{V}\sum_{\pm,\mathbf{k}} v_{\pm,\mathbf{k}}u_{\pm,\mathbf{k}}N_{\pm,k}. \tag{1.33}$$

Substituting equation (1.15) into equations (1.32) and (1.33), replacing the sum over k by an integral $\sum_{\mathbf{k}} \to V\int_0^{\infty} d^3k/(2\pi)^3$, and using the fact that $2N(x) + 1 = \coth(x/2)$, one obtains

$$\tilde{n} = \frac{1}{2}\int\frac{d^3k}{(2\pi)^3}\left[\frac{E_k + \mu_{\pm}}{\varepsilon_{k\pm}} - 1\right] + \frac{1}{2}\int\frac{d^3k}{(2\pi)^3}\frac{E_k + \mu_{\pm}}{\varepsilon_{k\pm}}\left[\coth\left(\frac{\varepsilon_k}{2T}\right) - 1\right], \tag{1.34}$$

and

$$\tilde{m} = -\frac{1}{2}\int \frac{d^3k}{(2\pi)^3}\frac{\mu_\pm}{\varepsilon_{k\pm}} - \frac{1}{2}\int \frac{d^3k}{(2\pi)^3}\frac{\mu_\pm}{\varepsilon_{k\pm}}\left[\coth\left(\frac{\varepsilon_k}{2T}\right) - 1\right]. \tag{1.35}$$

First terms in equations (1.34) and (1.35) are the zero-temperature contribution to the noncondensed and anomalous densities, respectively. Second terms represent the contribution of the so-called thermal fluctuations.

Remarkably, the zero temperature term of the anomalous density (1.35) is ultraviolet divergente, this problem can be circumvented employing the same renormalization of the coupling constants (1.22). Therefore, the renormalized anomalous density takes the form:

$$\tilde{m} = -\int \frac{d^3k}{(2\pi)^3}\left[\frac{1}{\varepsilon_k} - \frac{n_j^2 g_j^2}{2E_k} - \frac{n_1 n_2 g_{12}^2}{2E_k}\right]. \tag{1.36}$$

Equations (1.34) and (1.36) are appealing since they enable us to determine in a self-consistent way the quantum fluctuations that are responsible for the stabilization of the quantum droplet in Bose mixtures.

1.3 Quantum droplets

1.3.1 Experimental realization

Quantum droplets in the full 3D space were created in a weakly interacting binary condensate composed of two hyperfine states of ^{39}K [48]. The experiment utilized a cross dipole potential generated by three red-detuned laser beams, along with an optical levitation potential. The perpendicular beams were employed to initialize the condensate, while the latter component aided in minimizing residual confinement in all spatial directions. As shown in figure 1.3 (a), when the external magnetic field B is less than a critical value, the binary condensate may be either a quantum droplet or an LHY gas. When released from the external dipole trap in the attractive regime, the condensate keeps a constant size (see figure 1.3 (b)), which demonstrates a well-defined quantum droplet.

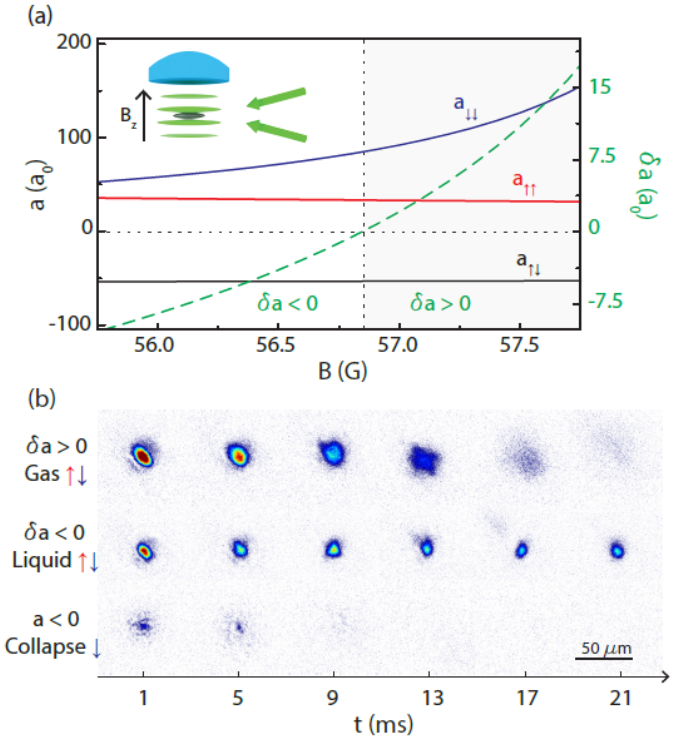

Figure 1.3: Observation of quantum droplets. Taken from [48]

1.3.2 Stabilization mechanism

In what follows we consider a symmetric mixture where $n_1 = n_2 = n$ and $g_1 = g_2 = g$. Therefore, the ground-state energy (1.20) turns out to be given as:

$$\frac{E}{V} = (g + g_{12})n^2 + \frac{8}{15\pi^2} m^{3/2} g^{5/2} n^{5/2} f\left(1, \frac{g_{12}^2}{g^2}, 1\right). \tag{1.37}$$

As we have mentioned above, when the attraction energy between the two atomic species in a Bose-Bose mixture becomes larger than the single species average repulsion energy, ($g_{12}^2 > g^2$), the mixture is expected to collapse according to the mean-field theory. Following the procedure outlined in [46] and consider the unstable case, where the mean-field energy is slightly negative. It is convenient then to introduce $\delta g_+ = g + g_{12} < 0$ and assume it small, $\delta g_+ \ll g$. In such a situation, the mixture is expected to collapse in the mean-field formalism, $|\delta g_+| n^2 < 0$, and the LHY term is positive and depends only on the contact interaction g. Because of its

steeper density scaling ($\propto n^{5/2}$) the quantum LHY repulsion neutralizes the mean-field attraction ($\propto n^2$) and stabilizes the system against collapse, giving rise to a self-bound solution: the so-called *quantum liquid droplet*, around a fixed equilibrium density $n^{(0)}$ which depends only on s-wave contact interactions and the droplet is therefore isotropic.

The stabilization mechanism is shown in figure 1.4, where we can see that the ground-state energy has a minimum for a fixed density.

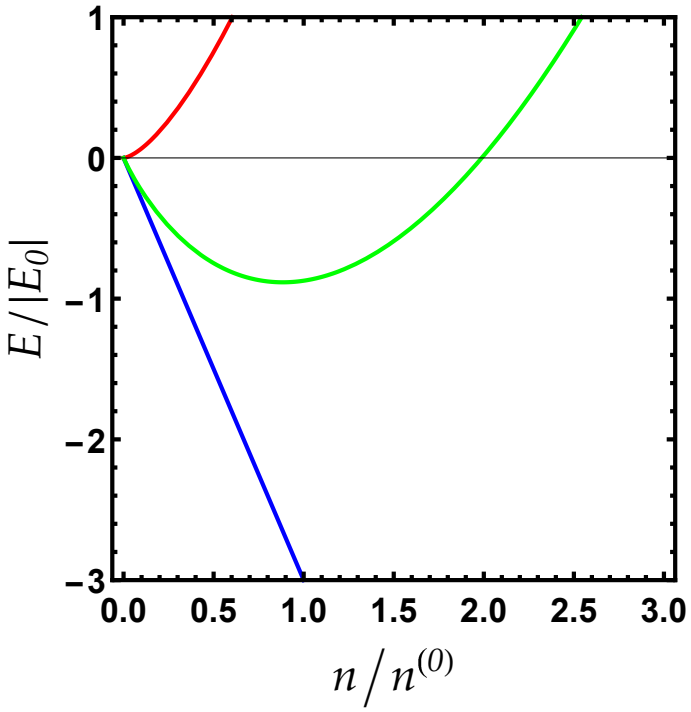

Figure 1.4: The blue line represents the mean-field energy, the red line is LHY energy, and the green line is the sum of the two terms for $g_{12}/g = -1.05$. Here $|E_0|/N = 25\pi^2\hbar^2|\delta a_+/a|^3/(49152ma^2)$.

The equilibrium density of the droplet is given by the relation [46]

$$n^{(0)} = \frac{25\pi\left(\delta a_+/a\right)^2}{16384a^3}, \tag{1.38}$$

where $\delta a_\pm/a = 1 \pm a_{12}/a$.

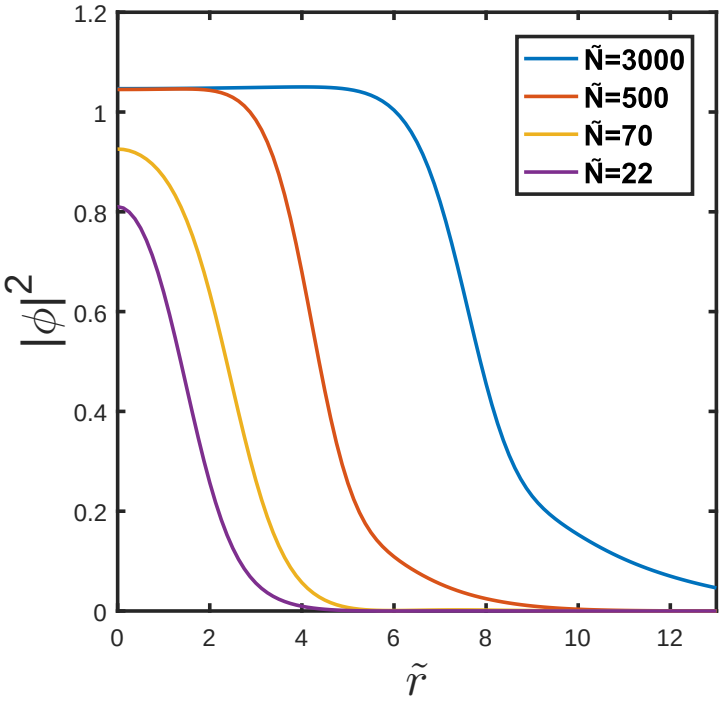

Figure 1.5: Density profile of the droplet for different values of $\tilde{N}$. For large atom numbers the pick density saturates to a fixed value, giving rise to a flat-top bulk.

1.3.3 Generalized Gross-Pitaevskii equation

Following Petrov in his famous work [46], we can describe the properties of the mixture in a simpler manner without using the set of coupled GPE. In the miscible phase and close to the collapse point, we can describe the system with an effective low-energy theory [116], where we treat the mixture as an effective single component BEC by setting

$$\Phi_j(\mathbf{r},t) = \sqrt{n_j^{(0)}}\phi(\mathbf{r},t), \tag{1.39}$$

where $\phi(\mathbf{r},t)$ is a scalar wavefunction common to both species.

By inserting equation (1.39) into equation (1.7), the corresponding energy density functional of a homogenous mixture reads

$$\mathcal{E}(\phi,\phi^*) = \frac{\hbar^2}{2m}n^{(0)}|\nabla\phi|^2 + \frac{\delta g_+}{4}n^{(0)^2}|\phi|^4 + \frac{64g\sqrt{\frac{a^3}{\pi}}}{15.2^{5/2}}n^{(0)^{5/2}}\sum_{\pm}\left(\frac{\delta a_\pm}{a}\right)^{5/2}|\phi|^5. \tag{1.40}$$

The generalized GPE can be derived through $i\partial\phi/\partial t = \partial\mathcal{E}/\partial\phi^*$. This yields

$$i\frac{\partial\phi(\mathbf{r},t)}{\partial t} = \left(\frac{-\hbar^2\Delta}{2m} + \frac{\delta g_+}{2}n^{(0)}|\phi|^2 + \frac{8g\sqrt{\frac{a^3}{2\pi}}}{3}n^{(0)^{3/2}}\sum_{\pm}\left(\frac{\delta a_\pm}{a}\right)^{5/2}|\phi|^3\right)\phi(\mathbf{r},t). \tag{1.41}$$

Using the dimensionless coordinates $\tilde{\mathbf{r}} = \mathbf{r}/\xi$ and $\tilde{t} = t/\tau$, where

$$\tau = \frac{3\hbar}{|\delta g_+|n_j^{(0)}}, \qquad \text{and} \qquad \xi = \sqrt{\frac{3\hbar^2}{m|\delta g_+|n_j^{(0)}}}, \tag{1.42}$$

we thus find the dimensionless generalized GPE

$$i\frac{\partial\phi(\tilde{\mathbf{r}},\tilde{t})}{\partial\tilde{t}} = \left(-\frac{1}{2}\Delta_{\tilde{\mathbf{r}}} - 3|\phi|^2 + \frac{5}{2}|\phi|^3\right)\phi(\tilde{\mathbf{r}},\tilde{t}). \tag{1.43}$$

Here we neglected the imaginary term in the LHY contribution, $(\delta a_+/a)^{5/2}$, by assuming $\delta a_+/a \ll 1$ and hence, $\delta a_-/a \simeq 2$.

The scalar wavefuction of the ground-state can be obtained by solving a generalized GPE using $\phi(\tilde{\mathbf{r}},\tilde{t}) = \phi_0(\tilde{\mathbf{r}})e^{-i\mu\tilde{t}}$ [46]

$$\mu\phi_0(\tilde{\mathbf{r}}) = \left(-\frac{1}{2}\Delta_{\tilde{\mathbf{r}}} - 3|\phi_0|^2 + \frac{5}{2}|\phi_0|^3\right)\phi_0(\tilde{\mathbf{r}}). \tag{1.44}$$

The chemical potential μ is fixed by the normalization condition: $\tilde{N} = \int d\tilde{\mathbf{r}}|\phi_0|^2$, where $\tilde{N}$ is related to the number of particles of the j-th component by $N_j = n_j^{(0)}\xi^3\tilde{N}$.

As depicted in figure 1.5, for large atom number the system exhibits a flat-top density profile and the size of the droplet increases with N. This is the regime of a uniform liquid (bulk). For small atom number, the droplet has a profile dominated by surface effects.

1.3.4 Variational method

An alternative way to derive the equilibrium properties of the droplet is to use a Gaussian ansatz for the wavefunction of the ground state. This approach has been recently used to evaluate the width, critical atom number, and the collective modes of a self-bound droplet in the presence of higher-order quantum corrections [62]. The key to the approximation consists of writing the density of the system as:

$$n(\tilde{r}) = \frac{\tilde{N}}{2\sqrt{2}\pi^{3/2}\sigma^3} e^{-\tilde{r}^2/(2\sigma^2)}, \tag{1.45}$$

where σ is the droplet width. Assuming that the associated wavefunction is $\phi(\mathbf{r}, t) = \sqrt{n(\mathbf{r}, t)}$ without considering phase terms which are not relevant in the study of the equilibrium properties of the system. Inserting the ansatz (1.45) into equation (1.40) and integrating over $\mathbf{r}$, one finds for the energy functional:

$$\tilde{E} = \int d\mathbf{r}\tilde{\mathcal{E}}(\phi, \phi^*) = \frac{3\tilde{N}}{4\sigma^2} - \frac{3\tilde{N}^2}{4\sqrt{2}\pi^{3/2}\sigma^3} + \frac{2}{5}\frac{\tilde{N}^{5/2}}{\pi^{9/4}\sigma^{9/2}}. \tag{1.46}$$

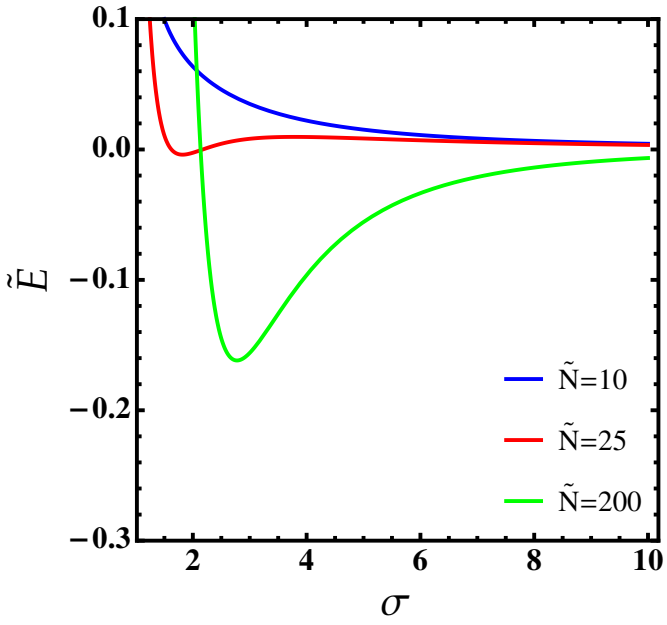

Figure 1.6: Total energy $\tilde{E}$ as a function of the width σ for different values of atom numbers, $\tilde{N}$.

Figure 1.6 shows that by decreasing the atom number, the minimum of $E(\sigma)$

corresponding to the self-bound droplet (green line) first becomes positive revealing that the system is in a metastable state (red line). Below a certain critical atom number, $N < N_{\rm cr}$, the minimum in energy disappears (blue line) signaling the occurrence of a liquid-to-gas phase transition (the self-bound state cannot exist). The critical number of particles is calculated by minimizing the total energy (1.46). This yields $N_{\rm cr} = 19.6204$.

1.4 One-dimensional quantum droplets in Bose-Bose mixtures

Studying 1D quantum systems is of great importance, since it provides valuable insights and serves as a foundation for understanding more complex systems. For instance 1D systems offer a level of simplicity that allows for more rigorous mathematical treatment and analytical solutions. The reduced dimensionality makes it easier to describe and analyze the behavior of quantum particles, enabling a deeper understanding of fundamental quantum principles. Another reason is that 1D quantum systems can be solved exactly, meaning their quantum states and properties can be determined precisely. This allows for a detailed examination of the underlying physics without resorting to approximations or numerical methods. In addition the interplay between quantum effects and the low dimensionality can give rise to emergent phenomena, such as quantum phase transitions, and the formation of exotic states of matter.

Since the experimental observation of the liquid-like state, 1D quantum droplet has become the subject of intense theoretical research. In 1D geometry, the LHY correction is attractive, in contrast to higher dimensions counterparts [61]. So, 1D quantum droplets occur due to the competition between attractive beyond mean-field LHY effects and repulsive mean-field term. An important feature is that in 1D configuration, the self-bound state can survive for any particle number and even

in a strongly-interacting regime. Moreover, the beyond mean-field can be boosted by decreasing the density without compromising the system's lifetime [61]. Based on the generalized GPE Astrakharchik *et. al.* have demonstrated that such an exotic state of matter exists in two different regimes, namely: Gaussian-like shape for relatively small number of particles and flat-top plateau in the case of a large number of atoms [124, 125]. A 1D quantum droplet can be realized by confining a dilute gas of ultracold bosonic atoms in an elongated, highly anisotropic trap (i.e. the trap must have a stronger confinement in the elongated direction compared to the transverse directions).

1.4.1 Energy and the equilibrium density

We consider again a symmetric homogeneous Bose mixture ($n_1 = n_2 = n$ and $g_1 = g_2 = g$) in a box of size L, where $g_j = -2\hbar^2/(ma_j)$. Despite the fact that a true BEC does not exist in 1D configuration, the Bogoliubov theory can correctly predict the energy of a weakly interacting Bose gas [128]. In the droplet regime where $\delta g_+ > 0$, the ground-state energy can be obtained from equations (1.20) and (1.21) by replacing the sum over k by an integral $\sum_{\mathbf{k}} \to V \int_0^\infty dk/(2\pi)$. This yields

$$\frac{E}{L} = \frac{\delta g_+}{4} n^2 - \frac{2\sqrt{m}}{3\pi\hbar} \sum_{\pm} \mu_\pm^{3/2}, \tag{1.47}$$

where $\delta g_+ = g + g_{12}$, and $\mu_\pm = n\delta g_\pm$. In figure 1.7 we show the results for the ground-state energy per particle from equation (1.47) valid in the limit $\delta g_+/g \to 0$. We observe that in the high density regime, the energy exhibits a minimum at a nonzero density, which is the hallmark of a liquid state. Whereas, in the limit of low density, the energy increases monotonically indicating the formation of a gas phase as is foreseen above. The same figure depicts also that the energy is decreasing with the interaction parameter, δg_+.

The equilibrium density of the droplet can be obtained by minimizing the ground-

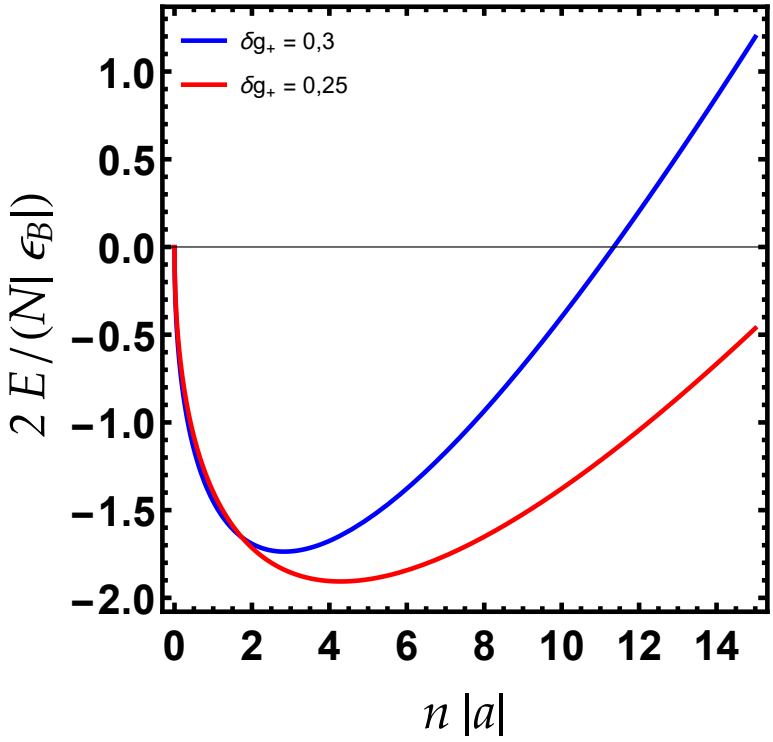

Figure 1.7: Energy per particle of a 1D droplet as a function of the density for two different value of δg_+.The energy is normalized by the binding energy of dimers composed from atoms from different components $\varepsilon_B = -\hbar^2/(ma_{12}^2)$.

state energy (1.47) with respect to the density. This gives [61]

$$n^{(0)} = \frac{8gm}{9\pi^2\hbar^2(\delta g_+/g)^2}, \tag{1.48}$$

and the corresponding chemical potential equals $\mu_0 = -\delta g_+ n_0/2$.

1.4.2 1D Generalized GPE

Following the same fashion as in 3D case, we derive the underlying 1D generalized GPE [46]

$$i\hbar\frac{\partial\Phi(x,t)}{\partial t} = \left(-\frac{\hbar^2}{2m}\frac{\partial^2}{\partial x^2} + \frac{\delta g_+}{2}|\Phi|^2 - \frac{\sqrt{m}}{\pi\hbar}g^{3/2}|\Phi|\right)\Phi(x,t), \tag{1.49}$$

where $\Phi(x,t)$ satisfies the condition $\int_{-\infty}^{+\infty}|\Phi(x,t)|^2dx = N$.

Let us introduce characteristic units of length $\tilde{x} = x/\xi$, time $\tilde{t} = t\hbar/(m\xi^2)$, energy

$\hbar^2/m\tilde{x} = \hbar/\tilde{t}$, where

$$\xi = \frac{\pi\hbar^2}{mg}\left(\frac{\delta g_+}{2g}\right)^{1/2}, \tag{1.50}$$

is the healing length. This yields for the wavefunction [124, 125]

$$\phi = \sqrt{\pi\xi}\left(\frac{\delta g_+}{2g}\right)^{3/4}\Phi, \tag{1.51}$$

and casts equation (1.49) in the following dimensionless form:

$$i\frac{\partial\phi(\tilde{x},\tilde{t})}{\partial\tilde{t}} = \left(-\frac{1}{2}\frac{\partial^2}{\partial\tilde{x}^2} + |\phi|^2 - |\phi|\right)\phi(\tilde{x},\tilde{t}), \tag{1.52}$$

with a new normalization condition $\int_{-\infty}^{+\infty}|\phi(\tilde{x},\tilde{t})|^2 d\tilde{x} = \tilde{N}$, where $\tilde{N}$ is the rescaled atom number. A peculiarity of the 1D geometry is that the generalized GPE (1.52)

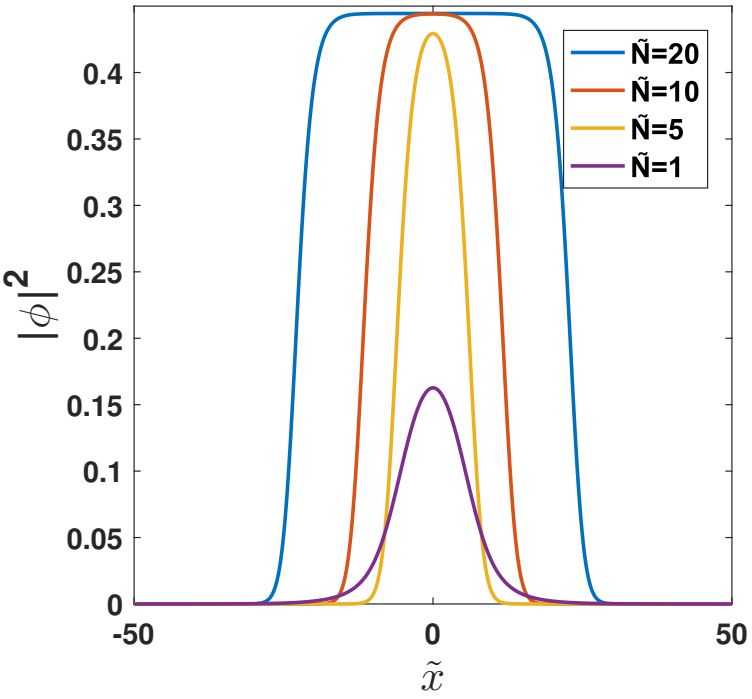

Figure 1.8: Density profiles of 1D droplets for different values of $\tilde{N}$

admits exact solution [61, 124]

$$\phi(\tilde{x},\tilde{t}) = -\frac{3\mu\exp\left(-i\mu\tilde{t}\right)}{1+\sqrt{1+(9\mu/3)}\cosh(\sqrt{-2\mu}\tilde{x})}, \tag{1.53}$$

where μ is the chemical potential.

The normalization condition gives a relation between the chemical potential and the atom number [124]

$$\tilde{N} = \frac{4}{3}\left[\ln\left(\frac{\sqrt{-9\mu/2}+1}{\sqrt{9\mu/2+1}} - \sqrt{-9\mu/2}\right)\right]. \tag{1.54}$$

We can distinguish mainly two different regimes of the self-bound droplet. (i) A flat-top (large) droplet corresponds to $\mu \to -2/9$ and large N [125] (see blue curve in figure (1.8)). (ii) A small droplet corresponds to a small N and μ. In such a limit, the mean-field cubic nonlinearity can be ignored, thus the droplet features an approximately Gaussian shape [124, 125] (see purple curve in figure (1.8)).

One should stress that in the case of negative δg_+ and large N, equation (1.52) becoming the integrable GPE with the cubic nonlinearity characterized by the bright soliton [125].

1.5 Finite-temperature effects

As a self-bound object, the energy of single-particle/collective excitations is bounded from above by the particle-emission threshold making the droplet automatically lose its thermal energy and hence reach zero temperature (self-evaporation) [46]. The experimental observation of this is still challenging. Indeed, the experimentally observed binary liquid mixtures might have a low but nonzero temperature in the realistic time-scale of experiments [47, 48, 49]. At such low temperatures, a fraction of unbound atoms (droplet depletion) appears as a halo surrounding the droplet due to the presence of thermal fluctuation effects [126, 127].

Let us first discuss the case of self-bound droplets in 3D Bose mixtures. The free

energy (1.26) can be then written in terms of density as:

$$\frac{F}{NE_0} = \frac{E}{NE_0} - \frac{\sqrt{\pi}}{720}(na^3)^{-5/2}\left(\frac{T}{E_0}\right)^4 \sum_{\pm}(\delta a_{\pm}/a)^{-3/2}, \tag{1.55}$$

where $E_0 = \hbar^2/ma^2$.

In figure 1.9. (a) we show the behavior of free energy (1.55) at different temperatures. We see that the local minimum disappears at the critical temperature $T_c/|E_0| \simeq 1.437 \times 10^{-4}$ at which the thermal fluctuations compensate the repulsive quantum fluctuations. At higher temperatures $TN/|E_0| > 1.5 \times 10^{-4}$, the self-bound droplet completely evaporates due to the strong thermal fluctuations. These latter can overcome the attractive forces, leading to the dissociation of the droplet above a certain critical (evaporation) temperature. Figure 1.9. (b) depicts that the critical temperature T_c is decreasing with $|a_{12}/a|$.

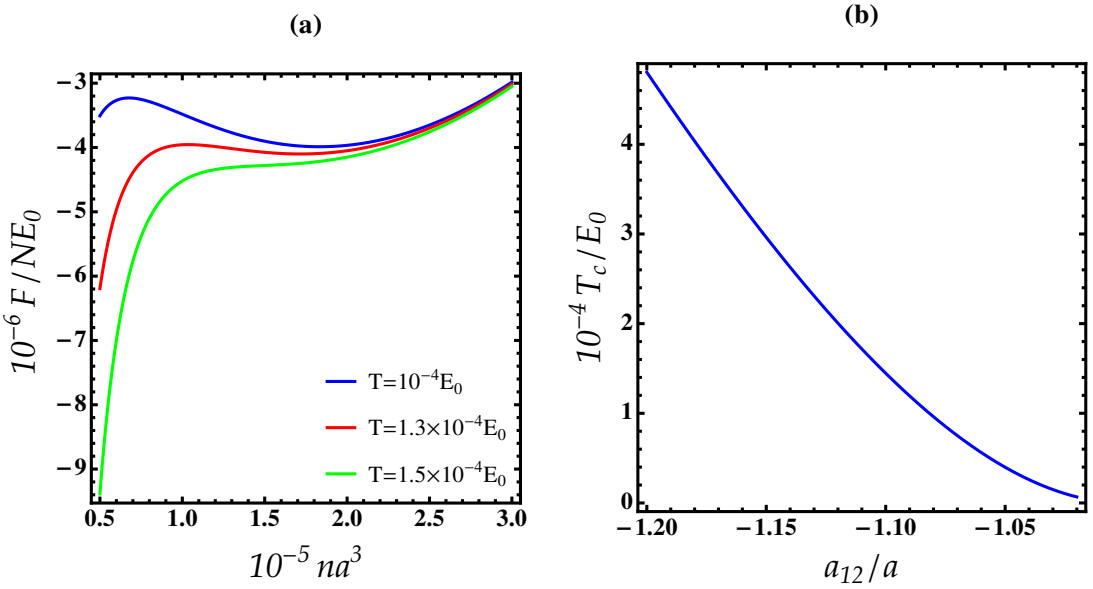

Figure 1.9: (a) Free energy of a 3D droplet as a function of the density calculated from equation (1.55) at different temperatures, and for $\delta a_+/a = 0.1$. (b) Critical temperature of a 3D droplet as a function of interspecies interactions a_{12}/a.

In a 1D liquid droplet, equation (1.26) gives for the free energy in terms of the

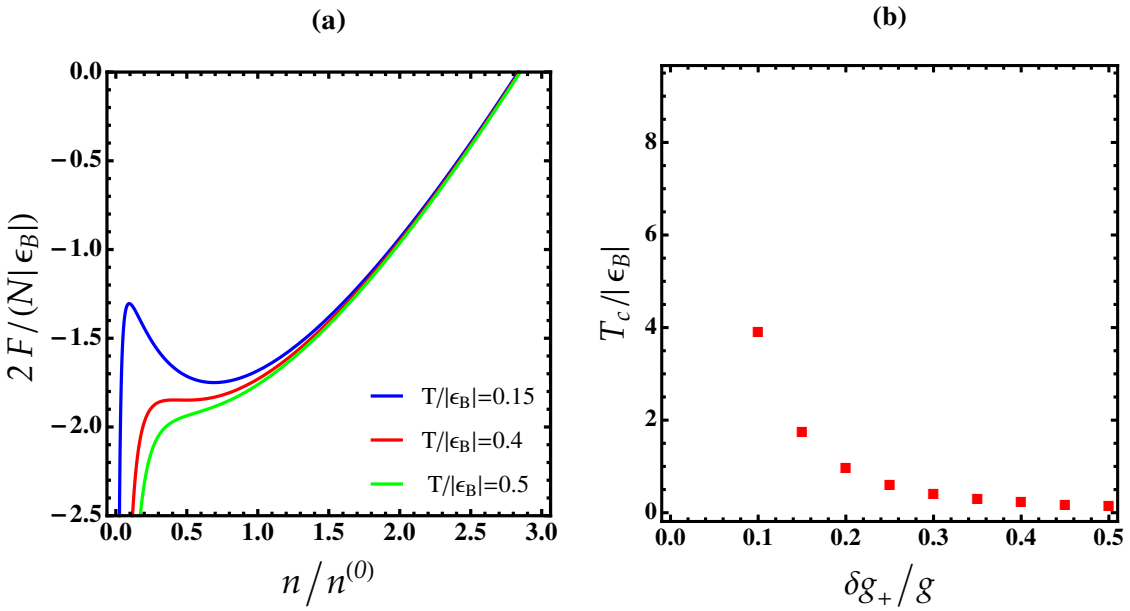

Figure 1.10: (a) Free energy of a 1D droplet as a function of the density calculated from equation (1.55) at different temperatures, and for $\delta g_+/g = 0.3$. (b) Critical temperature of a 1D droplet as a function of interspecies interactions $\delta g_+/g$.

equilibrium density (1.48):

$$\frac{2F}{N|\varepsilon_B|} = \frac{2E}{N|\varepsilon_B|} - \frac{\pi(g/g_{12})^2}{6}\left(\frac{32(n/n^{(0)})}{9\pi^2(\delta g_+/g)^2}\right)^{-3/2}\left(\frac{T}{|\varepsilon_B|}\right)^2\sum_{\pm}\left(\frac{\delta g_\pm}{g}\right)^{-1/2}. \quad (1.56)$$

In figure 1.10. (a) we present the 1D free energy (1.55) at different temperatures. At very low temperature, i.e., $T = 0.15\,|\varepsilon_B|$, the free energy exhibits a local minimum at the density $0.7n^{(0)}$, thus the droplet state satisfies the self-bound condition [69]. Increasing temperature ($T = 0.4\,|\varepsilon_B|$), the equilibrium density becomes smaller and the droplet starts to evaporate. At higher temperatures i.e. ($T = 0.5\,|\varepsilon_B|$), the free energy decreases monotonically as the density decays to zero. Hence, the self-bound liquid evaporates at a critical temperature $0.4|\varepsilon_B| \leq T_c < 0.5|\varepsilon_B|$.

Figure 1.10. (b) shows the critical temperature as a function of $\delta g_+/g$. We observe that T_c decreases with increasing $\delta g_+/g$ since the ground-state energy is proportional to $1/(\delta g_+/g)$ in contrast to the 3D case [68, 69, 42]. Large interspecies interaction may jeopardize the formation of a stable quantum liquid droplet [68].

Note that the experimental measurement of the predicted thermal effects of a

self-bound droplet is a complicated task due to the lack of efficient thermometry at low temperatures [129].

Chapter 2

Tools for ultracold atomic gases in disordered potentials

Disorder is an intrinsic property of all real systems. In the context of quantum physics, disorder refers to any form of randomness or irregularity in the properties of a physical system. Disorder can arise in a quantum mechanical system, from a variety of sources, including impurities, defects, thermal fluctuations, or external perturbations. Studying the effect of a disordered potential on a BEC is of significant importance in the field of quantum physics and condensed matter physics. Understanding the interplay between disorder and the underlying quantum mechanics is crucial for advancing our understanding of many-body quantum systems and for developing practical applications in areas such as quantum computing, quantum sensing, and materials science.

Disorder can give rise to a range of fascinating phenomena that are not present in ordered systems. One of the key phenomena associated with disorder in quantum systems is Anderson localization. This latter refers to the absence of diffusion in a disordered system, leading to the confinement of wavefunctions in localized regions. This effect was first predicted by Philip Anderson in 1958 [73] and has since been observed in various physical systems, including ultracold atomic gases (see for e.g.[81,

130]). The interplay between disorder and interactions may exhibit critical behavior and quantum phase transitions that differ from conventional ordered or disordered phases such as Bose glasses or Griffiths-McCoy phases [86].

This chapter is devoted to introduce the fundamental concepts and review the main features on disordered potentials, used to describe disordered ultracold atomic systems, thus serves as an introduction to the rest of this thesis. We review the statistical properties of random potentials, then introduce the different possibilities that can be followed to produce disordered potentials for ultracold neutral atoms. Finally we present the theoretical tools to be used when dealing with Bose gases in disordered potentials.

2.1 Statistical properties of random potentials

We call random potential or disordered potential the type of potential seen by the system studied, whose amplitude and/or spatial variations are random. In this section, we will define the statistical features associated with disorder. One important way to characterize the disorder is to know all the n-point correlation functions

$$R_n(\mathbf{r_1}, \mathbf{r_2}, \cdots, \mathbf{r_n}) = \langle U(\mathbf{r_1})U(\mathbf{r_2})\cdots U(\mathbf{r_n})\rangle\,, \tag{2.1}$$

where $\langle\cdots\rangle$ indicates statistical averaging over many disorder realizations. As a consequence each quantity examined must be averaged over a large number of realizations of the random potential when studying the influence of disorder.

Two statistical properties, defining the kind of disorder, which we will assume to be verified: homogeneity of space, and vanishing long-range correlations.

2.1.1 Homogeneity of space

The random potential is homogeneous, this implies that its statistical features are independent of the absolute position in the sample:

$$\langle U(\mathbf{r_1}+\mathbf{z})U(\mathbf{r_2}+\mathbf{z})\cdots U(\mathbf{r_n}+\mathbf{z})\rangle = \langle U(\mathbf{r_1})U(\mathbf{r_2})\cdots U(\mathbf{r_n})\rangle\,, \tag{2.2}$$

where $\mathbf{z}$ is a vector.

This assumption of homogeneity implies the symmetries :

$$R_2(\mathbf{r}) = R_2(-\mathbf{r}) \quad \text{and} \quad R_2(\mathbf{k}) = R_2(-\mathbf{k}), \tag{2.3}$$

where $R_2(\mathbf{r}) = R(\mathbf{r})$ is the two-point auto-correlation function, and its Fourier transform $R(\mathbf{k}) = \int d^d r R(\mathbf{r}) e^{-i\mathbf{k}.\mathbf{r}}$.

Another consequence of space homogeneity, is that the single-point properties which are determined by the probability distribution $P(U)$, do not depend on position. Therefore, we can assume a vanishing statistical average, $\langle U\rangle = 0$, thus the standard deviation reads $U_R^2 = \langle U^2\rangle$. The two-point correlation function, or auto-correlation function, depends only on one relative coordinate $R = \langle U(\mathbf{r}')U(\mathbf{r}+\mathbf{r}')\rangle$.

2.1.2 Vanishing long-range correlations

The second assumption on the random potential is the disappearance of statistical correlations between values of the potential at points with infinitely large separation [131].

$$\langle U(\mathbf{r_1})\cdots U(\mathbf{r_n})U(\mathbf{r_{n+1}}+\mathbf{z})U(\mathbf{r_m}+\mathbf{z})\rangle \longrightarrow_{|\mathbf{z}|\to\infty} \langle U(\mathbf{r_1})U(\mathbf{r_n})\rangle \langle U(\mathbf{r_{n+1}})\cdots U(\mathbf{r_m})\rangle\,. \tag{2.4}$$

In particular, the two-point correlator, R, drops to zero at infinity, as a result of the assumption $\langle U(\mathbf{r})\rangle = 0$, on a typical length-scale called the correlation length,

σ. The correlation length is the minimal length scale characterizing the spatial variations of the potential, it can be used to define a dimensionless autocorrelation function $c_2(\mathbf{r})$ by [132]

$$R(\mathbf{r}) = U_R^2 c_2(\mathbf{r}/\sigma), \tag{2.5}$$

and in Fourier space with d-dimension

$$R(\mathbf{k}) = U_R^2 \sigma^d c_2(\mathbf{k}\sigma_R). \tag{2.6}$$

2.2 How to produce a disordered potential

Unlike condensed matter physics, cold atom physics allows for the employment of completely described and controlled disordered potentials. Furthermore, the characteristics of the disorder that we impose on the system can be varied in a very wide range. Disorder may be introduced in ultracold systems in several ways. Speckle potentials, quasiperiodic lattices, and impurity disorder, are among the most commonly implemented models of disorder. In this section, we briefly review their main features.

2.2.1 Speckle potentials

Optical speckle patterns can be generated by a transmission of a laser light through a material surface with a roughness on the scale of an optical wavelength [133]. The laser speckle is the figure formed by a coherent beam after traveling through a random medium (rough diffusive plate), which is then focused by a convergent lens (as illustrated in figure 2.1), such that the intensity distribution in the far field corresponds to the interference of a large number of random phase sources. At any spatial position x, the randomly phased partial waves originating from different scattering sites of the rough surface total up, resulting in constructive or destructive interferences [133].

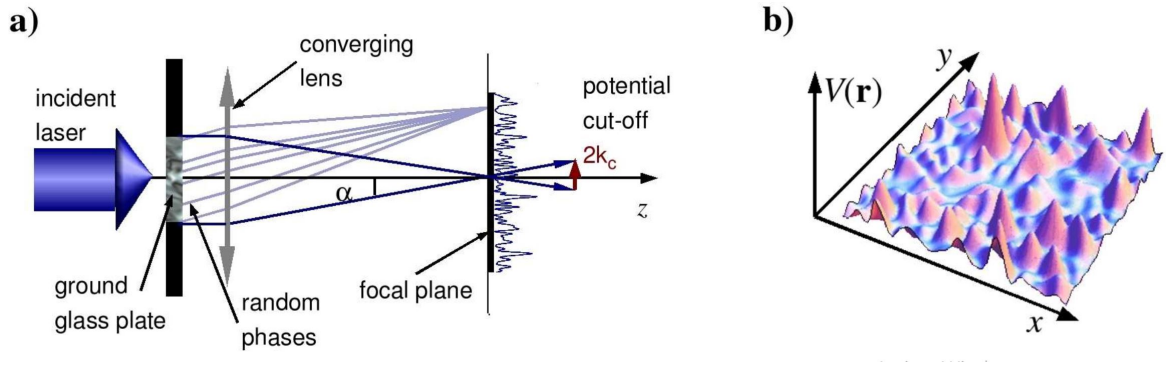

Figure 2.1: Optical speckle potentials. a) Optical configuration. b) Two-dimensional representation of a speckle potential. Figure extracted from [134]

Speckle patterns are an excellent approach to generate disordered potential in a controlled way. The fact that the intensity of the speckle pattern may be immediately recorded by a CCD camera allows for exact measurement of the statistical and correlation features of the disordered potential [135]. The speckle phenomenon is not limited to optical fields but is also used in several other applications such as in radar [136], ultrasound medical imagery [137], and spectral analysis of random processes [138].

Speckle potentials offer benefits from both practical and fundamental perspectives. Firstly, they can be readily created using basic optical components, and their statistical characteristics are thoroughly understood [131, 132]. Secondly, speckle potentials are characterized by correlated random patterns, and the correlation functions can be tailored by adjusting the optical setup's geometry used in their generation. Speckle potentials are also an example of non-Gaussian potentials, appropriate for analytical computations [132].

2.2.2 Multichromatic lattices

The autocorrelation length is a significant indicator of speckle potentials because it estimates the minimal length scale beyond which the potential loses its random nature and becomes correlated. The random potential produced by speckles is often with correlation length, σ, of the order of several microns, what makes the

random potential too coarse-grained [135]. However, It is simple to generate optical standing waves with spatial periodicities that can also be smaller than half a micron. This implies that by integrating many optical standing waves with distinct non-commensurate spacings, it is possible to create a disordered potential with very small correlation length.

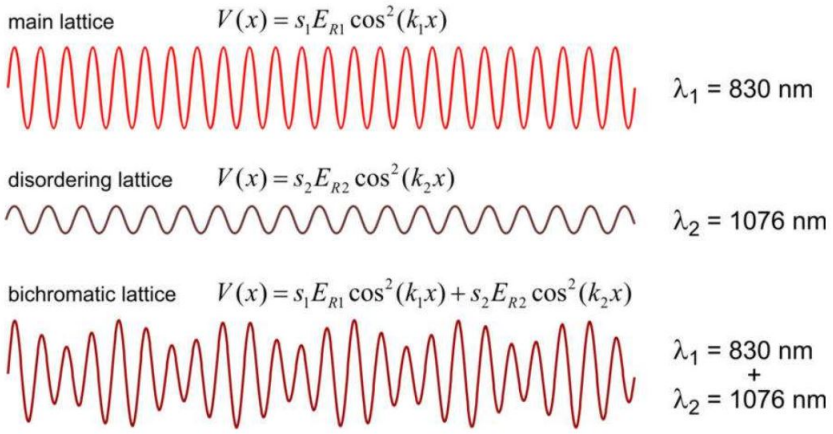

Figure 2.2: A bichromatic optical lattice, the main lattice is perturbed by the addition of a secondary lattice with different wave length. Figure extracted from [135]

To create a multichromatic lattice, multiple laser beams with different frequencies (colors) are employed. Each laser beam generates a distinct optical lattice potential, resulting in a superposition of different-colored lattices. The specific arrangement and periodicity of these lattices depend on the laser beam parameters and on the interference between them. As an example a bichromatic lattice is formed by combining two incommensurate wavelength lattices (see figure 2.2). Actually, this kind of disorder are not exactly disordered potentials, they differ from purely random potentials in their statistical and correlation properties. They are quasiperiodic potentials.

2.2.3 Impurity disorder

An alternative suggestion to generate disordered potentials, which does not entail the dipolar force, is the impurity disorder. It refers to the presence of foreign atoms

or particles within an otherwise homogeneous atomic system. Impurity disorder is introduced by intentionally adding a small number of atoms or particles of a different species into the atomic system, creating a localized region of distinct properties within the overall atomic cloud, often referred to as a disorder potential. This potential can arise due to the difference in the energy levels, scattering lengths, or masses of the impurity and host atoms. The main species experiences the impurity potential created by the second species

$$U(\mathbf{r}) = \sum_i f(\mathbf{r} - \mathbf{r}_i), \tag{2.7}$$

where $\mathbf{r}_i$ denote the random positions of the impurities, and f is the single impurity potential. Quite often, the single-impurity potential is assumed to be proportional to a Dirac distribution, in which case the disorder is uncorrelated [139].

2.3 Common disorder correlations

In the context of disorder in BECs or other systems, two common types of disorder correlations are uncorrelated disorder and correlated disorder, characterized by different correlation functions.

2.3.1 Uncorrelated disorder

Uncorrelated disorder (or white noise disorder) is a potential where there is no spatial coherence. In other words, there is no correlation between the disorder values at different positions. Mathematically, the autocorrelation function is delta-correlated [132, 140, 141]

$$R(\mathbf{r}) = R_0\delta(\mathbf{r}), \tag{2.8}$$

where δ is the d-dimensional Dirac function, and R_0 characterizes the strength of the potential which has the dimension of $(\text{energy})^2(\text{length})^d$. White noise disorder

is largely used in cold atom experiments because of its simplicity and universality, uncorrelated disorder makes it easier to compare experimental results with theoretical models. Theoretical calculations and simulations often assume uncorrelated disorder to simplify the analysis and make predictions about the behavior of the system.

2.3.2 Gaussian correlation

Correlated disorder involves disorder potentials with a nonzero correlation between disorder values at different positions. The correlation function describes the degree of correlation or spatial dependence between disorder values, in the case of Gaussian autocorrelation, it follows a Gaussian distribution. The correlation function reads [100, 142]

$$R(\mathbf{r}) = R_0 e^{-\mathbf{r}^2/\sigma^2}, \tag{2.9}$$

which can be witten in Fourier space as:

$$R(\mathbf{k}) = R_0 e^{-\sigma^2\mathbf{k}^2/2}. \tag{2.10}$$

For disorder with a Gaussian autocorrelation function, the spatial correlation length σ is an extremely important parameter. It controls how quickly the correlation between disorder quantities decays as the distance between locations grows larger. A shorter correlation length suggests that disorder values are more closely correlated at adjacent locations, whereas a longer correlation length shows weaker correlation over greater distances. The Gaussian autocorrelation function provides a well-defined and mathematically tractable foundation for theoretical computations and simulations.

2.3.3 Speckel with uniform apertures

Speckle patterns with uniform apertures refer to a specific type of disorder potential used in cold atom experiments. These patterns are created by introducing uniform

apertures into the optical setup used to generate speckle patterns, it provides a flexible and controllable approach for generating disorder potentials in cold atom experiments. Considering the case of isotropic apertures, the correlation function reads [132]

$$R(\mathbf{r}) = U_R^2 \mathrm{sinc}^2(\mathbf{r}/\sigma), \tag{2.11}$$

The corresponding Fourier transform in the 3D case, has the form

$$R(\mathbf{k}) = U_R \sigma^3 \frac{\pi^2}{\mathbf{k}\sigma} \Theta(2 - \mathbf{k}\sigma), \tag{2.12}$$

where Θ is the Heaviside step function.

In a 1D configuration, it reads:

$$R(k) = U_R^2 \sigma \pi \left(1 - \frac{k\sigma}{2}\right) \Theta\left(1 - \frac{k\sigma}{2}\right). \tag{2.13}$$

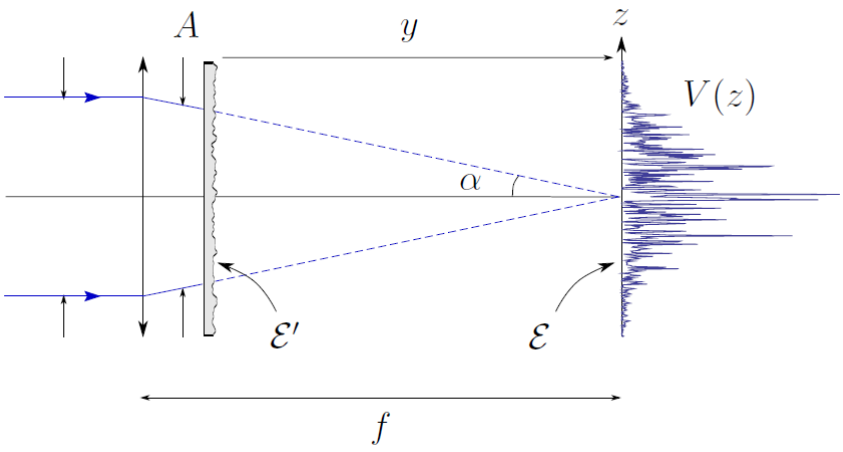

Figure 2.3: Typical set-up for an experiment with speckle potentials. The correlation functions of the speckle field ε can be designed by choosing the shape and size of the aperture A and the intensity profile of the free laser beam [143].

Optical potentials have demonstrated their effectiveness in the confinement and control of ultracold atoms. When exposed to laser light that is nearly resonant with a transition from the ground state to an excited state. The precise level of manipulation provided by optical dipole potentials has been harnessed to confine

ultracold atoms within low-dimensional structures and to generate lattice potentials for these atoms.

The disordered distribution of light can be imaged onto the atoms, producing a disordered potential $V(\mathbf{r})$ proportional to the local laser intensity $I(\mathbf{r})$ [135]. Typically, when the light's wavelength significantly deviates from the atomic resonance, there is no absorption of the light, and the resulting mechanical impact can be characterized using a potential energy represented by the following equation:

$$V(\mathbf{r}) = \frac{3\pi c^2}{2\omega_0^3}\left(\frac{\Gamma}{\Delta}\right) I(\mathbf{r}), \tag{2.14}$$

where c is the speed of light, ω_0 is the frequency of the atomic resonance, Γ its radiative linewidth, $\Delta = \omega - \omega_0$ the detuning, and $I(\mathbf{r})$ the intensity distribution. The sign of this potential depends on Δ. For $\Delta < 0$ (red detuning), $V(\mathbf{r})$ is negative, hence maxima of light intensity correspond to potential minima: atoms will move towards higher-intensity regions. Instead, when $\Delta > 0$ (blue detuning), $V(\mathbf{r})$ is positive, hence maxima of light intensity correspond to potential maxima: atoms will move towards lower-intensity regions.

The correlation functions can be directly controlled in the experiments by changing the aperture of the optical system. A typical experimental setup is sketched in figure 2.3. A lens is introduced in front of the diffusive plate to focus the laser power onto the atoms. However, it is important to note that the wavefront curvature introduced by the lens does not alter the correlation characteristics of the speckle pattern in the back focal plane. On the contrary, the aperture A plays a different role by restricting the area of the diffuser that receives illumination, and its specific design is employed to manipulate the correlation functions [143].

2.4 Bose-Einstein condensates in disordered potentials

Weakly interacting BECs in a disorder environment have long been a challenging topic in the field of condensed matter physics due to the intriguing interplay between superfluidity and localization. In this section we discuss the possibility of Bose-Glass and Anderson localization transition in a BEC in a disordered medium.

2.4.1 Localization

In contrast to condensed-matter systems, ultracold atomic gases can be realized in the presence of controlled disorder, opening possibilities for investigations of localization effects[89, 90, 91, 92]. The remarkable benefit provided by atomic systems lies in the extraordinary opportunity to manipulate perfectly isolated samples at nearly absolute zero temperature, with experimental control over a wide range of Hamiltonian parameters, such as the lattice depth or the strength of atom-atom interactions, which can be finely adjusted, even in real-time [135].

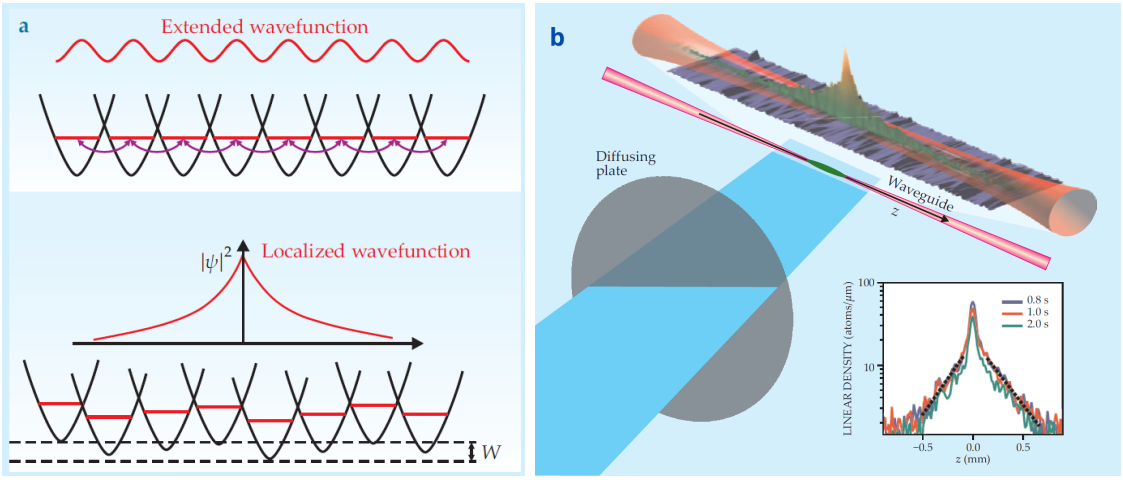

Figure 2.4: (a) Difference between extended and localized wavefunctions. (b) Andesrson localisation of ultra cold atoms in a 1D speckle disorder. When a small BEC initially confined along z-axis, is released in the disordered potential, its expanssion stops after about 5s,after which astationary density profile whith exponentially decaying wings emerges, taken from[144].

Among the most intriguing phenomena observed in the wave propagation within disordered systems is Anderson localization. This phenomenon is named after P.

W. Anderson, who, in 1958, elucidated the pivotal significance of disorder in the transition from metal to insulator that is observed in solid-state systems [73]. In the subsequent years, it became evident that Anderson localization is a significantly broader phenomenon, applying to the propagation of various types of linear waves in disordered mediums.

In the presence of disorder, the wavefunction which characterizes a BEC can be Anderson localized. This wavefunction (more precisely, the squared modulus of it) can be directly observed by imaging the condensate with a CCD camera [135]. The occurrence of Anderson localization is significantly influenced by the dimension of the system. Disorder exerts its most pronounced impact in 1D, where particles are scattered either forward or backward, leading to individual particles becoming exponentially localized over a specific length scale. As we see in figure 2.4, by releasing a BEC in 1D speckle disorder, the evolution of the atomic wavefunction shows an impressive behavior. After an initial expansion, the atomic wave packet stops expanding and its wings decay exponentially [144].

2.4.2 Phase transitions

A highly intriguing and as-yet unresolved issue concerns the influence of interactions on localization. Initially, Anderson developed his theory for non-interacting quantum particles. Yet, when one takes into account genuinely interacting particles, the situation may differ considerably. The interplay between disorder and interactions in the physics of localization has been the subject of extensive theoretical exploration. It quickly became apparent that repulsive interactions have the potential to counteract disorder and ultimately disrupt localization. Nevertheless, in systems with strong interactions, distinct regimes can emerge, leading to the attainment of new quantum phases where interactions and disorder work together to localize the system in glassy states.

A logical initial step in understanding the behavior of the BEC within a disor-

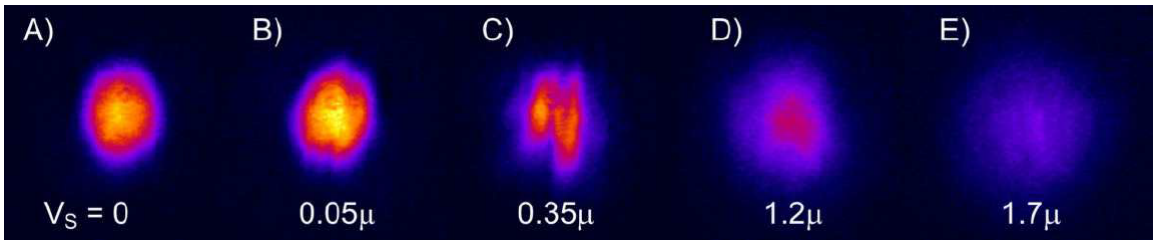

Figure 2.5: Density profile of the BEC after 28 ms of expansion from the combined magnetic and speckle potential for varying speckle potential intensities V_S[80].

dered potential is to examine the configuration of the atomic density distribution once it has been released from the confining potential. We can consider the case of disordered potentials created with optical speckles, first investigated with ^{87}Rb in [80]. In figure 2.5 one can observe three different regimes, depending on the ratio between the speckle potential intensity V_S and the BEC chemical potential μ. For very small optical potentials $V_S = 0.1\mu$ one does not observe any significant deviation from the ordinary Thomas-Fermi shape of the BEC expanding from the harmonic trap (figure 2.5. B). For higher speckle heights $0.1\mu \leq V_S \leq \mu$ one observes that the density distribution is strongly modified by the appearance of complex structures in the form of elongated stripes (figure 2.5.C). By increasing the speckle height to $V_S \geq \mu$, the expanded density profile ceases to be characterized by stripes (figure 2.5 E) [135]. In this case, the BEC is localized in the wells of the high random potential.

In [145] a Lifshitz glass phase has been introduced to describe the system's ground-state when interactions are weak. Lifshitz states, a specific category of localized states, demonstrate "weaker" localization characteristics compared to Anderson-localized states. This means that they exhibit exponential decay primarily in their distant tails, while their shape near the peak is significantly influenced by the local properties of the potential. In figure 2.6 we can see the phase diagram of the interacting disordered BEC derived in [145] as a function of the BEC chemical potential and of the speckle height. Starting with the Lifshitz glass phase and escalating the level of interactions, a phase characterized by fragmented interacting BECs has been suggested. This phase serves as a precursor to the Bose glass phase.

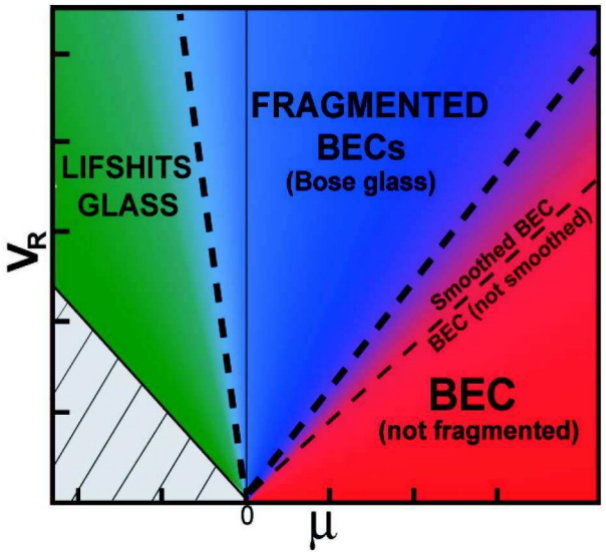

Figure 2.6: Schematic quantum-state diagram of an interacting ultracold Bose gas in 1D disorder. The dashed lines represent the boundaries. V_R is the amplitude of the random potential. [145].

2.5 Theoretical tools

The interplay between interaction and disorder in a BEC is an interesting and complex topic that develops when both atom interactions and disorder potentials are present in the system. This interaction produces a wide range of physical phenomena and has the potential to profoundly impact the behavior and features of the condensate. In the last decade there was an extended theoretical and experimental efforts in understanding the influence of disorder on samples of cold atoms (see e.g.[91, 74, 76, 77, 140]). In this section we introduce the key theoretical models by which we might describe weakly interacting Bose gases in weak random potentials.

2.5.1 Bogoliubov-Huang-Meng theory

In order to study the properties of interacting bosons in a random potential, Huang and Meng proposed a Bogoliubov theory, which was applied to the case of superfluid helium in porous media [140]. Huang and Meng calculated the condensate density n_c in terms of the particle density n of a Bose gas with contact interaction at low temperatures in a random potential within a Bogoliubov theory and found

perturbatively two different depletions of the condensate density which are : the known depletion due to the particle interaction, and a depletion induced by the disorder potential. Here we present the main concepts of HM theory for a weakly-interacting disordered Bose gas.

We consider a 3D ultracold Bose gas in a weak random potential. The Hamiltonian of the system can be expressed as:

$$\hat{H} = \int d\mathbf{r}\hat{\psi}^{\dagger}(\mathbf{r}) \left[\frac{-\hbar^2\nabla^2}{2m} + U(\mathbf{r})\right] \hat{\psi}(\mathbf{r}) + \frac{g}{2}\int d\mathbf{r}\hat{\psi}^{\dagger}(\mathbf{r})\hat{\psi}^{\dagger}(\mathbf{r})\,\hat{\psi}(\mathbf{r})\,\hat{\psi}(\mathbf{r}), \qquad (2.15)$$

where $\hat{\psi}^{\dagger}(\mathbf{r})$ and $\hat{\psi}(\mathbf{r})$ are creation and annihilation field operators, obeying the usual bosonic commutation relations, $g = 4\pi\hbar^2 a/m$ is coupling constant, with a being the s-wave scattering length, and $U(\mathbf{r})$ represents the random potential. We assume that the average over the random potential vanishes $\langle U(\mathbf{r})\rangle = 0$ and that it has some kind of correlation $\langle U(\mathbf{r})U(\mathbf{r}')\rangle = R(\mathbf{r}-\mathbf{r}')$[99, 146].

With the help of a Fourier transformation (1.9) we can rewrite the Hamiltonian (2.15) in momentum space according to

$$\hat{H} = \sum_{\mathbf{k}} \left(\frac{\hbar^2\mathbf{k}^2}{2m}\right) \hat{a}^{\dagger}_{\mathbf{k}}\hat{a}_{\mathbf{k}} + \frac{1}{V}\sum_{\mathbf{p},\mathbf{k}} U_{\mathbf{p}-\mathbf{k}}\hat{a}^{\dagger}_{\mathbf{p}}\hat{a}_{\mathbf{k}} + \frac{g}{2V}\sum_{\mathbf{p},\mathbf{k},\mathbf{q}} \hat{a}^{\dagger}_{\mathbf{k}+\mathbf{q}}\hat{a}^{\dagger}_{\mathbf{p}-\mathbf{q}}\hat{a}_{\mathbf{p}}\hat{a}_{\mathbf{k}}, \qquad (2.16)$$

where $E_{\mathbf{k}} = \hbar^2\mathbf{k}^2/(2m)$. At very low temperature the number of the particles in the ground-state N_c becomes macroscopically large. In this case we can use the Bogoliubov prescription described in the previous chapter which stipulates that $\hat{a}_0 = \hat{a}_0^{\dagger} = \sqrt{N_c}$. As a consequence, the respective momentum summations in the Hamiltonian (2.16) is decomposed into their ground state $\mathbf{k} = 0$ and excited states $\mathbf{k} \neq 0$. Assuming a weakly interacting system, we can then ignore terms which contain creation and annihilation operators of the excited states, which are of third and fourth order. On the other hand, for weak enough disorder we can neglect terms $U_{\mathbf{p}-\mathbf{k}}\hat{a}^{\dagger}_{\mathbf{p}}\hat{a}_{\mathbf{k}}$ with both $\mathbf{k} \neq 0$ and $\mathbf{p} \neq 0$ [99].

In order to diagonalize the Hamiltonian (2.16), Huang and Meng [140] introduces

the following Bogoliubov transformation [119]

$$\begin{aligned} \hat{a}_{\mathbf{k}} &= u_{\mathbf{k}}\hat{b}_{\mathbf{k}} - v_{\mathbf{k}}\hat{b}^{\dagger}_{-\mathbf{k}} - \beta_{\mathbf{k}}, \\ \hat{a}^{\dagger}_{\mathbf{k}} &= u_{\mathbf{k}}\hat{b}^{\dagger}_{\mathbf{k}} - v_{\mathbf{k}}\hat{b}_{-\mathbf{k}} - \beta^{*}_{\mathbf{k}}, \end{aligned} \tag{2.17}$$

where $\hat{b}_{\mathbf{k}}$ and $\hat{b}^{\dagger}_{\mathbf{k}}$ are operators of elementary excitations which obey the usual Bose commutation relations (1.14), the functions $u_{\mathbf{k}}$,$v_{\mathbf{k}}$ are defined as

$$u_{\mathbf{k}}, v_{\mathbf{k}} = \frac{1}{2}\left(\sqrt{\frac{\varepsilon_{\mathbf{k}}}{E_{\mathbf{k}}}} \pm \sqrt{\frac{E_{\mathbf{k}}}{\varepsilon_{\mathbf{k}}}}\right), \tag{2.18}$$

and the disorder translation β_k is defined as:

$$\beta_{\mathbf{k}} = \sqrt{\frac{n_c}{V}}\frac{E_{\mathbf{k}}}{\varepsilon^2_{\mathbf{k}}}U_{\mathbf{k}}. \tag{2.19}$$

The Bogoliubov excitations energy is given by [100, 146]

$$\varepsilon_{\mathbf{k}} = \sqrt{E^2_{\mathbf{k}} + 2gn_cE_{\mathbf{k}}}. \tag{2.20}$$

The diagonal form of the Hamiltonian (2.16) can be obtained using (2.18) and averaging over the disorder. This yields

$$\hat{H} = E + \sum_{\mathbf{k}\neq 0}\varepsilon_{\mathbf{k}}\hat{b}^{\dagger}_{\mathbf{k}}\hat{b}_{\mathbf{k}}, \tag{2.21}$$

where E stands for the ground-state energy defined as:

$$\frac{E}{V} = \frac{g}{2}n^2 + \frac{1}{2V}\sum_{\mathbf{k}}\left[\varepsilon_{\mathbf{k}} - E_{\mathbf{k}} - n_cg\right] + E_R, \tag{2.22}$$

and

$$E_R = -\sum_{\mathbf{k}} n_c\left\langle|U_{\mathbf{k}}|^2\right\rangle\frac{E_{\mathbf{k}}}{\varepsilon^2_{\mathbf{k}}} = -\sum_{\mathbf{k}} n_cR_{\mathbf{k}}\frac{E_{\mathbf{k}}}{\varepsilon^2_{\mathbf{k}}}. \tag{2.23}$$

is the disorder contribution to the ground-state energy.

The noncondensed density can be calculated through equations (1.28) and (2.17)

$$\tilde{n} = \frac{1}{V}\sum_{\mathbf{k}} \left[v_{\mathbf{k}}^2 + (v_{\mathbf{k}}^2 + u_{\mathbf{k}}^2)N_{\mathbf{k}} + \langle|\beta_{\mathbf{k}}|^2\rangle\right]. \tag{2.24}$$

The anomalous density can be computed using equations (1.29) and (2.17)

$$\tilde{m} = -\frac{1}{V}\sum_{\mathbf{k}} \left[v_{\mathbf{k}}u_{\mathbf{k}}(1 + 2N_k) + \langle|\beta_{\mathbf{k}}|^2\rangle\right]. \tag{2.25}$$

The leading term in equations (2.24) and (2.25) represents the quantum contribution to the noncondensed and anomalous densities, the subleading term accounts for thermal contribution, and the last terme, $n_R = \frac{1}{V}\sum_{\mathbf{k}}\langle|\beta_{\mathbf{k}}|^2\rangle$, is the disorder fluctuations known as *glassy fraction*. It originates from the accumulation of density near the potential minima and density depletion around the maxima [100, 146].

To be concrete, we apply the above HM results to a delta-correlated random potential (2.8), its Fourier transform is given by $R(\mathbf{k}) = R$.

$$n_R = \int \frac{d^3k}{(2\pi)^3}\frac{E_k^2}{\varepsilon_k^4}R(\mathbf{k}) = \frac{m^2R}{8\pi^{3/2}\hbar^4}\sqrt{\frac{n}{a}}. \tag{2.26}$$

We see that the density of BEC in a weak disorder potential is depleted due to localization effects [140], this was found first by Huang and Meng in 1992. For BEC at zero temperature, a large number of atoms occupy the lowest energy state, forming a coherent matter wave. This condensate state is characterized by a macroscopic occupation of a single quantum state. However, interactions between atoms or with the surrounding environment can cause scattering events that transfer atoms from the condensate state to other states. When disorder is introduced, it breaks the coherence and induces the formation of localized regions or domains within the condensate. These localized regions are characterized by different local densities and phases. As a result the condensate depletion consists of two contributions, one due to the quantum fluctuations (1.28) and another one due to the disorder potential, this

latter depletion is called **glassy fraction**. It is obvious from equation (2.26) that when a vanishes, n_R becomes infinite ($n_R \propto \sqrt{1/a}$). This means that the system would collapse, and eventually destabilizes, if there were no repulsive interactions between atoms.

2.5.2 Perturbative approach

The perturbative approach is most suitable when the disorder in the BEC is relatively weak, meaning that the energy scale associated with disorder is much smaller than the energy scale associated with particle interactions. This condition allows for the use of perturbation theory. It is a valuable tool for studying disordered BECs. It helps us to understand how disorder affects the properties and behavior of BECs. The perturbative theory for disordered BECs has been used in many theoretical works (see e.g. [74, 76, 77, 75, 78, 79]).

Let us consider weakly interacting Bose gases at zero temperature in a weak random potential $U(\mathbf{r})$, the system is described by the static GPE

$$\mu\Phi(\mathbf{r}) = \left[-\frac{\hbar^2}{2m}\nabla^2 + U(\mathbf{r}) + g|\Phi(\mathbf{r})|^2+\right]\Phi(\mathbf{r}). \tag{2.27}$$

If the disorder is sufficiently weak, it is possible then to solve the GPE (2.27) perturbatively in powers of U using the expansion [74, 76, 77, 75, 78, 79]

$$\Phi(\mathbf{r}) = \Phi^{(0)} + \Phi^{(1)}(\mathbf{r}) + \Phi^{(2)}(\mathbf{r}) + \cdots, \tag{2.28}$$

where the index i in the real valued functions $\Phi^{(i)}(\mathbf{r})$ signals the i-th order contribution with respect to the disorder potential.

Inserting the ansatz (2.28) into equation (2.27), we get up to first-order in U

$$\begin{aligned}&\left(g\Phi^{(0)2}-\mu\right)\Phi^{(0)}+\left[\hat{h}\Phi^{(1)}(\mathbf{r})+U(\mathbf{r})\Phi^{(0)}\right] \\ &+\left[\hat{h}\Phi^{(2)}(\mathbf{r})+U(\mathbf{r})\Phi^{(1)}(\mathbf{r})+3g\Phi^{(0)}\Phi^{(1)2}(\mathbf{r})\right]+\cdots=0,\end{aligned} \tag{2.29}$$

with the operator $\hat{h}=-(\hbar^2/2m)\nabla^2-\mu+3g(\Phi^{(0)})^2$.

Equating the coefficients leads to one equation for each order.

Zeroth-order calculation gives

$$\Phi^{(0)}=\sqrt{\frac{\mu}{g}}. \tag{2.30}$$

First-order term, $\Phi^{(1)}(\mathbf{r})$, can be obtained by solving

$$\hat{h}\Phi^{(1)}(\mathbf{r})=-U(\mathbf{r})\Phi^{(0)}. \tag{2.31}$$

Performing a Fourier transformation leads to an algebraic equation which is solved by

$$\Phi^{(1)}(\mathbf{k})=\frac{-U(\mathbf{k})\Phi^{(0)}}{E_{\mathbf{k}}-\mu+3g\Phi^{(0)2}}. \tag{2.32}$$

Following the same fashion, second-order term, $\Phi^{(2)}(\mathbf{r})$, is determined by solving

$$\hat{h}\Phi^{(2)}(\mathbf{r})=-\Phi^{(1)}(\mathbf{r})[U(\mathbf{r})+3g\Phi^{(0)}\Phi^{(1)}(\mathbf{r})]. \tag{2.33}$$

Using the Fourier transformation of a product of two functions

$$\int d^3r\Phi^{(1)}(\mathbf{r})U(\mathbf{r})e^{-i\mathbf{kr}}=\int\frac{d^3k'}{(2\pi)^3}\Phi^{(1)}\left(\mathbf{k}-\mathbf{k}'\right)U\left(\mathbf{k}'\right), \tag{2.34}$$

we obtain

$$\Phi^{(2)}(\mathbf{k})=-\frac{\int\frac{d^3k'}{(2\pi)^3}\Phi^{(1)}\left(\mathbf{k}-\mathbf{k}'\right)\left[U\left(\mathbf{k}'\right)+3g\Phi^{(0)}\Phi^{(1)}\left(\mathbf{k}'\right)\right]}{E_{\mathbf{k}}-\mu+3g\Phi^{(0)2}}. \tag{2.35}$$

Now we calculate the depletion induced by disorder (glassy fraction) is given by

$$n_R = n - n_c, \tag{2.36}$$

where

$$n_c = \langle \Phi(\mathbf{r}) \rangle^2 = \Phi^{(0)2} + 2\Phi^{(0)} \langle \Phi^{(1)}(\mathbf{r}) \rangle + 2\Phi^{(0)} \langle \Phi^{(2)}(\mathbf{r}) \rangle + \langle \Phi^{(1)}(\mathbf{r}) \rangle^2 + \cdots , \tag{2.37}$$

is the condensed density, and

$$n = \langle \Phi(\mathbf{r})^2 \rangle = \Phi^{(0)2} + 2\Phi^{(0)} \langle \Phi^{(1)}(\mathbf{r}) \rangle + 2\Phi^{(0)} \langle \Phi^{(2)}(\mathbf{r}) \rangle + \langle \Phi^{(1)2}(\mathbf{r}) \rangle + \cdots \tag{2.38}$$

is the total density.

The property $\langle U(\mathbf{r}) \rangle = 0$ implies that $\langle \Phi^{(1)}(\mathbf{r}) \rangle = 0$, then equations (2.37) and (2.38) reduce to

$$n_c = \Phi^{(0)2} + 2\Phi^{(0)} \langle \Phi^{(2)}(\mathbf{r}) \rangle + \cdots , \tag{2.39}$$

and

$$n = \Phi^{(0)2} + 2\Phi^{(0)} \langle \Phi^{(2)}(\mathbf{r}) \rangle + \langle \Phi^{(1)2}(\mathbf{r}) \rangle + \cdots . \tag{2.40}$$

Therefore, the glassy fraction takes the form

$$\begin{aligned} n_R &= \langle \Phi^{(1)2}(\mathbf{r}) \rangle + \cdots \\ &= \int \frac{d^3k}{(2\pi)^3} \int \frac{d^3k'}{(2\pi)^3} \frac{\langle U(\mathbf{k}) U(\mathbf{k}') \rangle \Phi^{(0)2}}{(E_{\mathbf{k}'} - \mu + 3g\Phi^{(0)2})(E_{\mathbf{k}} - \mu + 3g\Phi^{(0)2})} e^{i(\mathbf{k}+\mathbf{k}').\mathbf{r}} + \cdots . \end{aligned} \tag{2.41}$$

Making use of $\langle U(\mathbf{k}) U(\mathbf{k}') \rangle = (2\pi)^3 \delta(\mathbf{k} + \mathbf{k}') R(\mathbf{k})$, and $\mu = g\Phi^{(0)2} = gn$, we obtain

$$n_R = n \int \frac{d^3k}{(2\pi)^3} \frac{R(\mathbf{k})}{(E_{\mathbf{k}} + 2gn)^2} + \cdots \tag{2.42}$$

Equation (2.42) shows that the disorder correlation deforms the condensate causing the occurrence of a depletion due to localization effects.

As an illustration, let us discuss the glassy fraction for a delta-correlation function of (2.8). A straightforward calculation using (2.42), yields $n_R = (m^2 R/8\hbar^4\pi^{3/2})\sqrt{n/a}$ which coincides with the seminal HM result (2.26) [140].

In next chapters we will use both theoretical models (HM theory and perturbative approach) to study effects of weak random potentials on the equilibrium and dynamical properties of Bose mixtures and on quantum droplets.

Chapter 3

Binary Bose-Einstein condensates in weak disordered potentials

In this chapter we present a comprehensive study of equilibrium and nonequilibrium behaviors of two-component BECs with weak disorder potentials.

We start with the equilibrium case and analyze some ground-state and thermodynamic aspects of disordered mixtures. To this end, we extend the perturbative theory applicable to the single component bosonic gas, described in Chapter 2, and present a detailed analysis of weakly interacting homogeneous two-component Bose gases subjected to both correlated and uncorrelated disorder potentials. The effects of the disorder on the miscibility-immiscibility condition are also deeply investigated. We derive useful expressions for the glassy fraction, the equation of state (EoS), the compressibility, and the superfluid density. We look at how each species is influenced by the disorder and how the interaction between disordered bosons influences the coupling and the phase transition between the two components. In the decoupling regime where the interspecies interaction goes to zero, we find good agreement with the analytical results obtained within the Huang-Meng model [140] and perturbative theory for a single component BEC.

On the other hand, we analyze the dynamical properties of two BECs in a Gaus-

sian disorder potential with time-periodic driving using the aforementioned time-dependent perturbation theory. The complex combination of atomic interactions, the disorder potential, and time-periodic perturbations may uncover new phenomena in dirty Bose mixtures such as *Floquet states* (see for review [147]). In the field of ultracold quantum gases, this concept could offer powerful techniques to reach novel phase transitions (see [27, 147, 148, 149, 150, 151, 152, 153, 154, 155, 156] and references therein). Our theory predicts an oscillatory behavior of the condensate deformation during the time evolution. It is found in addition that the disorder drives the growth of the disorder fraction with time, reducing the condensed fraction in each species. Interestingly, a long time analysis predicts the existence of stationary states resembling to the Floquet states due to the combination of many-body effects, the drive frequency and disorder correlations.

3.1 Equilibrium of a disordered mixture

In this section we investigate the impacts of a weak disorder potential on the quantum fluctuations and on the superfluidity of two-component BECs in the equilibrium state.

3.1.1 Model

Consider weakly interacting binary Bose gases at zero temperature in a weak random potential fulfilling the mean-field miscibility criterion, the system is described by the coupled GPE:

$$\mu_j \Phi_j = \left[-\frac{\hbar^2}{2m_j}\nabla^2 + U_j + g_j|\Phi_j|^2 + g_{12}|\Phi_{\bar{j}}|^2 \right] \Phi_j, \tag{3.1}$$

where Φ_j is the wavefunction of each condensate, the indice j is the species label, $\bar{j} = 3 - j$, μ_j is the chemical potential of each condensate, $g_j = (4\pi\hbar^2/m_j)a_j$ and $g_{12} = g_{21} = 2\pi\hbar^2(m_1^{-1} + m_2^{-1})a_{12}$ with a_j and a_{12} being the intraspecies and

the interspecies scattering lengths, respectively. The gas parameter satisfies the condition $n_j a_j^3 \ll 1$. The disorder potential $U_j(\mathbf{r})$ is described by vanishing ensemble averages $\langle U(\mathbf{r})\rangle = 0$, and a finite correlation of the form $\langle U(\mathbf{r})U(\mathbf{r}')\rangle = R(\mathbf{r}-\mathbf{r}')$. For weak disorder, equation (3.1) can be solved using straightforward perturbation theory in powers of U using the expansion [74, 75, 78, 76, 77, 79]

$$\Phi_j = \Phi_j^{(0)} + \Phi_j^{(1)}(\mathbf{r}) + \Phi_j^{(2)}(\mathbf{r}) + \cdots, \qquad j = 1, 2 \tag{3.2}$$

where the index i in the real valued functions $\Phi^{(i)}(\mathbf{r})$ signals the i-th order contribution with respect to the disorder potential. They can be determined by inserting the perturbation series (3.2) into equation (3.1) and by collecting the terms up to U^2. The zeroth-order gives

$$\Phi_j^{(0)} = \sqrt{\frac{\mu_j - g_{12}\Phi_{\bar{j}}^{(0)2}}{g_j}}, \tag{3.3}$$

which is the uniform solution in the absence of a disorder potential. Combining equations (3.3), yields

$$\Phi_j^{(0)} = \sqrt{\frac{\mu_j}{g_j}\left(1 - \frac{g_{12}}{g_{\bar{j}}}\frac{\mu_{\bar{j}}}{\mu_j}\right)\frac{\Delta}{\Delta - 1}}, \tag{3.4}$$

where $\Delta = g_j g_{\bar{j}}/g_{12}^2$ is the miscibility parameter which characterizes the miscible-immiscible transition. For $\Delta > 1$, the mixture is miscible while it is immiscible for $\Delta < 1$.

First-order equations read

$$-\frac{\hbar^2}{2m_j}\nabla^2\Phi_j^{(1)}(\mathbf{r}) + U_j(\mathbf{r})\Phi_j^{(0)} + 2g_j\Phi_j^{(0)2}\Phi_j^{(1)}(\mathbf{r}) + 2g_{12}\Phi_j^{(0)}\Phi_{\bar{j}}^{(0)}\Phi_{\bar{j}}^{(1)}(\mathbf{r}) = 0, \tag{3.5}$$

Performing a Fourier transformation:

$$\Phi(\mathbf{r}) = \int \frac{d\mathbf{k}}{(2\pi)^3} e^{i\mathbf{k}.\mathbf{r}} \Phi(\mathbf{k}), \tag{3.6}$$

one obtains the first-order solution:

$$\Phi_j^{(1)}(\mathbf{k}) = -\frac{\left[U_j(\mathbf{k}) + 2g_{12}\Phi_{\bar{j}}^{(0)}\Phi_{\bar{j}}^{(1)}(\mathbf{k})\right]\Phi_j^{(0)}}{E_{kj} + 2g_j\Phi_j^{(0)2}}, \tag{3.7}$$

where $E_{kj} = \hbar^2 k^2/2m_j$.

For $E_{kj} \ll 2g_j\Phi_j^{(0)2} = \mu_j\left(1 - g_{12}\mu_{\bar{j}}/g_{\bar{j}}\mu_j\right)\Delta/(\Delta-1)$, the kinetic energy is negligible compared to the random potential energy then, the mixture deformation sustains only the potential effects. Therefore, the coupled GPE (3.1) yield for the total density $n_j(\mathbf{r}) = \Phi_j^{(0)2} + n_j^{(1)}(\mathbf{r})$, where

$$n_j^{(1)} = \frac{\Delta}{(\Delta-1)}\left(n_{0j} - \frac{g_{12}}{g_j}n_{0\bar{j}}\right), \tag{3.8}$$

with $n_{0j} = (\mu_j - V_j)/g_j$ being the decoupled condensate density which is nothing else than the standard Thomas-Fermi-like shape.

For $E_k \gg \mu_j\left(1 - g_{12}\mu_{\bar{j}}/g_{\bar{j}}\mu_j\right)\Delta/(\Delta-1)$, the densities of the two condensates follow the modulations of a smoothed disorder potential where the variations of U have been smoothed out.

Second-order term is governed by the following equations

$$\begin{aligned} &-\frac{\hbar^2}{2m_j}\nabla^2\Phi_j^{(2)}(\mathbf{r}) + U_j(\mathbf{r})\Phi_j^{(1)} + g_j\left[2\Phi_j^{(0)2}\Phi_j^{(2)}(\mathbf{r}) + 3\Phi_j^{(0)}\Phi_j^{(1)2}(\mathbf{r})\right] \\ &+ g_{12}\left[2\Phi_{\bar{j}}^{(0)}\Phi_{\bar{j}}^{(1)}(\mathbf{r})\Phi_j^{(1)}(\mathbf{r}) + \Phi_j^{(0)}\Phi_{\bar{j}}^{(1)2}(\mathbf{r}) + 2\Phi_j^{(0)}\Phi_{\bar{j}}^{(0)}\Phi_{\bar{j}}^{(2)}(\mathbf{r})\right] = 0. \end{aligned} \tag{3.9}$$

The solution of these coupled equations in the momentum space reads

$$\Phi_j^{(2)}(\mathbf{k}) = -\int \frac{d\mathbf{k}'}{(2\pi)^3} \frac{\Phi_j^{(1)}(\mathbf{k}-\mathbf{k}')\left[U_j(\mathbf{k}') + 3g_j\Phi_j^{(0)}\Phi_j^{(1)}(\mathbf{k}')\right]}{E_{kj} + 2g_j\Phi_j^{(0)2}} - g_{12}\frac{2\Phi_{\bar{j}}^{(0)}\Phi_j^{(0)}\Phi_{\bar{j}}^{(2)}(\mathbf{k})}{E_{kj} + 2g_j\Phi_j^{(0)2}} - g_{12}\int \frac{d\mathbf{k}'}{(2\pi)^3}\Phi_{\bar{j}}^{(1)}(\mathbf{k}-\mathbf{k}')\frac{\left[2\Phi_{\bar{j}}^{(0)}\Phi_j^{(1)}(\mathbf{k}') + \Phi_{\bar{j}}^{(1)}(\mathbf{k}')\Phi_j^{(0)}\right]}{E_{kj} + 2g_j\Phi_j^{(0)2}}. \tag{3.10}$$

Equations (3.10) enable us to selfconsistently determine the chemical potential of the system (see below).

Finally, the validity of the present perturbation approach requires the condition:

$$U \ll g_j\Phi_j^{(0)2} \simeq g_j n_j, \tag{3.11}$$

where $\Phi_j^{(0)}$ is given in equation (3.4), tells us that the densities do not vary much around the homogeneous values. For $g_{12} = 0$, one recovers the well-known condition ($U \ll g\Phi^{(0)2}$) established for a disordered single BEC [79]. Indeed, this simple assumption indicates how localization can be destroyed in the regime of weak interactions. However, the perturbation approach is no longer valid in the regime of strong disorder.

Glassy fraction

Now, we evaluate the glassy fraction inside each component. As we have shown in Chapter 2, the disorder contribution to the condensate can be given as the variance of the wavefunction $n_{Rj} = n_j - n_{cj}$ [76, 77], where

$$n_j = \langle\Phi_j^2(\mathbf{r})\rangle = \Phi_j^{(0)2} + \langle\Phi_j^{(1)2}(\mathbf{r})\rangle + 2\Phi_j^{(0)}\langle\Phi_j^{(2)}(\mathbf{r})\rangle + \cdots \tag{3.12}$$

and

$$n_{cj} = \langle\Phi_j(\mathbf{r})\rangle^2 = \Phi_j^{(0)2} + 2\Phi_j^{(0)}\langle\Phi_j^{(2)}(\mathbf{r})\rangle + \cdots \tag{3.13}$$

is the condensed density.

Subtracting equations (3.13) from (3.12), one obtains $n_{Rj} = \langle \Phi_j^{(1)2}(\mathbf{r})\rangle + \cdots$, which is in fact analog to the Edwards-Anderson order parameter of a spin glass [77, 157, 158].

From now on, we shall consider $U_1 = U_2 = U$ and $m_1 = m_2 = m$. Employing the Fourier transform of $\Phi_j^{(1)}(\mathbf{r})$ of equation (3.7), and using the fact that $\langle U(\mathbf{k}')U(\mathbf{k}'')\rangle = (2\pi)^3 R(\mathbf{k}')\delta(\mathbf{k}'+\mathbf{k}'')$, the glassy fraction, n_{Rj}, takes the form

$$n_{Rj} = n_j \int \frac{\mathbf{dk}}{(2\pi)^3} R(\mathbf{k}) \left[\frac{E_k + 2n_{\bar{j}}\big(g_{\bar{j}} - g_{12}\big)}{\mathcal{E}_k}\right]^2, \tag{3.14}$$

where $\mathcal{E}_k = \big(E_k + 2g_j n_j\big)\big(E_k + 2g_{\bar{j}} n_{\bar{j}}\big) - 4g_{12}^2 n_j n_{\bar{j}}$, and $R(\mathbf{k})$ is the disorder correlation in Fourier space.

Equation of state

The EoS can be calculated by substituting equations (3.3)-(3.10) into equation (3.12) and solving the equation $\langle \Phi_j^2(\mu_{bj})\rangle = n(\mu_{bj})$, where μ_{bj} represents the bare chemical potential. It diverges for uncorrelated disorder [77, 78]. We then obtain

$$\begin{aligned}\mu_{bj}(n_j, n_{\bar{j}}) = g_j n_j + g_{12} n_{\bar{j}} - \int \frac{d\mathbf{k}}{(2\pi)^3} \frac{R(\mathbf{k})}{(g_j g_{\bar{j}} - g_{12}^2)\mathcal{E}_k} \Bigg\{ & (g_j g_{\bar{j}} - g_{12}^2)[E_k - 2n_{\bar{j}}(g_{12} - g_{\bar{j}})] \\ + g_{12} g_j [E_k - 2n_j(g_{12} - g_j)] - & \frac{2g_{12} g_j g_{\bar{j}} n_{\bar{j}} [E_k - 2n_j(g_{12} - g_j)]^2 - 2g_j^2 g_{\bar{j}} n_j [E_k - 2n_{\bar{j}}(g_{12} - g_{\bar{j}})]^2}{\mathcal{E}_k} \\ - 2g_{12} n_{\bar{j}} (g_j g_{\bar{j}} - g_{12}^2)[E_k - 2n_j(g_{12} - g_j)] & \frac{[E_k - 2n_{\bar{j}}(g_{12} - g_{\bar{j}})]}{\mathcal{E}_k} - \frac{2g_{12} g_j g_{\bar{j}} n_j^{3/2} [E_k - 2n_{\bar{j}}(g_{12} - g_{\bar{j}})]^3}{(g_j g_{\bar{j}} - g_{12}^2)\mathcal{E}_k^2} \Bigg\},\end{aligned} \tag{3.15}$$

To overcome this unphysical ultraviolet divergence, we renormalize the chemical potential. The renormalized chemical potential is defined as:

$$\mu_j(n_j, n_{\bar{j}}) = \mu_{bj}(n_j, n_{\bar{j}}) - \mu_{bj}(0), \tag{3.16}$$

where

$$\mu_{bj}(0) = -\int \frac{d\mathbf{k}}{(2\pi)^3} R(\mathbf{k}) \left[\frac{1}{E_k} + \frac{g_j g_{12}}{(g_j g_{\bar{j}} - g_{12}^2) E_k} \right], \tag{3.17}$$

Omitting higher order in g_{12}, we obtain, in second-order of the disorder strength, the following renormalized EoS

$$\mu_j = g_j n_j + g_{12} n_{\bar{j}} + \int \frac{d\mathbf{k}}{(2\pi)^3} \frac{R(k)}{(g_j g_{\bar{j}} - g_{12}^2)\mathcal{E}_k^2 E_k} \Bigg\{ 4 g_j^2 g_{\bar{j}} n_j \left(E_k + g_j n_j\right) \left(E_k + 2 g_{\bar{j}} n_{\bar{j}}\right)^2$$
$$+ 4 g_j g_{\bar{j}} g_{12} n_{\bar{j}} \Big[(E_k + g_{\bar{j}} n_{\bar{j}})(E_k + 2 g_j n_j)^2 + E_k^2 (E_k + 2 g_{\bar{j}} n_{\bar{j}}) \Big] \Bigg\}. \tag{3.18}$$

3.2 Delta-correlated disorder

White-noise (or uncorrelated) disorders are widely used, mostly because at low-energy, many continuous random potentials can be replaced by a white-noise potential. Its autocorrelation function is defined in equation (2.8). This model is valid when the correlation length of the correlation function $R(\mathbf{r}-\mathbf{r}')$ is sufficiently shorter than the healing length.

Substituting equation (2.8) into equation (3.14), we get useful formula for the glassy fraction:

$$\frac{n_{Rj}}{n_j} = 4\pi R_j' \sqrt{\frac{n_j a_j^3}{\pi}} f_j(\Delta), \tag{3.19}$$

where $R_j' = R_0 / g_j^2 n_j$ is a dimensionless disorder strength and,

$$f_j(\Delta) = \left[\frac{(2\beta_j)^{-3/2}}{\sqrt{1 + \bar{\mu}_j + \sqrt{\beta_j}}} - \frac{(2\beta_j)^{-3/2}}{\sqrt{(1 + \bar{\mu}_j) - \sqrt{\beta_j}}} \right] \bar{f}_1(\Delta) \tag{3.20}$$
$$+ \left[\frac{\sqrt{2}\beta_j^{-1}}{4\sqrt{1 + \bar{\mu}_j + \sqrt{\beta_j}}} + \frac{\sqrt{2}\beta_j^{-1}}{4\sqrt{(1 + \bar{\mu}_j) - \sqrt{\beta_j}}} \right] \bar{f}_2(\Delta),$$

where

$$\bar{f}_1(\Delta) = (1+\bar{\mu}_j)^3 + 2\alpha_j (1+\bar{\mu}_j)^2 - 4(1+\bar{\mu}_j)\left[2\bar{\mu}_j \left(\frac{\Delta - 1}{\Delta} \right) + \alpha_j^2 \right] + 8\bar{\mu}_j \alpha_j \left(\frac{\Delta - 1}{\Delta} \right),$$

$$\bar{f}_2(\Delta) = (1+\bar{\mu}_j)^2 + 2\alpha_j(1+\bar{\mu}_j) - 6\bar{\mu}_j\left(\frac{\Delta-1}{\Delta}\right) - 2\alpha_j^2,$$

where $\beta_j = (1+\bar{\mu}_j)^2 - 4\bar{\mu}_j\left[(\Delta-1)/\Delta\right]$, $\alpha_j = \bar{\mu}_j\left(1-\sqrt{g_j/\left(g_{\bar{j}}\Delta\right)}\right)$, $\bar{\mu}_j = n_{\bar{j}}g_{\bar{j}}/n_j g_j$. Equation (3.19) is appealing since it describes the glassy fraction in terms of the miscibility parameter. The total disorder density is given by $n_R = n_{R1} + n_{R2}$. For $\Delta \to \infty$ (or $g_{12} \to 0$, equivalently), we find from equation (3.19) that $f_1(\infty) = f_2(\infty) = 1/2$. Therefore, we should reproduce the famous HM result [140], $n_R/n = 2\pi R'\sqrt{na^3/\pi}$ for the single component disorder fraction. The intriguing interplay between the strong intercomponent coupling and the disorder effects in the regime $\Delta - 1 \ll 1$ would cause a sharp increase in the functions $f_j(\Delta)$. Near the phase separation i.e. $\Delta \to 1$ (or $g_{12} \to \sqrt{g_1 g_2}$, equivalently), the functions $f_j(\Delta)$ are diverging. They are complex for $\Delta < 1$ and hence, the mixture undergoes instability.

The disorder functions f_j have the following asymptotic behavior for small a_{12}

$$f_j(a_{12}) = \frac{1}{2} - \frac{n_{\bar{j}}}{n_j a_j\left(1+\sqrt{\frac{n_{\bar{j}}a_{\bar{j}}}{n_j a_j}}\right)^2}a_{12} + \cdots,$$

and for large a_{12}

$$f_j(a_{12}) = \frac{\left(\sqrt{a_{\bar{j}}/a_j} - 1\right)^2}{2\left(\frac{n_{\bar{j}}a_{\bar{j}}}{n_j a_j}+1\right)^{3/2}\sqrt{\left(a_j a_{\bar{j}}/a_{12}^2\right) - 1}} + \cdots.$$

It is straightforward to check that these asymptotic results perfectly agree with the solutions shown in figure 3.1 (a) in the asymptotic regime.

As an illustration of our theoretical formalism, we consider a two-component Bose condensate of rubidium atoms in two different internal states ^{87}Rb-^{87}Rb. We have taken the intra-component scattering lengths : $a_1 = 100.4\,a_0$ and $a_2 = 95.44\,a_0$ (a_0 is the Bohr radius) [159], and the densities: $n_1 = 1.5 \times 10^{21}$ m $^{-3}$, and $n_2 = 10^{21}$ m^{-3}. Thus, the parameter $n_j a_j^3$ is as small as $\sim 10^{-4}$.

Figure 3.1 (a) shows that for $a_{12}/a_0 \leq 97.89$, the functions f_j are decreasing

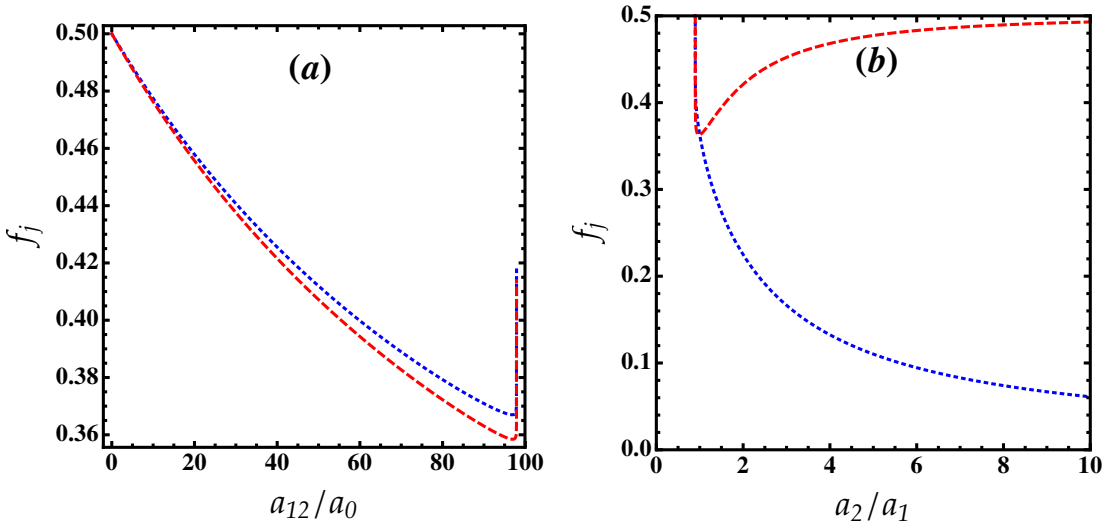

Figure 3.1: (a) Behavior of the disorder functions f_j as a function of the interspecies interaction strength a_{12} for ^{87}Rb-^{87}Rb mixture. (b) Behavior of the disorder functions f_j as a function of the ratio a_2/a_1 for $a_{12} = 90a_0$. Blue dotted lines: f_1. Red dashed lines: f_2. Here a_{12} can be adjusted via Feshbach resonance.

with the interspecies interaction giving rise to the delocalization of both species. In the vicinity of the transition between the miscible and immiscible phases i.e. $a_{12}/a_0 = 97.89$, the functions f_j exhibit an anomalous behavior where they develop a small minimum. Then they start to increase for $a_{12}/a_0 > 97.89$. In such a regime, both species are strongly localized in the local wells of the random potential.

The situation is quite different for fixed a_{12} and varying the interaction ratio a_2/a_1. The disorder functions f_1 and f_2 decrease/increase with the ratio a_2/a_1 as is shown in figure 3.1 (b). The function f_2 develops a minimum at $a_2 \simeq a_1$. For $a_2/a_1 \geq 5$, f_1 is very small and thus, the first component becomes almost superfluid due to the suppression of the localization, while the second BEC remains localized regardless of the value of a_{12}.

One can conclude that the localization of each species does not depend only on the disorder strength but depends also on the interspecies interactions and the ratio of intraspecies interactions. Importantly, the localization of one component does not trigger the localization of the second component due to the interplay of the intra- and interspecies interactions and the disorder potential.

For delta-correlated disorder, the EoS (3.18) turns out to be given as:

$$\mu_j = g_j n_j + g_{12} n_{\bar{j}} + 16\pi g_j n_j R'_j \sqrt{\frac{n_j a_j^3}{\pi}} h_j(\Delta), \tag{3.21}$$

where

$$h_j(\Delta) = \frac{1}{(2\beta_j)^{3/2}} \frac{\Delta}{\Delta - 1} \left[\bar{h}_1(\Delta) + \frac{n_{\bar{j}} g_{12}}{n_j g_j} \bar{h}_2(\Delta) \right], \tag{3.22}$$

and

$$\begin{aligned}
\bar{h}_1(\Delta) = & \left(\frac{1}{\sqrt{1 + \bar{\mu}_j + \sqrt{\beta_j}}} - \frac{1}{\sqrt{(1 + \bar{\mu}_j) - \sqrt{\beta_j}}} \right) H_1(\Delta) \\
& + \left(\frac{\sqrt{\beta_j}}{\sqrt{1 + \bar{\mu}_j + \sqrt{\beta_j}}} + \frac{\sqrt{\beta_j}}{\sqrt{(1 + \bar{\mu}_j) - \sqrt{\beta_j}}} \right) H_2(\Delta), \\
\bar{h}_2(\Delta) = & \left(\frac{1}{\sqrt{1 + \bar{\mu}_j + \sqrt{\beta_j}}} - \frac{1}{\sqrt{(1 + \bar{\mu}_j) - \sqrt{\beta_j}}} \right) H_3(\Delta) \\
& + \left(\frac{\sqrt{\beta_j}}{\sqrt{1 + \bar{\mu}_j + \sqrt{\beta_j}}} + \frac{\sqrt{\beta_j}}{\sqrt{(1 + \bar{\mu}_j) - \sqrt{\beta_j}}} \right) H_4(\Delta),
\end{aligned}$$

$$h_j(\Delta) = \frac{1}{(2\beta_j)^{3/2}} \frac{\Delta}{\Delta - 1} \left[\bar{h}_1(\Delta) + \frac{n_{\bar{j}} g_{12}}{n_j g_j} \bar{h}_2(\Delta) \right],$$

and

$$\begin{aligned}
\bar{h}_1(\Delta) = & \left(\frac{1}{\sqrt{1 + \bar{\mu}_j + \sqrt{\beta_j}}} - \frac{1}{\sqrt{(1 + \bar{\mu}_j) - \sqrt{\beta_j}}} \right) H_1(\Delta) \\
& + \left(\frac{\sqrt{\beta_j}}{\sqrt{1 + \bar{\mu}_j + \sqrt{\beta_j}}} + \frac{\sqrt{\beta_j}}{\sqrt{(1 + \bar{\mu}_j) - \sqrt{\beta_j}}} \right) H_2(\Delta), \\
\bar{h}_2(\Delta) = & \left(\frac{1}{\sqrt{1 + \bar{\mu}_j + \sqrt{\beta_j}}} - \frac{1}{\sqrt{(1 + \bar{\mu}_j) - \sqrt{\beta_j}}} \right) H_3(\Delta) \\
& + \left(\frac{\sqrt{\beta_j}}{\sqrt{1 + \bar{\mu}_j + \sqrt{\beta_j}}} + \frac{\sqrt{\beta_j}}{\sqrt{(1 + \bar{\mu}_j) - \sqrt{\beta_j}}} \right) H_4(\Delta),
\end{aligned}$$

where

$H_1(\Delta) = (1+\bar{\mu}_j)^3 + (1+\bar{\mu}_j)^2\left[\frac{1}{2}+2\bar{\mu}_j-\frac{1}{2}\bar{\mu}_j\left(\frac{\Delta}{\Delta-1}\right)\right] - 4(1+\bar{\mu}_j)\left[\bar{\mu}_j^2+\bar{\mu}_j\left(1+2\left(\frac{\Delta-1}{\Delta}\right)\right)\right]+2\bar{\mu}_j\left(\frac{\Delta-1}{\Delta}\right)(1+4\bar{\mu}_j)+6\bar{\mu}_j^2,$

$H_2(\Delta) = (1+\bar{\mu}_j)^2+\frac{1}{2}(1+\bar{\mu}_j)\left[1+\bar{\mu}_j\left(\frac{\Delta}{\Delta-1}\right)\right]-6\bar{\mu}_j\left(\frac{\Delta-1}{\Delta}\right),$

$H_3(\Delta) = 2(1+\bar{\mu}_j)^3 + (1+\bar{\mu}_j)^2\left[-2+\frac{3}{2}\bar{\mu}_j-\frac{1}{2}\left(\frac{\Delta}{\Delta-1}\right)\right] + 2\bar{\mu}_j\left\{3+\left(\frac{\Delta-1}{\Delta}\right)\left[-8(1+\bar{\mu}_j)+3\bar{\mu}_j+4\right]\right\}$, and

$H_4(\Delta) = 2(1+\bar{\mu}_j)^2+\frac{1}{2}(1+\bar{\mu}_j)\left[\frac{1}{2}\left(\frac{\Delta}{\Delta-1}\right)+3\bar{\mu}_j\right]-12\bar{\mu}_j\left(\frac{\Delta}{\Delta-1}\right).$

The last term in equation (3.21) accounts for the disorder corrections to the EoS. For $\Delta \to \infty$ (or $g_{12} \to 0$, equivalently), one has $h_j(\infty) = 3/4$ (see also Figure 3.2) and thus, the EoS reduces to that of a single BEC namely; $\mu = gn(1+12\pi R'\sqrt{na^3/\pi})$, found in Refs.[141, 158, 160] using the HM theory.

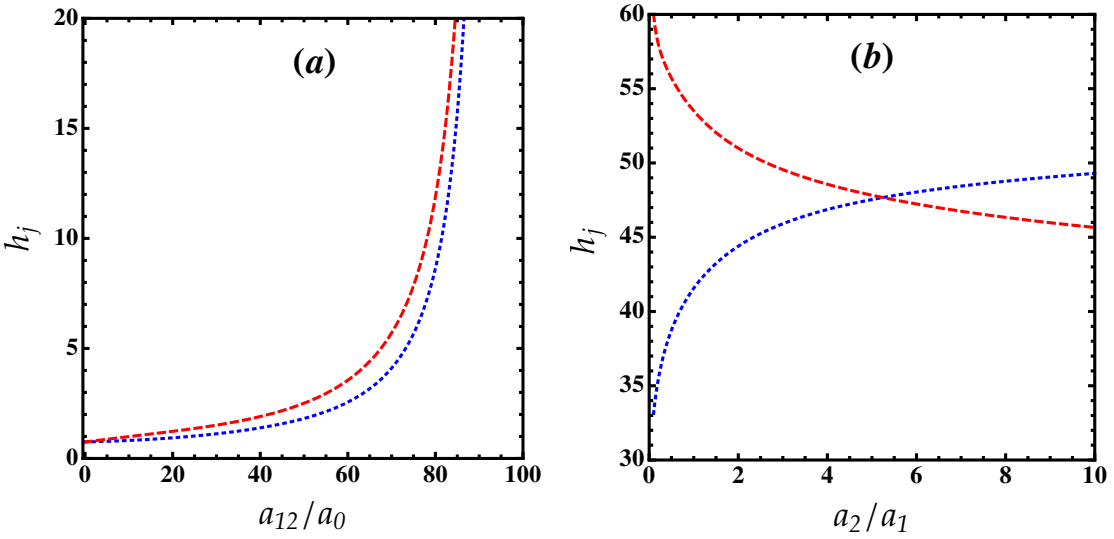

Figure 3.2: (a) Behavior of the disorder functions h_j as a function of a_{12} for ^{87}Rb-^{87}Rb mixture. (b) Behavior of the disorder functions h_j as a function of the ratio a_2/a_1 for $a_{12} = 90a_0$. Blue dotted lines: h_1. Red dashed lines: h_2.

Figure 3.2 (a) depicts that the functions h_j grow with a_{12} and diverge at $a_{12} \to \sqrt{a_1 a_2}$ results in an enhancement of the total chemical potential. In this case, the quantum fluctuations arising from interactions are viewed as being predominated by disorder effects.

Moreover, we see from figure 3.2 (b) that the disorder functions h_j behave differently with the interactions ratio a_2/a_1. Both functions diverge for $a_2/a_1 \to 0$ and

match at $a_2/a_1 = 5$. The chemical potential associated with the first component μ_1 enhances when h_1 rises, while μ_2 decays for lowering h_2. This reveals that the competition of the intraspecies interactions and the disorder potential may perceptibly alter the behavior of the EoS of the global mixture.

3.2.1 Miscibility conditions

We now discuss a possible energetic instability, associated with the presence of the disorder and the occurrence of miscible-immiscible phase transition. For a homogeneous mixture to be stable, the following conditions should be fulfilled [161]:

$$\frac{\partial \mu_j}{\partial n_j} > 0, \tag{3.23a}$$

$$\left(\frac{\partial \mu_j}{\partial n_j}\right)\left(\frac{\partial \mu_{\bar{j}}}{\partial n_{\bar{j}}}\right) > \left(\frac{\partial \mu_j}{\partial n_{\bar{j}}}\right)^2. \tag{3.23b}$$

These conditions are derived from the variation of the energy with respect to the densities. For the EoS (3.21), we obtain:

$$\frac{\partial \mu_j}{\partial n_j} = g_j \left[1 + 8\pi R'_j \sqrt{\frac{n_j a_j^3}{\pi}} \left(h_j + 2n_j \frac{\partial h_j(\Delta)}{\partial n_j}\right)\right]. \tag{3.24}$$

The second term in the r.h.s of equation (3.24) constitutes the disorder corrections to the inverse compressibility $\kappa_j^{-1} = n_j^2 \partial \mu_j / \partial n_j$. Figure 3.3 (a) shows that the disorder functions $n_j \partial h_j / \partial n_j$ possess identical behavior over almost the entire range of the interspecies interactions. They vanish for $a_{12} = 0$ where the two components are spatially separated and remain negligibly small in the domain $0 \leq a_{12}/a_0 \leq 65$, indicating that the disorder effect is marginally relevant in this regime. For $a_{12}/a_0 \geq 65, n_j \partial h_j / \partial n_j$ decrease and display a negative divergence at $a_{12} \to \sqrt{a_1 a_2}$, leading to substantially reduce the compressibility of the system. We observe from figure 3.3 (b) that the disorder functions $n_1 \partial h_1 / \partial n_1$ and $n_2 \partial h_2 / \partial n_2$ vary in the opposite way with the ratio a_2/a_1. They diverge for $a_2/a_1 \to 0$, and have minimum/maximum at

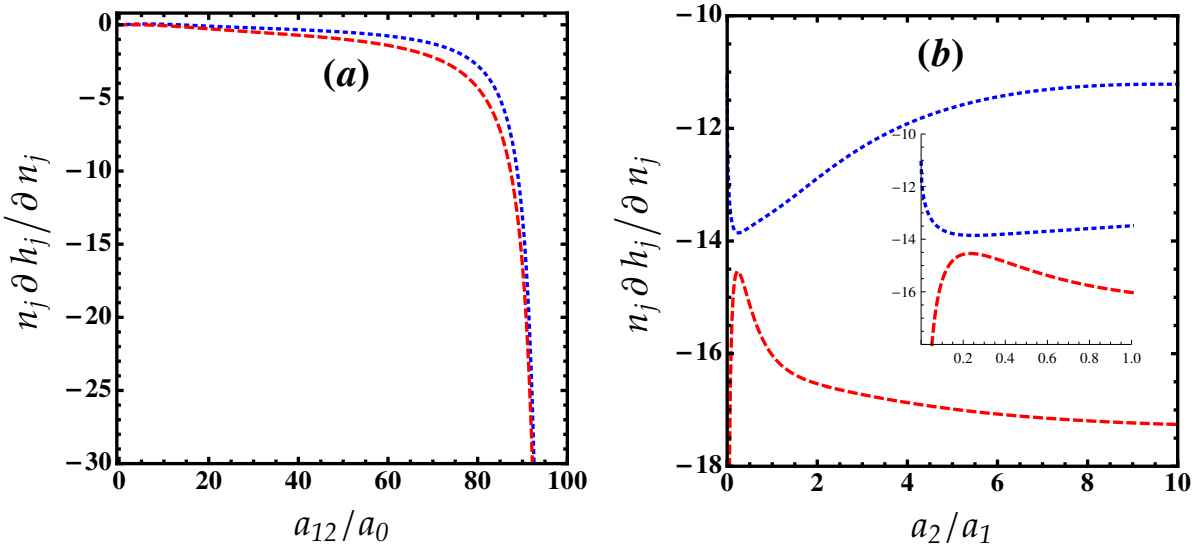

Figure 3.3: (a) Behavior of the disorder functions $\partial h_j/\partial n_j$ in units of n_j as a function of a_{12} for ^{87}Rb-^{87}Rb mixture. (b) Behavior of the disorder functions $\partial h_j/\partial n_j$ in units of n_j as a function of the ratio a_2/a_1 for $a_{12} = 90a_0$. Blue dotted lines: $n_1\partial h_1/\partial n_1$. Red dashed lines: $n_2\partial h_2/\partial n_2$.

$a_2/a_1 \simeq 0.2$, where the second component is extremely dilute compared to the first component, then they increase/decrease for $a_2/a_1 > 0.2$ (see the inset of Fig.3.3 (b)). This peculiar behavior can be attributed to the competition between the repulsive interactions, the miscibility and the disorder. The functions $\partial h_j/\partial n_j$ are negative in the whole range of interactions.

The stability conditions (3.23) turn out to be given as:

$$g_j \left[1 + 8\pi R'_j \sqrt{\frac{n_j a_j^3}{\pi}} \left(h_j + 2n_j \frac{\partial h_j(\Delta)}{\partial n_j}\right)\right] > 0, \tag{3.25a}$$

and

$$\Delta \left[1 + 8\pi R'_j \sqrt{\frac{n_j a_j^3}{\pi}} \left(h_j + 2n_j \frac{\partial h_j(\Delta)}{\partial n_j}\right)\right] \left[1 + 8\pi R'_{\bar{j}} \sqrt{\frac{n_{\bar{j}} a_{\bar{j}}^3}{\pi}} \left(h_{\bar{j}} + 2n_{\bar{j}} \frac{\partial h_{\bar{j}}(\Delta)}{\partial n_{\bar{j}}}\right)\right] > \left(1 + 16\pi R'_j \sqrt{\frac{n_j a_j^3}{\pi}} \frac{a_j}{a_{12}} n_j \frac{\partial h_j(\Delta)}{\partial n_{\bar{j}}}\right)^2. \tag{3.25b}$$

Expressions (3.25) clearly show that the miscibility condition for a mixture of two interacting BECs is significantly affected by the disorder potential. This gives rise

to a phase transition to an immiscible phase even though the cleaned mixture is miscible. For relatively large disorder strength, the mixture may drive a transition to an immiscible phase with complete spatial separation between the two BECs. For $R_j^{'} = 0$, the conditions (3.25) reduce to those of the cleaned binary BECs mentioned above.

The critical disorder strength above which a quantum miscible-immiscible phase transition occurs can be directly determined from (3.25b) as:

$$R_j^{\prime c} = \frac{-A_j - \sqrt{A_j^2 - 4B_j(\Delta - 1)/\Delta}}{16\pi\sqrt{n_j a_j^3/\pi}B_j}, \tag{3.26}$$

where $A_j = (h_j + 2n_j\partial h_j/\partial n_j) + \sqrt{g_j n_j/g_{\bar{j}} n_{\bar{j}}}\left(h_{\bar{j}} + 2n_{\bar{j}}\partial h_{\bar{j}}/\partial n_{\bar{j}}\right) - 4\Delta^{-1}\left(n_j g_j/g_{12}\right)\left(\partial h_j/\partial n_{\bar{j}}\right)$, and $B_j = \left(h_j + 2n_j\partial h_j/\partial n_j\right)\left(h_{\bar{j}} + 2n_{\bar{j}}\partial h_{\bar{j}}/\partial n_{\bar{j}}\right)\sqrt{g_j n_j/g_{\bar{j}} n_{\bar{j}}} - 4\Delta^{-1}\left(n_j g_j/g_{12}\right)^2\left(\partial h_j/\partial n_{\bar{j}}\right)^2$ with $R_{\bar{j}}^{\prime} = R_j^{\prime}\left(g_j^2 n_j/g_{\bar{j}}^2 n_{\bar{j}}\right)$.
In the case of ^{87}Rb $-$ ^{87}Rb mixture with parameters : $a_1 = 100.4a_0, n_1 = 1.5 \times 10^{21}$ m^{-3} and $a_2 = 95.44a_0, n_2 = 10^{21}$ m^{-3}, and $a_{12} = 90a_0$, the miscible-immiscible phase transition arises for disorder strengths $R_1^{\prime c} = 0.7$ and $R_2^{\prime c} = 1.16$.

3.2.2 Superfluid fraction

Let us consider a Bose mixture superfluid moving with velocity $\mathbf{v_{sj}} = \hbar\mathbf{k_{sj}}/m$, where $\mathbf{k_{sj}}$ is a wavevector corresponding to the velocity of superfluid, subjected to a moving weak random potential with the velocity $\mathbf{v_u} = \hbar\mathbf{k_u}/m$, where $\mathbf{k_u}$ is a wavevector corresponding to the velocity of disorder. At finite temperatures, the Bose fluid is separated into a superfluid density n_{sj} and a normal density n_{nj} that moves with the disorder component n_{Rj}. Then the coupled time-dependent GPE read

$$i\hbar\frac{\partial\Phi_j(\mathbf{r},t)}{\partial t} = \left(-\frac{\hbar^2}{2m}\nabla^2 + U(\mathbf{r} - \mathbf{v_u}t) + g_j|\Phi_j(\mathbf{r},t)|^2 + g_{12}|\Phi_{\bar{j}}(\mathbf{r},t)|^2\right)\Phi_j(\mathbf{r},t). \tag{3.27}$$

We treat the solution of equation (3.27) perturbatively by introducing the function

$$\Phi_j(\mathbf{r},t) = \left[\Phi_j^{(0)} + \Phi_j^{(1)}(\mathbf{r},t) + \Phi_j^{(2)}(\mathbf{r},t) + \cdots\right] e^{i\mathbf{k_{sj}}.\mathbf{r}} e^{-\frac{i}{\hbar}\left(\frac{\hbar^2\mathbf{k}_{sj}^2}{2m}+\mu_j\right)t}, \tag{3.28}$$

which corresponds to the clean-case solution [77, 78, 141]. After inserting the expansion (3.27) into equation (3.28), and using the transformation $\mathbf{r}' = \mathbf{r} + \mathbf{v_u}t$, one obtains

$$\left(-\frac{\hbar^2}{2m}\nabla^2 - i\frac{\hbar^2}{m}\mathbf{K}_j.\nabla + U(\mathbf{r}') - \mu_j + g_j|\Phi_j(\mathbf{r}')|^2 + g_{12}|\Phi_{\bar{j}}(\mathbf{r}')|^2 \right)\Phi_j(\mathbf{r}') = 0, \tag{3.29}$$

where $\mathbf{K_j} = \mathbf{k_{sj}} - \mathbf{k_u}$.

In the two-fluid model, the total momentum $\mathbf{P}(\mathbf{r})$ of the moving system is defined as:

$$\mathbf{P}_j = -i\hbar\langle\Phi_j|i\mathbf{k}_{sj} + \nabla|\Phi_j\rangle = \hbar\mathbf{k}_{sj}n_j - i\hbar\langle\Phi_j^*\nabla\Phi_j\rangle. \tag{3.30}$$

We neglect higher than linear terms in $\mathbf{k}_{sj}$ and keeping in mind that in zeroth order $\mathbf{P}_j$ does not depend on $\mathbf{k}_{sj}$. This yields

$$\mathbf{P}_j = \hbar\mathbf{k}_{sj}n_j - i\hbar\langle\Phi_j^{*(1)}\nabla\Phi_j^{(1)}\rangle + \cdots, \tag{3.31}$$

where the first-order correction to the wavefunction is given in Fourier space by

$$\Phi_j^{(1)}(\mathbf{k}) = \frac{-U(\mathbf{k})\Phi_j^{(0)}(E_k - \frac{\hbar^2}{m}\mathbf{k}.\mathbf{K_j})\left[-E_k^2 - 2E_k\Phi_{\bar{j}}^{(0)2}(g_{\bar{j}} - g_{12}) + (\frac{\hbar^2}{m}\mathbf{k}.\mathbf{K_{\bar{j}}})^2\right]}{4\Phi_{\bar{j}}^{(0)2}\Phi_j^{(0)2}g_{12}^2E_k^2 - \left(E_k^2 + 2E_kg_{\bar{j}}\Phi_{\bar{j}}^{(0)2} - (\frac{\hbar^2}{m}\mathbf{k}.\mathbf{K_{\bar{j}}})^2\right)\left(E_k^2 + 2E_kg_j\Phi_j^{(0)2} - (\frac{\hbar^2}{m}\mathbf{k}.\mathbf{K_j})^2\right)}. \tag{3.32}$$

For small K_j, the normal density reads

$$n_{nj} = n_j - \frac{1}{\hbar}\frac{\partial P_j}{\partial K_j}\Big|_{K_j=0}. \tag{3.33}$$

In the case of delta-correlated random potential (2.8), we get for the normal

fraction

$$n_{nj} = \frac{16\pi}{3} R'_j \sqrt{\frac{n_j a_j^3}{\pi}} f_j(\Delta) = \frac{4}{3} n_{Rj}. \tag{3.34}$$

We see that equation (3.34) well recovers the HM results for a single component BEC with contact interaction [140]. The fact that n_{nj} is larger than n_{Rj} is due to the localization of bosons in the respective minima of the random potential which leads to reduction of the superfluid density. Obviously, the interplay of the disorder potential, interspecies interaction and the ratio of intraspecies interactions may strongly affect the superfluid fraction $n_{sj} = 1 - (4/3)n_{Rj}$.

3.3 Gaussian correlated disorder

We consider now the case of a correlated Gaussian disorder model, which allows for unique control of the interplay between the disorder potential and interactions. In this case the mixture deformation due to the disorder can be obtained by substituting equation (2.10) into the expression (3.14):

$$n_{Rj}^{\mathrm{eq}} = n_{j\mathrm{HM}} f_j(\Delta, \sigma_j), \tag{3.35}$$

where $n_{j\mathrm{HM}} = 2\pi R'_j n_j \sqrt{n_j a_j^3/\pi}$ is the HM result for equilibrium deformation of each BEC with $R'_j = R_0/g_j^2 n_j$ being a dimensionless disorder strength, $\sigma_j = \sigma/\xi_j$, $\Delta = g_j g_{\bar{j}}/g_{12}^2$, and $\xi_j = \hbar/\sqrt{m n_j g_j}$ is the healing length of each component. The disorder functions of the glassy fraction $f_j(\Delta, \sigma_j)$ of equation (3.35) can be written

as:

$$
\begin{aligned}
f_j(\Delta,\sigma_j) = \frac{\sqrt{2/\pi}}{\sqrt{\beta_j\alpha_j}(\alpha_j-\beta_j)^3}\Bigg\{ & -2\sigma_j\sqrt{\alpha_j\beta_j}(\alpha_j-\beta_j)\Big[2\nu_j^2+\alpha_j^2+\beta_j^2-2\nu_j(\alpha_j+\beta_j)\Big] \\
& + \sqrt{\pi}e^{\sigma_j^2\beta_j}\Big[3\nu_j^2\beta_j\sqrt{\alpha_j}+\sqrt{\beta_j}(\alpha_j\beta_j)^{3/2}(5-4\sigma_j^2\nu_j)+\sqrt{\alpha_j}[\nu_j^2\alpha_j+2\nu_j\beta_j\alpha_j(-3+\sigma_j^2\nu_j) \\
& - 2\nu_j\beta_j^2(1+\sigma_j^2\nu_j)+\beta_j^3(-1+2\sigma_j^2(2\nu_j+\alpha_j))-2\sigma_j^2\beta_j^4]\Big] \\
& + \sqrt{\pi}e^{\sigma_j^2\beta_j}\sqrt{\alpha_j}(\beta_j-\nu_j)\Big[\nu_j[\alpha_j+(3+2\sigma_j^2(\alpha_j-\beta_j))\beta_j]+\beta_j[-5\alpha_j+\beta_j-2\sigma_j^2\beta_j(\alpha_j-\beta_j)]\Big] \\
& \times\left[1-\mathrm{erfc}\left(\sqrt{\sigma_j^2\beta_j}\right)\right] \\
& + \sqrt{\pi}e^{\sigma_j^2\alpha_j}\sqrt{\beta_j}(\alpha_j-\nu_j)\Big[\alpha_j[\alpha_j+2\sigma_j^2\alpha_j(\alpha_j-\beta_j)-5\beta_j]+\nu_j[\beta_j+\alpha_j(3-2\sigma_j^2(\alpha_j-\beta_j))]\Big] \\
& \times\mathrm{erfc}\left(\sqrt{\sigma_j^2\alpha_j}\right)\Bigg\}, \qquad (3.36)
\end{aligned}
$$

where $\mathrm{erfc}(x)$ is the complementary error function, $\alpha_j = 1+\bar{\mu}_j+\sqrt{(1+\bar{\mu}_j)^2-4\bar{\mu}_j\,(\Delta-1)\,/\Delta}$, $\beta_j = 1+\bar{\mu}_j-\sqrt{(1+\bar{\mu}_j)^2-4\bar{\mu}_j\,(\Delta-1)\,/\Delta}$, and $\nu_j = 2\bar{\mu}_j\left(1-g_{12}/g_{\bar{j}}\right)$. For $\sigma\to 0$, the disorder functions f_j tend to the delta-function obtained in equation (3.20). In the regime $\sigma\to 0$ and $\Delta\to\infty$ (or $g_{12}\to 0$, equivalently), one has $f_j(\infty,0)=1$. This immediately leads to reproduce the HM result [140] for the single component disorder fraction. If $\sigma\to 0$ and $\Delta\to 1$ (or $g_{12}\to\sqrt{g_1g_2}$, i.e in the vicinity of the phase separation), the functions $f_j(1,0)$ are diverging and become complex for $\Delta<1$.

For our simulations we consider the above ^{87}Rb-^{87}Rb mixture in two different internal states with the following parameters: $a_1 = 100.4\,a_0$, $a_2 = 95.44\,a_0$, and $n_1 = n_2 = 10^{21}$ m^{-3}.

The behavior of the disorder functions f_j versus the interspecies interactions and the disorder correlation length is displayed in figure 3.4. We see that for $\sigma<\xi_j$, the effects of the disorder fluctuations are important. Whereas they vanish in the case of $\sigma>\xi_j$ for any value of interspecies interactions leading to arrest the localization in both species. For fixed $\sigma<\xi_j$, the disorder functions f_j decrease with a_{12} and diverge near the vicinity of the transition between the miscible and immiscible phases

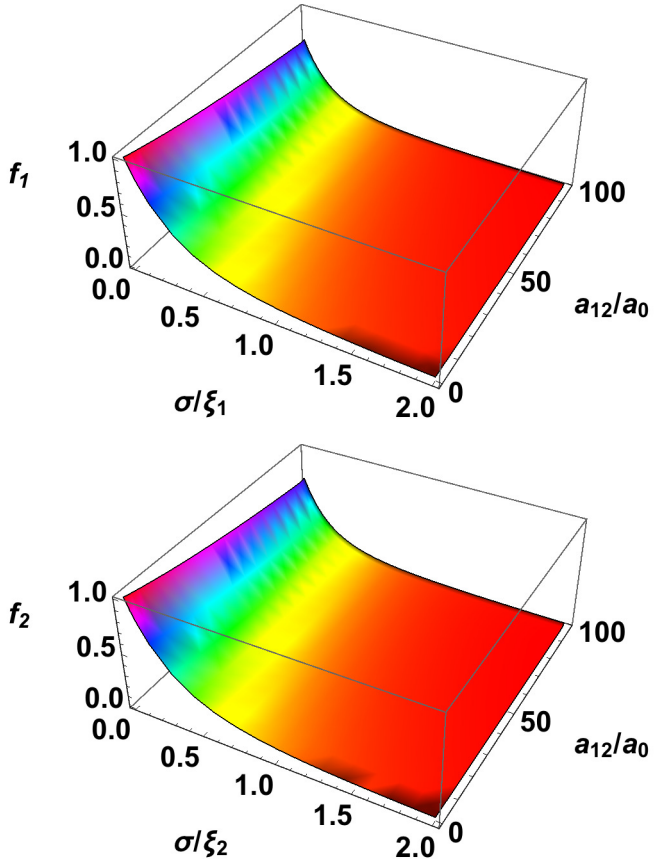

Figure 3.4: Behavior of the disorder functions f_j as a function of the interspecies interaction strength a_{12} and the disorder correlation length σ for ^{87}Rb-^{87}Rb mixture in two different internal states. Parameters are: $a_1 = 100.4\,a_0$ and $a_2 = 95.44\,a_0$ [159], and the densities: $n_1 = n_2 = 10^{21}\mathrm{m}^{-3}$.

$(a_{12} \simeq 98a_0)$.

The chemical potential of each component can be obtained from integral (3.18), which gives

$$\mu_j = g_j n_j + g_{12} n_{\bar{j}} + g_j n_{j\mathrm{HM}} h_j(\Delta, \sigma_j), \tag{3.37}$$

The disorder functions $h_j(\Delta, \sigma_j)$ associated with the EoS read:

$$h_j(\Delta, \sigma_j) = \left(\frac{\Delta}{\Delta - 1}\right)\left(H_{1j}(\Delta, \sigma_j) + \frac{g_{12} n_{\bar{j}}}{n_j g_j} H_{2j}(\Delta, \sigma_j)\right), \tag{3.38}$$

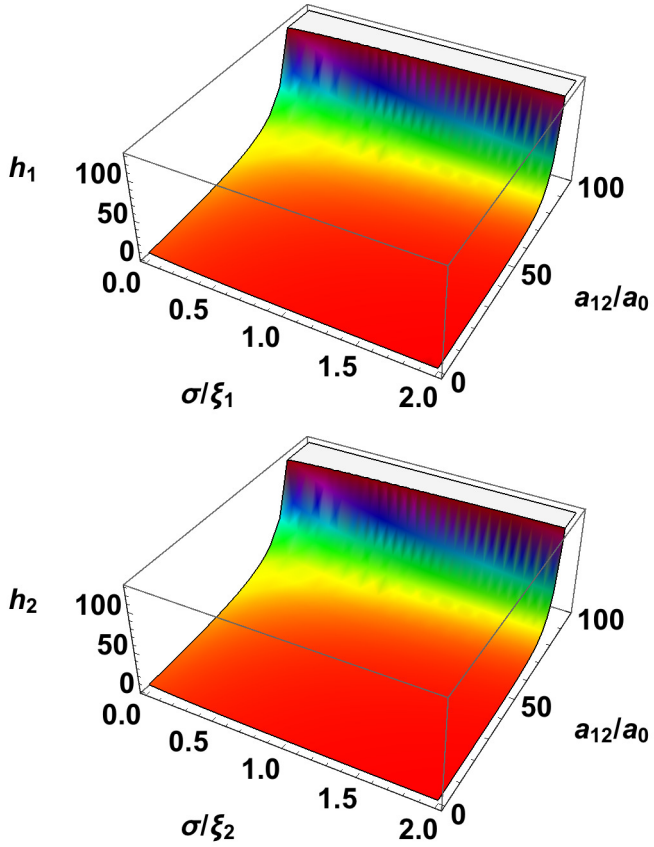

Figure 3.5: Behavior of the disorder functions h_j as a function of the interspecies interaction strength a_{12} and the disorder correlation length for ^{87}Rb-^{87}Rb mixture. Parameters are the same as in Fig.3.4.

where:

$$H_{1j}(\Delta,\sigma_j)=\frac{4\sqrt{2/\pi}}{(\alpha_j-\beta_j)^3}\Bigg\{$$
$$\frac{2\sigma_j(\alpha_j-\beta_j)}{\alpha_j\beta_j}\left[-\alpha_j\beta_j\left[8\bar{\mu}_j^2+\alpha_j^2+\beta_j^2-4\bar{\mu}_j(\alpha_j+\beta_j)\right]-8\bar{\mu}_j\alpha_j\beta_j+(\alpha_j+\beta_j)\left(4\bar{\mu}_j^2+\alpha_j\beta_j\right)\right]$$
$$+\frac{\sqrt{\pi}}{\alpha_j^{3/2}}e^{\sigma_j^2\alpha_j}(\alpha_j-2\bar{\mu}_j)\left[2\bar{\mu}_j\left[\alpha_j\left(-5+2\sigma_j^2(\alpha_j-\beta_j)\right)+\beta_j\right]+\alpha_j\left[\alpha_j-2\sigma_j^2\alpha_j(\alpha_j-\beta_j)+3\beta_j\right]\right.$$
$$\left.+\alpha_j\left[\alpha_j\left(\alpha_j+2\sigma_j^2\alpha_j(\alpha_j-\beta_j)-5\beta_j\right)+2\bar{\mu}_j\left(\beta_j+\alpha_j\left(3-2\sigma_j^2(\alpha_j-\beta_j)\right)\right)\right]\right]\operatorname{erfc}\left(\sqrt{\sigma_j^2\alpha_j}\right)$$
$$-\frac{\sqrt{\pi}}{\beta_j^{3/2}}e^{\sigma_j^2\beta_j}(\beta_j-2\bar{\mu}_j)\left[2\bar{\mu}_j\alpha_j+\beta_j\left[2\bar{\mu}_j\alpha_j+3\alpha_j-2\bar{\mu}_j\left(5+2\sigma_j^2\alpha_j\right)\right]+\beta_j^2\left[1+6\bar{\mu}_j+4\bar{\mu}_j\sigma_j^2+\right.\right.$$
$$\left.\left.\alpha_j\left(-5+2\sigma_j^2(1+2\bar{\mu}_j)\right)\right]-\beta_j^3\left[-1+2\sigma_j^2(1+2\bar{\mu}_j+\alpha_j)\right]+2\sigma_j^2\beta_j^4\right]\operatorname{erfc}\left(\sqrt{\sigma_j^2\beta_j}\right)\Bigg\},$$

and

$$H_{2j}(\Delta,\sigma_j)=\frac{2\sqrt{2/\pi}}{(\alpha_j\beta_j)^{3/2}(\alpha_j-\beta_j)^3}\Bigg\{-2\sigma_j\sqrt{\alpha_j\beta_j}(\alpha_j-\beta_j)\left[2\alpha_j\beta_j\left[8+\alpha_j^2+\beta_j^2-4(\alpha_j+\beta_j)\right]\right.$$
$$\left.-2\bar{\mu}_j\left[-8\alpha_j\beta_j+(\alpha_j+\beta_j)(4+\alpha_j\beta_j)\right]\right]+\sqrt{\pi}e^{\sigma_j^2\alpha_j}\beta_j^{3/2}(\alpha_j-2)\left[\alpha_j\left[4\sigma_j^2\alpha_j^3+6\beta_j\bar{\mu}_j\right.\right.$$
$$\left.-2\alpha_j^2\left(-1+2\sigma_j^2(\beta_j+\bar{\mu}_j)\right)+\alpha_j\left(2\beta_j\left(-5+2\sigma_j^2\bar{\mu}_j\right)+2\bar{\mu}_j\right)\right]+2\left[-4\sigma_j^2\alpha_j^3+2\beta_j\bar{\mu}_j\right.$$
$$\left.\left.+2\alpha_j^2\left(3+2\sigma_j^2(\beta_j+\bar{\mu}_j)\right)+2\alpha_j\left(\beta_j-5\bar{\mu}_j-2\sigma_j^2\beta_j\bar{\mu}_j\right)\right]\right]\operatorname{erfc}\left(\sqrt{\sigma_j^2\alpha_j}\right)$$
$$+\sqrt{\pi}e^{\sigma_j^2\beta_j}\alpha_j^{3/2}(2-\beta_j)\left[4\beta_j\left[\alpha_j+2\sigma_j^2\alpha_j\beta_j+\beta_j\left(3-2\sigma_j^2\beta_j\right)\right]+4\bar{\mu}_j\left[\alpha_j-2\sigma_j^2\alpha_j\beta_j+\beta_j\left(-5+2\sigma_j^2\beta_j\right)\right.\right.$$
$$\left.\left.+\beta_j\left[\beta_j\left(2\beta_j\left(1+2\sigma_j^2(\beta_j-\bar{\mu}_j)\right)+2\bar{\mu}_j\right)+2\alpha_j\left(3\bar{\mu}_j+\beta_j\left(-5-2\sigma_j^2(\beta_j-\bar{\mu}_j)\right)\right)\right]\right]\operatorname{erfc}\left(\sqrt{\sigma_j^2\beta_j}\right)\Bigg\}$$
$$+\frac{4\sqrt{2/\pi}}{(\beta_j-\alpha_j)^3}\Bigg\{2\sigma_j(\alpha_j-\beta_j)\left[\alpha_j^2+\beta_j^2-2\bar{\mu}_j(\alpha_j+\beta_j)\right]$$
$$+\sqrt{\pi}\sqrt{\alpha_j}e^{\sigma_j^2\alpha_j}\left[2\sigma_j^2\alpha_j^3+\alpha_j^2\left[1-2\sigma_j^2(\beta_j+2\bar{\mu}_j)\right]+6\beta_j\bar{\mu}_j+\alpha_j\left[-5\beta_j+2\bar{\mu}_j+4\sigma_j^2\beta_j\bar{\mu}_j\right]\right]$$
$$\times\left[-1+\operatorname{erf}\left(\sqrt{\sigma_j^2\alpha_j}\right)\right]+\sqrt{\pi}\sqrt{\beta_j}e^{\sigma_j^2\beta_j}\left[\beta_j\left[\beta_j+2\sigma_j^2\beta_j(\beta_j-2\bar{\mu}_j)+2\bar{\mu}_j\right]\right.$$
$$\left.+\alpha_j\left[6\bar{\mu}_j+\beta_j\left(-5-2\sigma_j^2(\beta_j-2\bar{\mu}_j)\right)\right]\right]\operatorname{erfc}\left(\sqrt{\sigma_j^2\beta_j}\right)\Bigg\}.$$

Again in the limit $\sigma\to 0$, the disorder corrections to the EoS h_j reduces to that obtained for the delta-correlated disorder (3.21). For $\sigma\to 0$ and $\Delta\to\infty$ (or $g_{12}\to 0$, equivalently), one has $h_j(\infty,0)=6$ hence, the EoS (3.37) simplifies to that of a single component BEC namely; $\mu=gn(1+12\pi R'\sqrt{na^3/\pi})$ found in Refs.[141, 158, 160]. Figure 3.5 depicts that functions h_j are increasing with the interspecies interactions strength a_{12} results in an enhancement of the total chemical potential.

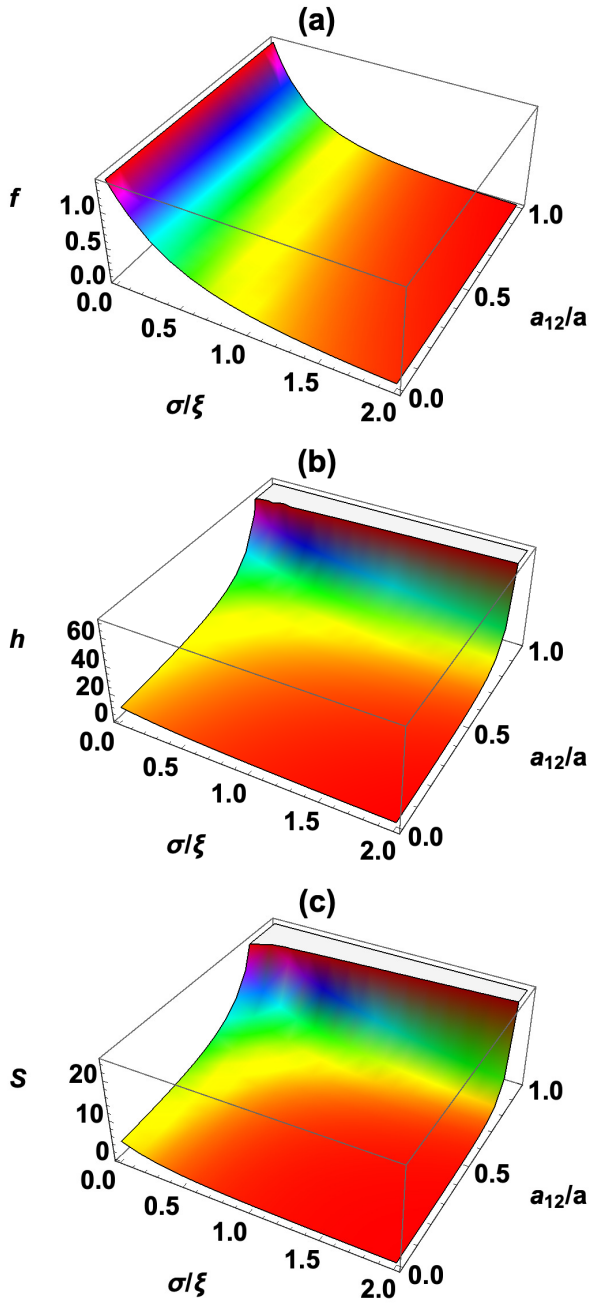

Figure 3.6: Behavior of the disorder functions f from Eq.(3.40) (a), h from Eq.(3.43) (b), and S from equation (3.46) (c) as a function of σ/ξ and a_{12}/a.

The symmetric case

To simplify the expressions we restrict ourselves to the case of a symmetric mixture where $a_1 = a_2 = a$ and $n_1 = n_2 = n$. the glassy fraction turns out to be given:

$$\frac{n_R}{n} = \frac{\xi_+}{\ell_L} f\left(\frac{\sigma}{\xi_+}\right), \tag{3.39}$$

where the disorder function reads

$$f\left(\frac{\sigma}{\xi_+}\right) = \sqrt{2} e^{\frac{\sigma^2}{\xi_+^2}} \left(\frac{2\sigma^2}{\xi_+^2} + 1\right) \operatorname{erfc}\left(\frac{\sigma}{\xi_+}\right) - \frac{2\sqrt{2}\sigma}{\sqrt{\pi}\xi_+}, \tag{3.40}$$

where $\operatorname{erfc}(x)$ is the complementary error function, $\xi_+ = \xi/\sqrt{\delta a_+}$ is the extended healing length for a symmetric mixture with short-range interactions, $\xi = \hbar/\sqrt{2mng}$, $\delta a_+ = 1 + a_{12}/a$, and $\ell_L = 4\pi\hbar^4/(m^2 R_0)$ accounts for the Larkin length which is associated with the pinning energy due to the disorder [160, 162, 163]. For $\sigma \to 0$, $f(0) = \sqrt{2}$, thus, the results of binary BECs with a weak delta-correlated disorder are recovered equation (3.20). For $\sigma \to 0$ and $a_{12} = 0$, one can reproduce the seminal HM findings for a dirty single BEC [140].

The behavior of the function (3.40) is shown in figure 3.6 (a). As expected, the function f is decreasing with the disorder correlation length σ/ξ regardless of the strength of interspecies interactions indicating that the condensate depletion due to the disorder effects is suppressed for $\sigma \gg \xi$. One might explain this delocalization as the results of a screening of disorder by interspecies interaction. The same situation takes place in single dirty dipolar and nondipolar BECs [76, 78, 100, 164, 165]. For fixed σ, n_R is decreasing with the interspecies interactions a_{12}/a.

The validity of the present perturbation theory requires to have the condensate depletion due to the disorder much smaller than the total density $n_R \ll n$. This implies that to have a weak disorder potential, the following condition must be

fulfilled

$$\ell_L \gg \xi_+ f\left(\frac{\sigma}{\xi_+}\right). \tag{3.41}$$

Equation (3.41) is a natural extension of the result of [162].

For the EoS in second-order of the disorder strength, we find:

$$\mu = ng\Big[\delta a_+ + \frac{\xi_-}{\ell_L} h\left(\delta a_\pm, \frac{\sigma}{\xi\pm}\right)\Big], \tag{3.42}$$

where the disorder functions read:

$$\begin{aligned} h\left(\delta a_\pm, \frac{\sigma}{\xi_\pm}\right) =& \frac{\sqrt{\frac{2}{\pi}}}{\delta a_-}\Bigg\{ \left(\frac{\sigma}{\xi_-}\right)\left[\frac{(\delta a_+ - \delta a_-)^2}{2\delta a_+ \delta a_-} - 2\right] + \frac{\sqrt{\pi\delta a_-}}{(\delta a_+ - \delta a_-)}\Big(A_- - A_+\Big) \\ &+ \frac{1}{\delta a_+}\Big[2\left(\frac{\sigma}{\xi_-}\right)(\delta a_- - \delta a_+) + \sqrt{\pi\delta a_-}\Big(B_+ - B_-\Big)\Big]\Bigg\}, \end{aligned} \tag{3.43}$$

where $\xi_- = \xi/\delta a_-$, $\delta a_- = 1 - a_{12}/a$, and

$$\begin{aligned} A_\pm =& \frac{e^{(\sigma/\xi_\pm)^2}}{(\delta a_\pm)^{3/2}} \mathrm{erfc}\left(\frac{\sigma}{\xi_\pm}\right)\Bigg[7 + \left(\frac{\sigma}{\xi_\mp}\right)^2 - \left(\frac{\sigma}{\xi_\pm}\right)^2 - 9\delta a_\pm \\ &- \frac{(\delta a_\mp - \delta a_\pm)^2}{4}\left(6 + \left(\frac{\sigma}{\xi_\mp}\right)^2 + 5\left(\frac{\sigma}{\xi_\pm}\right)^2\right)\Bigg], \end{aligned}$$

$$B_\pm = \sqrt{\delta a_\pm}\left[3 + 2\left(\frac{\sigma}{\xi\pm}\right)^2\right] e^{(\sigma/\xi_\pm)^2} \mathrm{erfc}\left(\frac{\sigma}{\xi_\pm}\right).$$

In the limit $\sigma \to 0$, one has:

$$\begin{aligned} h_{\sigma\to 0} =& \frac{1}{\sqrt{2}\sqrt{\delta a_-}\left(\frac{a_{12}}{a}\right)\left(1 - \left(\frac{a_{12}}{a}\right)^2\right)^{3/2}}\Bigg\{2\left(\sqrt{\delta a_-} - \sqrt{\delta a_+}\right) - 3\left(\frac{a_{12}}{a}\right)^2\left(\sqrt{\delta a_-} - 5\sqrt{\delta a_+}\right) \\ &-12\left(\frac{a_{12}}{a}\right)^3\left(\sqrt{\delta a_-} + \sqrt{\delta a_+}\right) + \left(\frac{a_{12}}{a}\right)\left(13\sqrt{\delta a_-} + \sqrt{\delta a_+}\right)\Bigg\} \end{aligned}$$

which is in agreement with the equation (3.22). Evidently, equation (3.42) shows that the EoS increases linearly with the disorder strength R_0. Figure 3.6 (b) shows

that the disorder function h is lowering with σ/ξ and rising with a_{12}/a. This signals that the interplay of the disorder effects and interspecies interaction could modify the behavior of the EoS of Bose mixtures.

Sound velocity

Corrections to the sound velocity of each component due to the disorder fluctuations are given by [102]:

$$c_{sj}^2 = \frac{n_j}{m_j}\frac{\partial \mu_j}{\partial n_j}. \tag{3.44}$$

In the case of a balanced mixture $a_1 = a_2 = a$ and $n_1 = n_2 = n$, we find after a straightforward calculation:

$$\frac{c_s^2}{c_{s0}^2} = 1 + \frac{\xi_-}{\ell_L} S\left(\delta a_\pm, \frac{\sigma}{\xi\pm}\right), \tag{3.45}$$

where $c_{s0} = \sqrt{gn/m}$ is the zeroth-order sound velocity and the disorder function $S(\delta a_\pm, \sigma/\xi\pm)$ is given as:

$$S(\delta a_\pm, \frac{\sigma}{\xi\pm}) = \frac{1}{2}\left(h + 2n\frac{\partial h}{\partial n}\right), \tag{3.46}$$

which has practically the same behavior as the function h as is displayed in figure 3.6(c).

3.4 Non-equilibrium evolution

The considerable interest in studying the dynamics of disordered BEC driven out-of-equilibrium by slow (adiabatic) or sudden (quenched) changes to system parameters such as the scattering length has been boosted by remarkable advances in the tunability of ultracold atomic gases [83, 124, 134, 166, 167]. Non-equilibrium evolution of BEC offers the unique opportunity to explore strongly correlated systems and transport in realistic physical systems. Chen et al.[168] have shown that for a weakly

non-equilibrium disordered Bose gas under a quantum quench in the interaction the disorder can substantially destroy superfluidity more than the condensate leading to the so-called dynamical Bose glass. Recent study demonstrates that the condensate deformation is a signature of the non-equilibrium feature of steady states of a Bose gas in a temporally controlled weak disorder [162]. Quite recently, experimental realization of ultracold bosonic gases in dynamic disorder with controlled correlation time have been reported in Ref.[169], where the microscopic origin of friction and dissipation has been well illustrated.

In this section we study the non-equilibrium evolution of binary BECs in the presence of a weak random potential with Gaussian correlation function using the time-dependent perturbation theory. The theory assumes weak interactions and weak disorder, hence it remains valid provided the depletion remains small throughout the full subsequent dynamics. We then apply the time-dependent perturbation theory to construct a closed set of equations that highlight the role of the spectacular interplay between the disorder and the interspecies interactions in the time evolution of the density induced by disorder in each component.

Let us consider two weakly interacting ultracold Bose gases subjected to a weak random potential $U(\mathbf{r},t) = u(\mathbf{r})F(t)$, such that $F(0) = 0$ and $0 \leq F(t) \leq 1$. The system evolution at $t \geq 0$ is described by the coupled time-dependent GPE which can be written as:

$$i\hbar\frac{\partial}{\partial t}\Phi_j(\mathbf{r},t) = \bigg(-\frac{\hbar^2}{2m}\nabla^2 + u(\mathbf{r})F(t) - \mu_{0j} + g_j|\Phi_j(\mathbf{r},t)|^2 + g_{12}|\Phi_{\bar{j}}(\mathbf{r},t)|^2 \bigg)\Phi_j(\mathbf{r},t). \tag{3.47}$$

For sufficiently small $u(\mathbf{r})$, the system can be treated perturbatively. Therefore, we can write the wavefunctions as:

$$\Phi_j(\mathbf{r},t) = \Phi_j^{(0)}(\mathbf{r}) + \Phi_j^{(1)}(\mathbf{r},t) + \Phi_j^{(2)}(\mathbf{r},t) + \cdots, \tag{3.48}$$

where $\Phi_j^{(0)}(\mathbf{r})$ are the equilibrium solutions of equation (3.1) at $t = 0$, and $\Phi_j^{(\alpha)}(r, 0) = 0$ for $\alpha \geq 1$. The particle densities $n_j = |\Phi_j(r)^{(0)}|^2$ determine the chemical potentials of the system in its equilibrium ground-state:

$$\mu_{0j} = g_j n_j + g_{12} n_{\bar{j}}. \tag{3.49}$$

The condensate deformation due to the disorder potential, can be given by

$$n_{Rj}(t) = \langle |\Phi_j(\mathbf{r}, t)|^2 \rangle - |\langle \Phi_j(\mathbf{r}, t) \rangle|^2. \tag{3.50}$$

Using the perturbative expansion (3.48) up to second-order, and assume that the disorder have a vanishing ensemble averages the deformation of each BEC becomes:

$$n_{Rj}(t) = \langle |\Phi_j^{(1)}(\mathbf{r}, t)|^2 \rangle. \tag{3.51}$$

The first-order coupled equations follow from equation (3.47) read:

$$\begin{aligned}
i\hbar \frac{\partial}{\partial t} \Phi_j^{(1)}(\mathbf{r}, t) &= \left(-\frac{\hbar^2}{2m} \nabla^2 + g_j n_j \right) \Phi_j^{(1)}(\mathbf{r}, t) + g_j n_j \Phi_j^{(1)*}(\mathbf{r}, t) + \sqrt{n_j} u(\mathbf{r}) f(t) \\
&\quad + g_{12} \sqrt{n_j n_{\bar{j}}} \left[\Phi_{\bar{j}}^{(1)}(\mathbf{r}, t) + \Phi_{\bar{j}}^{(1)*}(\mathbf{r}, t) \right], \\
-i\hbar \frac{\partial}{\partial t} \Phi_j^{(1)*}(\mathbf{r}, t) &= \left(-\frac{\hbar^2}{2m} \nabla^2 + g_j n_j \right) \Phi_j^{(1)*}(\mathbf{r}, t) + g_j n_j \Phi_j^{(1)}(\mathbf{r}, t) + \sqrt{n_j} u(\mathbf{r}) f(t) \\
&\quad + g_{12} \sqrt{n_j n_{\bar{j}}} \left[\Phi_{\bar{j}}^{(1)}(\mathbf{r}, t) + \Phi_{\bar{j}}^{(1)*}(\mathbf{r}, t) \right].
\end{aligned} \tag{3.52}$$

Working in Fourier space and using the Laplace transform

$$L[f](s) = \int_0^\infty dt\, f(t) e^{-st}, \tag{3.53}$$

equations (3.52) turn out to be given as:

$$\begin{aligned}
&(\hbar\omega_{\mathbf{k}} + g_j n_j - i\hbar s)\,\Phi_j^{(1)}(\mathbf{k},s) + g_j n_j \Phi_j^{(1)*}(\mathbf{k},s) + g_{12}\sqrt{n_j n_{\bar{j}}}\left[\Phi_{\bar{j}}^{(1)}(\mathbf{k},s) + \Phi_{\bar{j}}^{(1)*}(\mathbf{k},s)\right] \\
&= -\sqrt{n_j}u(\mathbf{k})f(s), \\
&(\hbar\omega_{\mathbf{k}} + g_j n_j + i\hbar s)\,\Phi_j^{(1)*}(\mathbf{k},s) + g_j n_j \Phi_j^{(1)}(\mathbf{k},s) + g_{12}\sqrt{n_j n_{\bar{j}}}\left[\Phi_{\bar{j}}^{(1)}(\mathbf{k},s) + \Phi_{\bar{j}}^{(1)*}(\mathbf{k},s)\right] \\
&= -\sqrt{n_j}u(\mathbf{k})f(s),
\end{aligned} \tag{3.54}$$

where $\hbar\omega_{\mathbf{k}} = E_k$ is the kinetic energy. Here we have made the identification $L[F](s) = f(s)$, for brevity of notation [162].

The solution of equations (3.54) reads

$$\begin{aligned}
\Phi_j^{(1)}(\mathbf{k},s) &= -\sqrt{n_j}u(\mathbf{k})f(s)\frac{(\omega_{\mathbf{k}} + is)\left[2g_{12}n_{\bar{j}}\omega_{\mathbf{k}} - \hbar(\Omega_{\mathbf{k}\bar{j}}^2 + s^2)\right]}{4g_{12}^2 n_j n_{\bar{j}}\omega_{\mathbf{k}}^2 - \hbar^2(\Omega_{\mathbf{k}\bar{j}}^2 + s^2)(\Omega_{\mathbf{k}j}^2 + s^2)}, \\
\Phi_j^{(1)*}(\mathbf{k},s) &= -\sqrt{n_j}u(\mathbf{k})f(s)\frac{(\omega_{\mathbf{k}} - is)\left[2g_{12}n_{\bar{j}}\omega_{\mathbf{k}} - \hbar(\Omega_{\mathbf{k}\bar{j}}^2 + s^2)\right]}{4g_{12}^2 n_j n_{\bar{j}}\omega_{\mathbf{k}}^2 - \hbar^2(\Omega_{\mathbf{k}\bar{j}}^2 + s^2)(\Omega_{\mathbf{k}j}^2 + s^2)},
\end{aligned} \tag{3.55}$$

where $\hbar\Omega_{\mathbf{k}j} = \sqrt{\hbar\omega_{\mathbf{k}}(\hbar\omega_{\mathbf{k}} + 2g_j n_j)}$ is the standard dispersion relation for a single BEC. Using the inverse Laplace transform we get:

$$\begin{aligned}
\Phi_j^{(1)}(\mathbf{k},t) &= -\frac{\sqrt{n_j}}{\hbar}u(\mathbf{k})\int_0^t dt^{'}\mathcal{K}_j(\mathbf{k},t-t^{'})f(t^{'}), \\
\Phi_j^{(1)*}(\mathbf{k},t) &= -\frac{\sqrt{n_j}}{\hbar}u(\mathbf{k})\int_0^t dt^{'}\mathcal{K}_j^{*}(\mathbf{k},t-t^{'})f(t^{'}),
\end{aligned} \tag{3.56}$$

where

$$\mathcal{K}_j(k,t) = \frac{\mathcal{K}_{j-}(k,t) - \mathcal{K}_{j+}(k,t)}{(\Omega_{kj+}^2 - \Omega_{kj-}^2)}, \tag{3.57}$$

and

$$\mathcal{K}_{j\pm}(k,t) = \left[i\cos(\Omega_{kj\pm}t) + \frac{\omega_{kj}}{\Omega_{kj\pm}}\sin(\Omega_{kj\pm}t)\right]\left[\Omega_{k\bar{j}}^2 - \Omega_{kj\pm}^2 - \frac{2g_{12}n_{\bar{j}}\omega_{k\bar{j}}}{\hbar}\right],$$

where the Bogoliubov spectrum of two-component BECs is given as (see e.g [29] and

references therein):

$$\Omega_{k\pm} = \sqrt{\omega_k^2 + k^2 c_{s\pm}^2}, \tag{3.58}$$

with

$$c_{s\pm}^2 = \left(c_{s1}^{(0)2}/2\right)\left[1 + \bar{\mu} \pm \sqrt{(1-\bar{\mu})^2 + 4\Delta^{-1}\bar{\mu}}\right],$$

being the sound velocities in the density (c_{s-}) and spin (c_{s+}) channels, and $\bar{\mu}_j = n_{\bar{j}} g_{\bar{j}}/n_j g_j$.

In the limit $k \to 0$, the total dispersion is phonon-like $\Omega_{k\pm} = c_{s\pm}k$.

Using the fact that $\langle \Phi_j^{(1)*}(\mathbf{k}, t)\rangle = 0$, the time-dependent disorder densities (3.50) take the form:

$$n_{R_j}(t) = \frac{n_j}{\hbar^2}\int \frac{d\mathbf{k}}{(2\pi)^3} R(\mathbf{k}) \left| \int_0^t dt' \mathcal{K}_j(\mathbf{k}, t-t') f(t') \right|^2. \tag{3.59}$$

To exemplify outrightly the form of the density (3.59), let us suppose a time-periodic disorder potential which is abruptly switched on at time $t = 0$

$$F(t) = \frac{1}{2}\left[1 - \cos(\omega t)\right]. \tag{3.60}$$

Therefore, the system earns a new stationary state as we shall see hereafter.

For a symmetric mixture where $a_1 = a_2 = a$ and $n_1 = n_2 = n$, the Boboliubov spectrum (3.59) reduces to the following dimensionless form:

$$\Omega_{k\pm} = \Omega_0(k\xi)\sqrt{(k\xi)^2 + 2(1 \pm a_{12}/a)}, \tag{3.61}$$

where $\Omega_0 = ng/\hbar$ is the inverse characteristic mean-field time scale. It is clearly seen that for $a_{12}/a > 1$, the spectrum associated with the density channel Ω_{k-} becomes complex leading to destabilize the system. Whereas for $a_{12}/a < -1$, the spectrum Ω_{k+} may become imaginary and thus, the mxiture would be destabilized.

Inserting equations (3.61) and (3.57) into equation (3.59), and keeping in mind

that terms associated with Ω_{k-} cancel, one finds for $n_R(t)$:

$$n_R(t) = \frac{n}{4\hbar^2}\int \frac{d\mathbf{k}}{(2\pi)^3}\frac{R(\mathbf{k})}{\Omega_{\mathbf{k}+}^4\left(\Omega_{\mathbf{k}+}^2-\omega^2\right)^2}\Big\{\omega^2\Omega_{\mathbf{k}+}^2\left[\Omega_{\mathbf{k}+}\sin(\omega t)-\omega\sin(\Omega_{\mathbf{k}+}t)\right]^2 + \omega_{\mathbf{k}}^2\left[\omega^2-\Omega_{\mathbf{k}+}^2+\Omega_{\mathbf{k}+}^2\cos(\omega t)-\omega^2\cos(\Omega_{\mathbf{k}+}t)\right]^2\Big\}. \tag{3.62}$$

This equation tells us that once the depletion due to disorder is known at $t = 0$, both the condensed density $n - n_R$ and n_R can be calculated in a somehow simpler way at time $t > 0$. For a given k and $\omega > 0$, the density (3.62) is peaked "resonant" at frequencies $\Omega_{k+} = \omega$ (i.e. when the external frequency nearly matches the eigenfrequencies). In terms of momenta this condition yields

$$k = k_{\text{res}} = \frac{mc_s\sqrt{1+a_{12}/a}}{\hbar\sqrt{-2+2\sqrt{1+\hbar^2\omega^2/m^2c_s^4(1+a_{12}/a)^2}}}.$$

For $k \geq k_{\text{res}}$, the disorder depletion becomes very large, $n_R(t)/n \gg 1$, indicating that the perturbation theory is no longer valid in such an unstable regime despite the fact that the disorder is naively weak. Therefore, the intuitive stability criterion reads $k < k_{\text{res}}$.

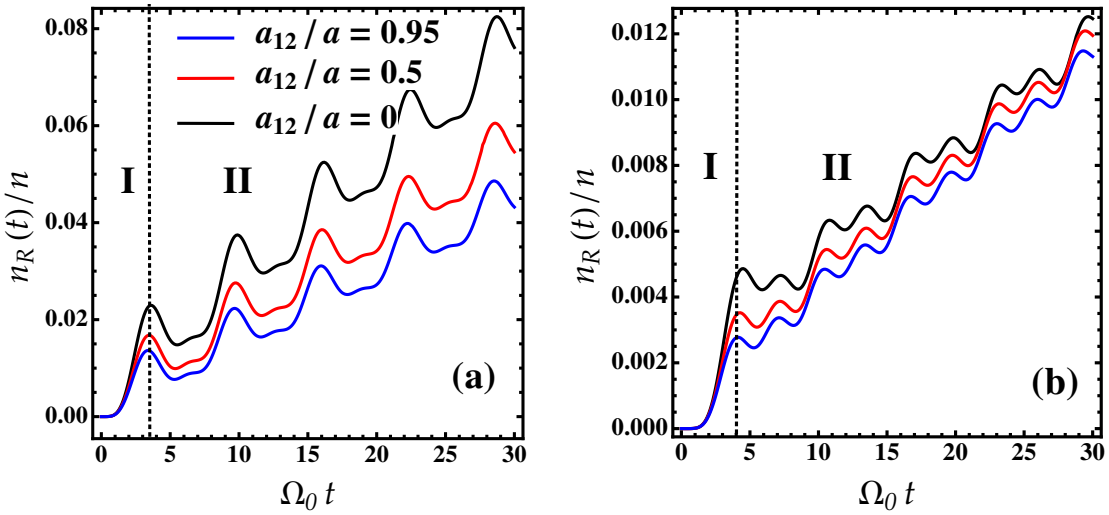

Figure 3.7: (a) Time evolution of the disorder fraction from Eq.(3.31) for different values of a_{12}/a. Parameters are : $a/a_0 = 95.44$, $n = 10^{21}\text{m}^{-3}$, $R' = 0.5$, $\omega/\Omega_0 = 1$, (a) $\sigma/\xi = 0.2$, and (b) $\sigma/\xi = 2$. Here $R' = R_0/g^2n$. There are two different regimes: I and II delineated by a vertical dotted line.

In order to substantiate the relevance of the above time-dependent perturbative mean-field approach for laboratory experiments, we consider the ^{87}Rb-^{87}Rb mixture in two different internal states, but our theory can be readily generalized to other mixtures. The scattering lengths and the densities are chosen to $a_1 = a_2 = a = 95.44\, a_0$ [159] with a_0 being the Bohr radius, and $n_1 = n_2 = n = 10^{21}$ m^{-3}, respectively, which are sufficient to ensure that the system meets the requirement of weakly interacting gas, $\sqrt{na^3} \simeq 10^{-2} \ll 1$.

The interspecies scattering length a_{12} which can be adjusted via Feshbach resonance is selected in such a way that the phase-separated condition is fulfilled throughout the dynamics. The disorder strength is fixed to be $R' = 0.5$ which gives $n_R/n \leq 1\%$, ensuring the sufficient criterion for the weak disorder regime. We employ various disorder driving frequencies and correlation lengths.

The numerical solutions of equation (3.62) is shown in figure 3.7. One can clearly identify two phases of evolution: In phase I, $\Omega_0 t \leq 4$, although the density $n_R(t)$ is somehow low, the dynamics follows an exponential growth due to the considerable effect of both quasiparticles and disorder onto the two BECs. In region II, $\Omega_0 t > 4$, we observe that as the disorder evolves in time, the glassy fraction increases and exhibits sinusoidal oscillations signaling that the system being completely depleted at a long time. This can be attributed to the motion of the Gaussian disorder which may create elementary excitations (i.e. the Bogoliubov phonons at low momenta/free particle in the high-energy regime) leading to enhance the disorder depletion. Therefore, whatever the strength and the frequency of the disordered potential, the condensates are localized since $n_R(t)$ extends to infinity at long times. In this region, the dynamics slightly slows down without any saturation and it presumably follows another growth law. It is worth noticing that a very similar change in behavior has been observed in the dynamics of periodically-driven BEC in a shaken 1D lattice [170].

Besides, it is clearly visible that in the case of $\sigma < \xi$, the time-dependent glassy

fraction is increasing with decreasing the interspecies interactions (see figure 3.7.(a)). Whereas for $\sigma > \xi$, $n_R(t)$ varies with small oscillations and remains almost insensitive to a_{12}/a which means that the disorder density is protected against interspecies interactions effects during its time evolution (see figure 3.7. (b)). Furthermore, as the healing length ξ decreases, the chemical potential rises and the density of two BECs n grows. In this situation the low-lying excitations are poorly affected by the disorder time evolution, gives rise to lower the glassy fraction.

In figure 3.8 we present the time evolution of the disorder fraction as a function of the relevant parameters. We see that at short times $\Omega_0 t \leq 4$ the atoms are almost delocalized i.e. $n_R(t)$ is vanishingly small. Whereas, $n_R(t)$ is increasing as the time goes on which implies a possibility for reducing the condensed fraction whatever the values of σ/ξ, ω/Ω_0, and a_{12}/a. The dynamics slows down significantly for small external frequencies $\omega < \Omega_0$, relatively strong interspecies interactions $a_{12} \geq 0.5a$ and for large disorder correlation $\sigma > \xi$ as is displayed in figures 3.8.(a), (b) and (c). Figures 3.8. (a) and (c) depict also that the oscillation strength of the condensate deformation strongly depends on σ/ξ and ω/Ω_0.

Most noteworthy, for fixed $\sigma > \xi$ and varying the ratio ω/Ω_0, the density $n_R(t)$ remains practically constant in time for $\Omega_0 t \geq 10$, apart from tenuous wigglings (see figure 3.8. (c)) which could be an indicator of the existence of stationary Floquet condensates [171, 172]. Frankly speaking, a qualitative analysis of these Floquet states in the presence of such periodic perturbations requires further thoughts.

One can expect that in the regime of a strong disorder, each component fragments into a number of low-energy, localized single-particle states with no gauge symmetry breaking forming the so-called Bose glass phase. The exploration of such a regime would need either a non-perturbative approach or Quantum Monte Carlo simulations. We believe that our study not only bridges the gap between superfluidity, interactions and disorder but also it is important from the viewpoint of elucidating the localization phenomenon and transport of two bosonic species.

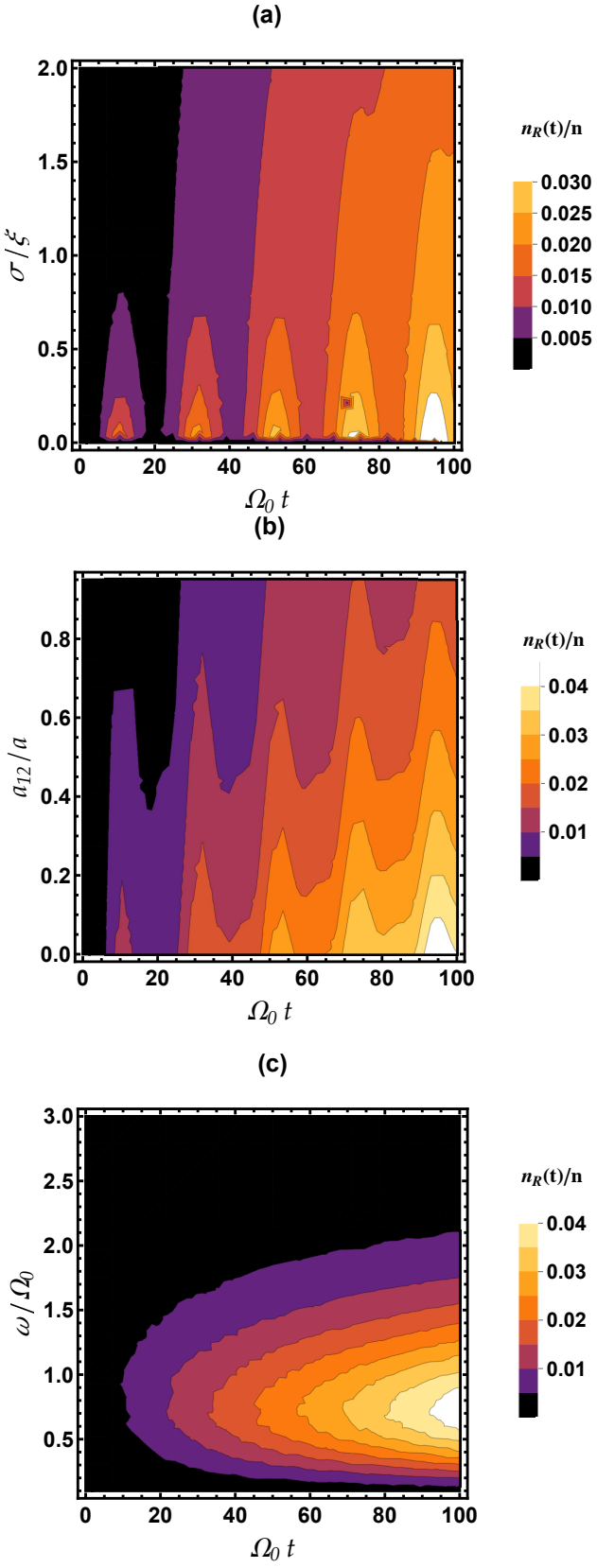

Figure 3.8: (a) Disorder fraction $n_R(t)/n$ from Eq.(3.62) as a function of $\Omega_0 t$ and σ/ξ for $a_{12}/a = 0.5$ and $\omega/\Omega_0 = 0.3$. (b) $n_R(t)/n$ as a function of $\Omega_0 t$ and a_{12}/a for $\sigma/\xi = 0.5$ and $\omega/\Omega_0 = 0.3$. (c) $n_R(t)/n$ as a function of $\Omega_0 t$ and ω/Ω_0 for $\sigma/\xi = 1.8$ and $a_{12}/a = 0.5$. Parameters are the same as in Fig.3.7.

Chapter 4

Self-bound droplets in weak three-dimensional random potentials

Studying quantum droplets in disordered potentials is an important area of research in the field of quantum physics. Investigating the behavior of disordered self-bound liquids contributes to fundamental research, offering a deeper understanding of many-body quantum systems, phase transitions, and the emergence of complex phenomena in strongly correlated systems.

Common wisdom is that the presence of an external random potential always enhance the escape of atoms from the condensate yielding a fragmentation of the condensate due to the formation of mini BECs in the minima of the random landscape. For sufficiently strong disorder the condensate turns out to be completely destroyed as all bosons are localized in the minima of the random potential. A critical issue of great importance is: how do disorder potentials affect the formation, the stability and the dynamics of a self-bound quantum droplet? Answering this question is crucial for determining the experimental observability and practical applications of such quantum droplets. It provides insights into the conditions under

which these droplets can maintain their coherence and structural integrity. A second interesting feature is the interplay between many-body effects and disorder which may give rise to intriguing quantum phase transitions such as Anderson localization, Bose glass, superglass and so on. Furthermore, the additional complexity introduced by the disorder may significantly alter the critical behavior and universality classes of quantum droplets.

In this chapter, we extend the Bogoliubov theory of Huang and Meng [140] presented in Chapter 1 for a single BEC to quantum droplets. Such an extension permits us to provide a comprehensive understanding of the characteristics of self-bound liquid droplets with weak 3D random potentials. Our focus lies in examining the role of the interplay of interspecies interactions, the LHY quantum fluctuations, and the disorder potential on the formation and stability of such self-bound droplets. The competition between these ingredients may dramatically change the quantum behavior of this exotic state of matter.

Initially, we investigate the drastic effects of an external random δ-correlated potential on the bulk properties of self-bound droplets at both zero and finite temperatures. The ground-state energy and the quantum fluctuations induced by disorder are computed utilizing the HM theory. We construct a useful stability phase-diagram for the resulting dirty droplets. At finite temperature, we calculate the free energy, and the thermal equilibrium density in terms of the disorder parameters.

Secondly, we study the bulk properties of self-bound liquid droplets in the presence of both speckle and Gaussian random potentials. To proceed, we derive useful formulas for the ground-state energy, the equilibrium density, the depletion, the anomalous density, and the glassy fraction inside the droplet by means of the developed HM theory. At finite temperature, we calculate the free energy, the thermal equilibrium density, and the critical temperature.

Finally, we deal with the static and dynamical properties of disordered self-bound droplets. We calculate in particular the density profiles by numerically solving the

underlying generalized disorder GPE which we derive selfconsistently. The width and the breathing modes of the droplet are also computed using a variational scheme based on a Gaussian ansatz.

4.1 Ground-state energy and quantum fluctuations

We consider a weakly interacting Bose mixture with equal masses $m_1 = m_2 = m$, subjected to a weak disorder potential $U(\mathbf{r})$. The disorder potential is assumed to have vanishing ensemble averages $\langle U(\mathbf{r})\rangle = 0$ and a finite correlation of the form $\langle U(\mathbf{r})U(\mathbf{r}')\rangle = R(\mathbf{r}-\mathbf{r}')$. The second quantized Hamiltonian of the system reads

$$\begin{aligned}\hat{H}=&\sum_{j,\mathbf{k}} E_k \hat{a}^\dagger_{j,\mathbf{k}}\hat{a}_{j,\mathbf{k}} + \frac{1}{V}\sum_{j,\mathbf{k},\mathbf{p}} U_{\mathbf{k}-\mathbf{p}}\hat{a}^\dagger_{j,\mathbf{k}}\hat{a}_{j,\mathbf{p}} + \frac{g_j}{2V}\sum_{j,\mathbf{k},\mathbf{p},\mathbf{q}} \hat{a}^\dagger_{j,\mathbf{k}}\hat{a}^\dagger_{j,\mathbf{p}}\hat{a}_{j,\mathbf{p}-\mathbf{q}}\hat{a}_{j,\mathbf{k}+\mathbf{q}} \\ &+\frac{g_{12}}{V}\sum_{\mathbf{k},\mathbf{p},\mathbf{q}} \hat{a}^\dagger_{1,\mathbf{k}}\hat{a}^\dagger_{2,\mathbf{p}}\hat{a}_{2,\mathbf{p}-\mathbf{q}}\hat{a}_{1,\mathbf{k}+\mathbf{q}}.\end{aligned} \tag{4.1}$$

Under the Bogoliubov prescription, described in previous chapters, the ground-state of ultradilute Bose mixtures is assumed to contain most of the atoms, we replace the operators $\hat{a}_{j,0}$ and $\hat{a}^\dagger_{j,0}$ by a c-number, i.e., $\hat{a}_{j,0} = \hat{a}^\dagger_{j,0} = \sqrt{N_j}$, where N_j is the number of particles.

Using the normalization relation:

$$N_j = \hat{a}^\dagger_{j,0}\hat{a}_{j,0} + \sum_{\mathbf{k}\neq 0} \hat{a}^\dagger_{j,\mathbf{k}}\hat{a}_{j,\mathbf{k}}, \tag{4.2}$$

the Hamiltonian (4.1), takes the form:

$$\hat{H} = \sum_j \left(\frac{U_0}{V} N_j + \frac{g_j}{2V} N_j^2 \right) + \frac{g_{12}}{V} N_1 N_2 + \frac{1}{V} \sum_{j,\mathbf{k}\neq 0} \sqrt{N_j}\, U_{\mathbf{k}} \left(\hat{a}^\dagger_{j,\mathbf{k}} + \hat{a}_{j,-\mathbf{k}} \right) \tag{4.3}$$
$$+ \sum_{j,\mathbf{k}\neq 0} \left(E_k + 2 g_j n_j + g_{12} n_{3-j} \right) \hat{a}^\dagger_{j,\mathbf{k}} \hat{a}_{j,\mathbf{k}} + \sum_{j,\mathbf{k}\neq 0} \frac{g_j}{2V} N_j \left(\hat{a}^\dagger_{j,\mathbf{k}} \hat{a}^\dagger_{j,-\mathbf{k}} + \hat{a}_{j,\mathbf{k}} \hat{a}_{j,-\mathbf{k}} \right)$$
$$+ \frac{g_{12}}{V} \sqrt{N_1 N_2} \sum_{\mathbf{k}\neq 0} \left(\hat{a}^\dagger_{1,\mathbf{k}} + \hat{a}_{1,-\mathbf{k}} \right) \left(\hat{a}^\dagger_{2,-\mathbf{k}} + \hat{a}_{2,\mathbf{k}} \right),$$

where $n_j = N_j/V$ is the density of each component. In equation (4.3) we kept only quadratic terms in $\hat{a}^\dagger_{j,\mathbf{k}\neq 0}$, $\hat{a}_{j,\mathbf{k}\neq 0}$ up to the second-order in the coupling constants. We also assumed that for weak enough disorder, disorder fluctuations decouple in the lowest order [140]. As a result we ignored the terms $U_{\mathbf{k}-\mathbf{p}} \hat{a}^\dagger_{j,\mathbf{k}} \hat{a}_{j,\mathbf{p}}$ with both $\mathbf{k} = 0$ and $\mathbf{p} = 0$.

Hamiltonian (4.3) can be diagonalized making the extended Bogoliubov-Huang-Meng transformation

$$\hat{a}_{1k} = (u_{+,k} \hat{b}_{1k} - v_{+,k} \hat{b}^\dagger_{1,-k} - \beta_{1,\mathbf{k}}) \cos\gamma - (u_{-,k} \hat{b}_{2k} - v_{-,k} \hat{b}^\dagger_{2,-k} - \beta_{2,\mathbf{k}}) \sin\gamma, \tag{4.4a}$$
$$\hat{a}^\dagger_{1k} = (u_{+,k} \hat{b}^\dagger_{1k} - v_{+,k} \hat{b}_{1,-k} - \beta^*_{1,\mathbf{k}}) \cos\gamma - (u_{-,k} \hat{b}^\dagger_{2k} - v_{-,k} \hat{b}_{2,-k} - \beta^*_{2,\mathbf{k}}) \sin\gamma, \tag{4.4b}$$
$$\hat{a}_{2k} = (u_{+,k} \hat{b}_{1k} - v_{+,k} \hat{b}^\dagger_{1,-k} - \beta_{1,\mathbf{k}}) \sin\gamma + (u_{-,k} \hat{b}_{2k} - v_{-,k} \hat{b}^\dagger_{2,-k} - \beta_{2,\mathbf{k}}) \cos\gamma, \tag{4.4c}$$
$$\hat{a}^\dagger_{2k} = (u_{+,k} \hat{b}^\dagger_{1k} - v_{+,k} \hat{b}_{1,-k} - \beta^*_{1,\mathbf{k}}) \sin\gamma + (u_{-,k} \hat{b}^\dagger_{2k} - v_{-,k} \hat{b}_{2,-k} - \beta^*_{2,\mathbf{k}}) \cos\gamma, \tag{4.4d}$$

where

$$\cos\gamma, \sin\gamma = \frac{1}{\sqrt{2}} \sqrt{1 \pm \frac{1-\alpha}{\sqrt{(1-\alpha)^2 + 4\Delta^{-1}\alpha}}},$$

$\alpha = n_2 g_2 / n_1 g_1$, $\Delta = g_1 g_2 / g_{12}^2$. The transformation (4.4) is canonical and the quasi-particle annihilation, $\hat{b}_{j,\mathbf{k}}$, and creation, $\hat{b}^\dagger_{j,\mathbf{k}}$, operators must obey the usual Bose commutation relations: $\left[\hat{b}_{j,\mathbf{k}}, \hat{b}^\dagger_{j,\mathbf{k}'} \right] = \delta_{\mathbf{k},\mathbf{k}'}$, $\left[\hat{b}_{j,\mathbf{k}}, \hat{b}_{j,\mathbf{k}'} \right] = \left[\hat{b}^\dagger_{j,\mathbf{k}}, \hat{b}^\dagger_{j,\mathbf{k}'} \right] = 0$. It allows us to decouple the quantum and random variables and get the bilinear form of the Hamiltonian.

The Bogoliubov quasiparticle amplitudes, $u_{\pm,k}$, $v_{\pm,k}$, and disorder translations, $\beta_{j,k}$, are calculated in order to make the coefficients of the non-diagonal terms $\hat{b}_{j,\mathbf{k}}\hat{b}_{j,-\mathbf{k}}$ and $\hat{b}^\dagger_{j,\mathbf{k}}\hat{b}^\dagger_{j,-\mathbf{k}}$ in the Hamiltonian (4.3) vanish. With this we immediately obtain

$$\begin{aligned} u_{\pm,k} &= \frac{1}{2}\left(\sqrt{\frac{\varepsilon_{\pm,k}}{E_k}} + \sqrt{\frac{E_k}{\varepsilon_{\pm,k}}}\right), \\ v_{\pm,k} &= u_{\pm,k} - \sqrt{\frac{E_k}{\varepsilon_{\pm,k}}}, \end{aligned} \tag{4.5}$$

and

$$\begin{aligned} \beta_{1,\mathbf{k}} &= \sqrt{\frac{n_1}{V}}\frac{|u_{+,k}-v_{+,k}|^2}{\varepsilon_{+,k}}U_{\mathbf{k}}, \\ \beta_{2,\mathbf{k}} &= \sqrt{\frac{n_2}{V}}\frac{|u_{-,k}-v_{-,k}|^2}{\varepsilon_{-,k}}U_{\mathbf{k}}, \end{aligned} \tag{4.6}$$

where the excitation spectrum energies $\varepsilon_{\pm,k}$ are defined below.

After a lengthy but straightforward algebra, the Hamiltonian (4.3) can be expressed as: $\hat{H} = \hat{H}_{\mathrm{BB}} + \hat{H}_{\mathrm{dis}}$, where

$$\begin{aligned} \hat{H}_{\mathrm{BB}} = {} & \sum_j \frac{g_j}{2V}N_j^2 + \frac{g_{12}}{V}N_1N_2 - \frac{1}{2}\sum_{j,\mathbf{k}}(E_{\mathbf{k}} + g_j n_j) + \frac{1}{2}\sum_{j,\mathbf{k}}\Bigg\{\Big[(E_{\mathbf{k}} + g_j n_j)\cos^2\gamma \\ & + (E_{\mathbf{k}} + g_{3-j}n_{3-j})\sin^2\gamma\Big]\left(u^2_{\pm\mathbf{k}} + v^2_{\pm\mathbf{k}}\right) - 2u_{\pm\mathbf{k}}v_{\pm\mathbf{k}}\left(g_j n_j\cos^2\gamma + g_{3-j}n_{3-j}\sin^2\gamma\right) \\ & + 2\frac{g_{12}}{V}\sqrt{N_1N_2}(u_{\pm\mathbf{k}} - v_{\pm\mathbf{k}})^2\cos\gamma\sin\gamma\Bigg\} \\ & + \sum_{j,\mathbf{k}}\Bigg\{\Big[(E_{\mathbf{k}} + g_j n_j)\cos^2\gamma + (E_{\mathbf{k}} + g_{3-j}n_{3-j})\sin^2\gamma\Big](u^2_{\pm\mathbf{k}} + v^2_{\pm\mathbf{k}}) \\ & - 2u_{\pm\mathbf{k}}v_{\pm\mathbf{k}}\left(g_j n_j\cos^2\gamma + g_{3-j}n_{3-j}\sin^2\gamma\right) + 2\frac{g_{12}}{V}\sqrt{N_1N_2}(u_{\pm\mathbf{k}} - v_{\pm\mathbf{k}})^2\cos\gamma\sin\gamma\Bigg\}\hat{b}^\dagger_{j,\mathbf{k}}\hat{b}_{j,\mathbf{k}}, \end{aligned} \tag{4.7}$$

and

$$\hat{H}_{\rm dis} = \sum_j \frac{U_0}{V} N_j - \frac{\sqrt{N_j}}{V} \sum_{j,\mathbf{k}} U_{j,\mathbf{k}} (\beta_{j\mathbf{k}} + \beta^*_{j\mathbf{k}}) \tag{4.8}$$
$$+ \sum_{j,\mathbf{k}} \left[(E_\mathbf{k} + 2g_j n_j) \cos^2\gamma + (E_\mathbf{k} + 2g_{3-j} n_{3-j}) \sin^2\gamma + 4\frac{g_{12}}{V}\sqrt{N_1 N_2}\cos\gamma\sin\gamma \right] |\beta_{j\mathbf{k}}|^2.$$

The resulting disorder Hamiltonian, $\hat{H}_{\rm dis}$, varies with each realization of the random potential. Thus, the final bilinear Hamiltonian of disordered binary BECs can be obtained by performing the disorder ensemble average, $\langle \hat{H}_{\rm dis} \rangle$ [140]. This yields

$$\hat{H} = E + \sum_{\mathbf{k}\neq 0} \left(\varepsilon_{+,k} \hat{b}^\dagger_{1,\mathbf{k}} \hat{b}_{1,\mathbf{k}} + \varepsilon_{-,k} \hat{b}^\dagger_{2,\mathbf{k}} \hat{b}_{2,\mathbf{k}} \right), \tag{4.9}$$

where the Bogoliubov spectra are given by

$$\varepsilon_{+,\mathbf{k}} = \left[(E_\mathbf{k} + g_1 n_1)\cos^2\gamma + (E_\mathbf{k} + g_2 n_2)\sin^2\gamma \right] (u^2_{+\mathbf{k}} + v^2_{+\mathbf{k}}) \tag{4.10}$$
$$- 2u_{+\mathbf{k}} v_{+\mathbf{k}} (g_1 n_1 \cos^2\gamma + g_2 n_2 \sin^2\gamma) + 2\frac{g_{12}}{V}\sqrt{N_1 N_2}(u_{+\mathbf{k}} - v_{+\mathbf{k}})^2 \cos\gamma\sin\gamma,$$

and

$$\varepsilon_{-,\mathbf{k}} = \left[(E_\mathbf{k} + g_2 n_2)\cos^2\gamma + (E_\mathbf{k} + g_1 n_1)\sin^2\gamma \right] (u^2_{-\mathbf{k}} + v^2_{-\mathbf{k}}) \tag{4.11}$$
$$- 2u_{-\mathbf{k}} v_{-\mathbf{k}} (g_2 n_2 \cos^2\gamma + g_1 n_1 \sin^2\gamma) + 2\frac{g_{12}}{V}\sqrt{N_1 N_2}(u_{-\mathbf{k}} - v_{-\mathbf{k}})^2 \cos\gamma\sin\gamma.$$

The ground-state energy reads

$$E = \sum_j \frac{g_j}{2V} N_j^2 + \frac{g_{12}}{V} N_1 N_2 + \sum_{\pm,\mathbf{k}} \varepsilon_{\pm,\mathbf{k}} v^2_{\pm,\mathbf{k}} + E_R, \tag{4.12}$$

where

$$E_R = \langle H_{\rm dis}\rangle = \sum_{j,\mathbf{k}} \Big[(E_{\mathbf{k}} + 2g_j n_j)\cos^2\gamma + (E_{\mathbf{k}} + 2g_{3-j} n_j)\sin^2\gamma + 4\frac{g_{12}}{V}\sqrt{N_1 N_2}\cos\gamma\sin\gamma \Big] \langle |\beta_{j\mathbf{k}}|^2\rangle - \frac{\sqrt{N_j}}{V}\sum_{j,\mathbf{k}} \langle U_{j,\mathbf{k}}(\beta_{j\mathbf{k}} + \beta^*_{j\mathbf{k}})\rangle, \tag{4.13}$$

is the disorder contribution to ground-state energy.

From now on we consider a symmetric mixture with, equal densities $n_1 = n_2 = n/2$, equal intraspecies $g_1 = g_2 = g$ and interspecies $g_{12} = g_{21}$ coupling constants, where $\cos\gamma\sin\gamma = 1/2$. Therefore, the Bogoliubov excitation energies take the form

$$\varepsilon_{k\pm} = \sqrt{E_k^2 + 2E_k n\delta g_\pm},$$

where we recall that $\delta g_\pm = g(1 \pm g_{12}/g)$.
Using the definitions (4.5) and (4.6), the ground-state energy including the disorder corrections turns out to be given in d-dimensions as:

$$\frac{E}{V} = \sum_{\pm}\left[\frac{1}{2}n^2\delta g_\pm - n\int \frac{d^dk}{(2\pi)^d}\, R_k \frac{E_k}{\varepsilon^2_{k\pm}} + \frac{1}{2}\int \frac{d^dk}{(2\pi)^d}\,(\varepsilon_{k\pm} - 2E_k - n\delta g_\pm)\right]. \tag{4.14}$$

The leading term is the mean-field energy. The subleading term gives the correction to the ground-state energy due to the external random potential. The last term accounts for the LHY quantum corrections to the ground-state energy.

The noncondensed and anomalous densities can be computed by introducing the transformation (4.4) into the definitions (1.28) and (1.29). This gives

$$\tilde{n}_\pm = \frac{1}{V}\sum_{\mathbf{k}\neq 0}\Big\{ \Big[v^2_{\pm k} + \big(u^2_{\pm k} + v^2_{\pm k}\big) N_{\pm k}\Big]\cos^2\gamma + \Big[v^2_{\mp k} + \big(u^2_{\mp k} + v^2_{\mp k}\big) N_{\mp k}\Big]\sin^2\gamma \Big\} + n_{R\pm}, \tag{4.15}$$

and

$$\tilde{m}_{\pm} = -\frac{1}{V}\sum_{\mathbf{k}\neq 0}\Big\{ [u_{\pm k}v_{\pm k}(1+2N_{\pm k})]\cos^2\gamma \\ + [u_{\mp k}v_{\mp k}(1+2N_{\mp k})]\sin^2\gamma\Big\} + n_{R\pm}, \tag{4.16}$$

where $N_{\pm,k} = \langle \hat{b}^{\dagger}_{\pm,\mathbf{k}}\hat{b}_{\pm,\mathbf{k}}\rangle = [\exp(\varepsilon_{k,\pm}/T)-1]^{-1}$ are occupation numbers for the excitations.

The last term in Eqs.(4.15) and (4.16) can be evaluated by performing the disorder ensemble average through equation (4.6):

$$n_{R\pm} = \frac{1}{V}\sum_{\mathbf{k}}\langle|\beta_{\mathbf{k}\pm}|^2\rangle = n\int \frac{d^dk}{(2\pi)^d}\frac{E_k^2}{\varepsilon_{k\pm}^4}R_k, \tag{4.17}$$

The total noncondensed, $\tilde{n}$, and anomalous, $\tilde{m}$ can readily be obtained

$$\tilde{n} = \sum_{\pm}\tilde{n}_{\pm} = \sum_{\pm}\left[\frac{1}{2}\int\frac{d^dk}{(2\pi)^d}\left[\frac{E_k+n\delta g_{\pm}}{\varepsilon_{k\pm}}\sqrt{I_{k\pm}}-1\right]+n_{R\pm}\right], \tag{4.18}$$

and

$$\tilde{m} = \sum_{\pm}\tilde{m}_{\pm} = \sum_{\pm}\left[-\frac{1}{2}\int\frac{d^dk}{(2\pi)^d}\frac{n\delta g_{\pm}}{\varepsilon_{k\pm}}\sqrt{I_{k\pm}}+n_{R\pm}\right], \tag{4.19}$$

where $I_{k\pm} = \coth^2(\varepsilon_{k\pm}/2T)$ with T being the temperature.

Calculating the depletion is indeed essential for investigating the stability, dynamics, and coherence properties of the droplet state .

4.2 Validity condition of the model

The Bogoliubov approximation is valid when the interactions between the particles in the condensate are weak compared to their kinetic energy. In an alternative scenario, the quantum fluctuation density is significantly smaller compared to the total density $\tilde{n} \ll n$. In the presence of disorder the validity condition of the

Bogoliubov theory depends on the strength of disorder and the interaction strength between the particles, thus an additional condition must be fulfilled.

Therefore, the validity of the present approach requires the condition:

$$n_R = \sum_{\pm} n_{R\pm} \ll n, \tag{4.20}$$

which means that the disorder fluctuations must be small.

4.3 Quantum droplets in a white-noise disorder

In this section we study the influence of a 3D uncorrelated (white-noise) weak disorder on the bulk properties of self-bound droplets in Bose-Bose mixtures. Uncorrelated disorder is considered a universal model for disorder in many physical systems (see e.g. [131, 132, 140, 175]). A standard model of uncorrelated disorder is the random impurity potential, in which the random potential arises from the contribution of identical and randomly placed impurities [160, 175, 176]. We recall that at very low temperatures, one may consider the limit of a δ-correlated type of disorder (2.8) in which the external potential is described by a single parameter as:

$$R(\mathbf{r} - \mathbf{r}') = R_0 \delta(\mathbf{r} - \mathbf{r}'), \tag{4.21}$$

where R_0 denotes the disorder strength which has dimension (energy) ^{2} $\times$ (length)^3. It depends on the concentration of the impurities and to the s-wave scattering length of the random scatterers [140, 141, 160].

4.3.1 Energy and stability analysis

The regime of interest corresponds to $a > 0$ and $a_{12} < 0$. In such a situation the ground-state energy becomes complex in the droplet phase. This issue can be cured either by taking into account higher-order quantum fluctuations [29, 41, 68, 69] or

by simply setting $\delta a_+/a \ll 1$ [46].

The integration with respect to k of equation (4.14) gives for the ground-state energy:

$$\frac{E}{NE_0} = 2\pi(na^3)\frac{\delta a_+}{a} + \sum_{\pm}\left\{\frac{128\sqrt{\pi}}{15}(na^3)^{3/2}\left(\frac{\delta a_\pm}{a}\right)^{5/2} + R(na^3/\pi)^{1/2}\left(\frac{\delta a_\pm}{a}\right)^{1/2}\right\}, \tag{4.22}$$

where $\delta a_\pm/a = 1 \pm (a_{12}/a)$, $E_0 = \hbar^2/ma^2$ and $R = R_0/(E_0^2 a^3)$. For $R = 0$, equation (4.22) reduces to that found for a clean Bose mixture [41, 46, 68, 69]. When $(\delta a_+/a) < 0$, the mean-field theory energy provides a term $\propto n^2$ becomes complex results in a collapse of a homogeneous state towards bright soliton formation. The beyond-mean-field LHY quantum corrections provide an extra repulsive terms $\propto n^{5/2} + n^{3/2}$ halting the attractive mean-field term, leading to the formation of a stable mixture self-bound droplet.

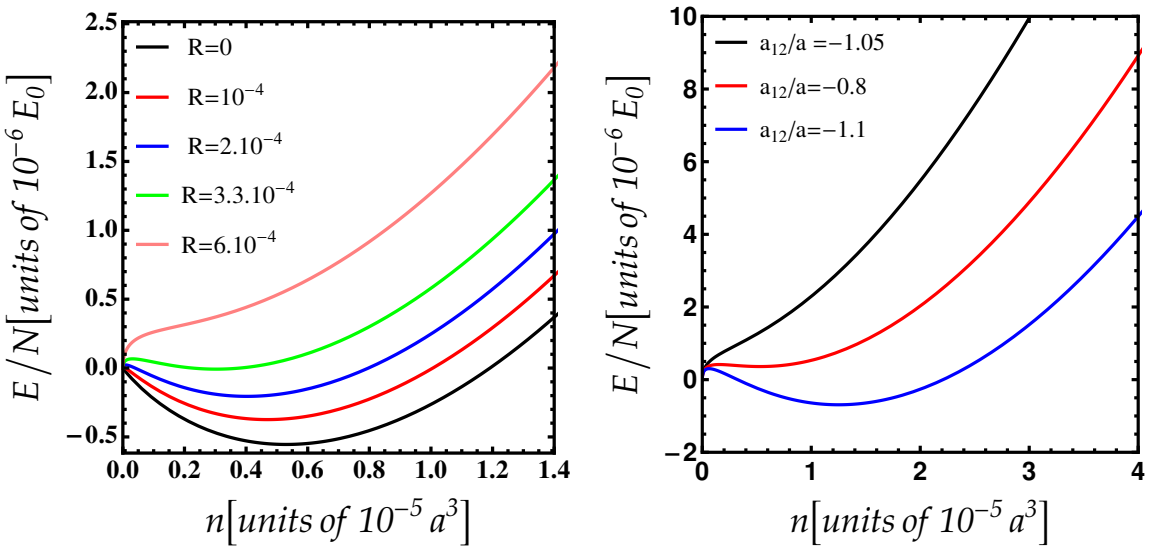

Figure 4.1: Ground-state energy from equation (4.22) as a function of the density n for different values of R, and $a_{12}/a = -1.05$. (b) Ground-state energy from equation (4.22) as a function of the density n for different values of a_{12}/a and $R = 2.10^{-4}$.

Figure 4.1 (a) shows that as the disorder strength R gets larger, the local minimum becomes shallow and the strength of the bond in the droplet is lowered. For $R \geq 3.3 \times 10^{-4}$, the energy becomes positive. This indicates the existence of a

critical value of R above which the self-bound droplet is completely destroyed. We see from figure 4.1 (b) that the droplet becomes less stable when a_{12}/a is increasing. For instance, if $a_{12}/a > -1.05$, the droplet evaporates.

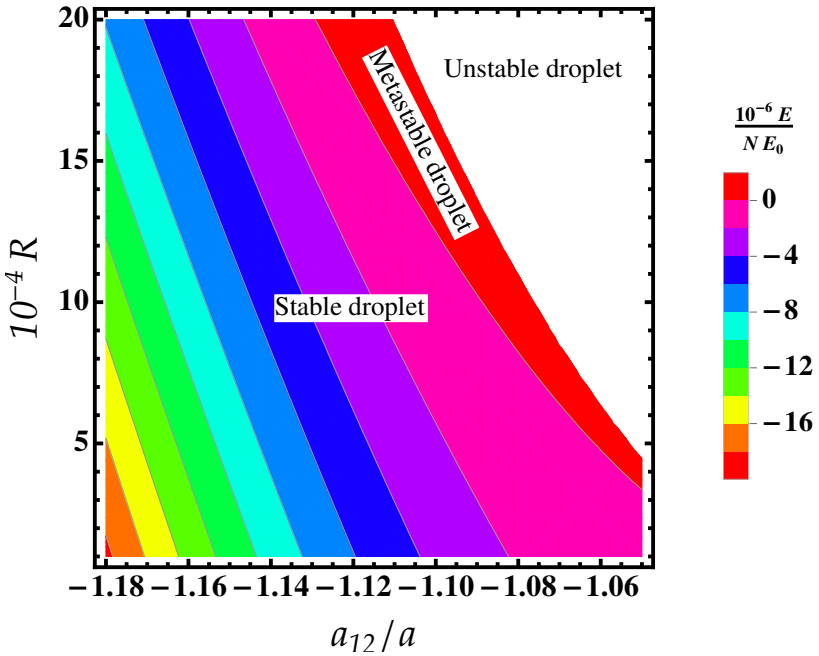

Figure 4.2: Phase diagram of self-bound solutions as a function of a_{12}/a and R calculated from equation (4.22). The colors show the energy of the solutions. The thick black line corresponds to $E = 0$.

The local minima corresponding to the energy (4.22) are captured in figure 4.2 in terms of the disorder strength R and the interspecies interactions a_{12}/a as a phase diagram. We delineate the phase boundary ($E = 0$) with a thick line, below which the droplet is stable. We see that localized solutions persist slightly beyond this region as metastable states notably for R. The self-bound state is unstable for large disorder strength and small interspecies interactions $|a_{12}/a|$. For any given value of $|a_{12}/a|$, there will be a critical value of R above which the localized solutions are unstable (see below). A stable and robust self-bound droplet survives for large $|a_{12}/a|$ and very weak disorder $R \ll 1$.

Equilibrium density

Minimizing the ground-state (4.22) with respect to the density in such a way that the condition $(\delta a_-/a) \simeq 2$ [46] must be fulfilled, we obtain the equilibrium density of the droplet in terms of disorder strength:

$$n_{\rm eq} = n^{(0)} \left(\frac{1}{2}(1 + \sqrt{1-\gamma}) - \frac{1}{4}\gamma \right), \tag{4.23}$$

where $n^{(0)}a^3 = 25\pi(\delta a_+/a)^2/32768$ is the equilibrium density of a clean droplet [46], and $\gamma = 256R/[5\pi^2(\delta a_+/a)^2]$. For $R = 0$, one recovers the equilibrium density of a clean droplet [46, 62]. Equation (4.23) shows that the equilibrium density is decreasing with increasing disorder strength. In such a case for a fixed total number of particles, the volume of the droplet enlarges when the disorder strength reaches its critical value, results in the system undergoes a transition to a gas phase.

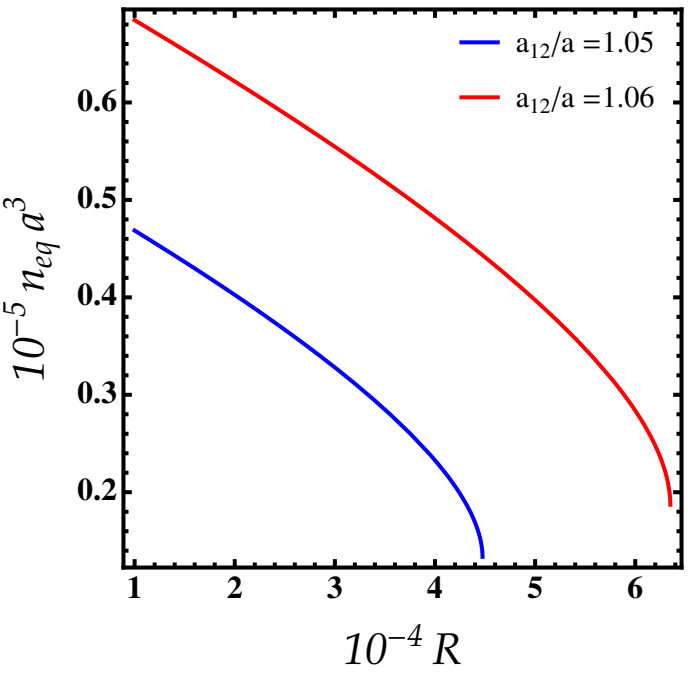

Figure 4.3: Equilibrium density from equation (4.23) as a function of the disorder strength for different values of a_{12}/a.

In figure 4.3 we plot the equilibrium density $n_{\rm eq}$ of the dirty droplet in units of $10^{-5}a^3$ as a function of the disorder strength for different values of interspecies

interactions. We observe that the equilibrium density is very sensitive to the interspecies interactions, and it decreases by increasing the disorder strength indicating that the liquid droplet becomes unstable.

Critical disorder strength

The critical disorder strength beyond which the droplet transforms into a gas phase (i.e. corresponds to disappearance of the local minimum of the energy) is given by:

$$R_c = \frac{5\pi^2(\delta a_+/a)^2}{32(\delta a_-/a)^3}. \tag{4.24}$$

Following the Petrov's prescription, $(\delta a_-/a) \simeq 2$ [46], equation (4.24) reduces to $R_c = 5\pi^2(\delta a_+/a)^2/256$ which strongly depends on the interspecies interactions, $\delta a_+/a$. For ^{39}K mixture droplets [47], with intraspecies scattering length $a_{12}/a = -1.09$, one has $R_c = 0.00137$.

Glassy fraction

As we have shown in section (4.2), the validity criterion of the HM model requires the condition (4.20) which implies:

$$\frac{n_{R-}}{n^{(0)}} = \frac{\sqrt{512}\sqrt{n/n^{(0)}}R}{5\pi^2|\delta a_+/a|\sqrt{\delta a_-/a}}. \tag{4.25}$$

Here we neglected the imaginary part n_{R+}, in the droplet regime.

The glassy fraction (4.25) is appealing since it explains the interplay between the disorder potential, the LHY quantum corrections and the attractive interspecies interaction. The behavior of n_{R-} from equation (4.25) as a function of a_{12}/a and R in the equilibrium regime is depicted in figure 4.4. We observe that for $a_{12}/a < -1.05$, the depletion due to the disorder, n_{R-}, increases linearly with the disorder strength, R, (see left panel). For fixed R, n_{R-} grows slightly with the interspecies interaction a_{12}/a (see right panel). Due to the restrictions of the Bogoliubov theory, this latter

is valid under the condition $n_{R-} \ll n$.

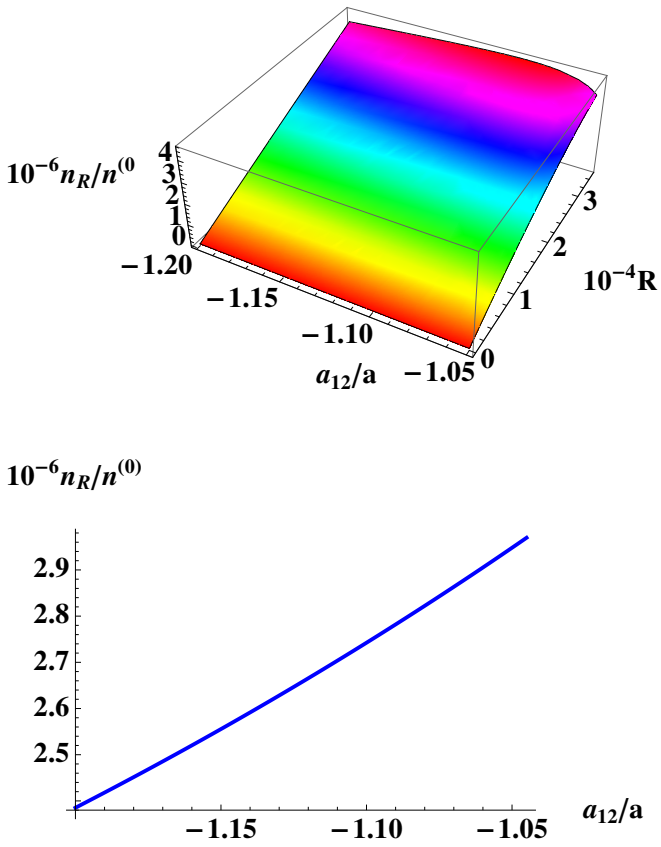

Figure 4.4: Top panel: Glassy fraction inside the droplet n_R as a function of a_{12}/a and R. Bottom panel: Glassy fraction inside the droplet n_R as a function of a_{12}/a for $R = 2 \times 10^{-4}$.

In next sections we investigate the behavior of quantum droplets in the presence of correlated disorders which allow for the exploration of non-universal phenomena. By studying droplets in correlated disorders, we gain a unique perspective compared to scenarios involving uncorrelated disorders. This perspective enables us to examine distinct spatial patterns, heightened localization effects, non-universal behavior, and practical applications. Furthermore, it provides opportunities to understand the role of correlations in disorder and how they impact quantum systems, thereby expanding our knowledge of complex environments and their influence on quantum phenomena.

4.4 Speckle disorder with uniform apertures

Let us consider a self-bound droplet subjected to a 3D weak speckle disorder which is often used with ultracold atoms experiments [80, 81, 83, 177, 133]. The speckle disorder is characterized by the autocorrelation function given in equation (2.11). Its Fourier transform reads [119, 178]:

$$R(\mathbf{k}) = U_R^2 \sigma^3 \frac{\pi^2}{k\sigma} \Theta(2 - k\sigma), \tag{4.26}$$

where Θ denotes the Heaviside function.

Stability of the droplet

Substituting equation (4.26) into (4.14) and integrating over k, we obtain the ground state energy. Normalizing the resulting energy and the density, to their equilibrium values obtained within the theory of Petrov for a clean droplet namley: $n^{(0)} = 25\pi(\delta a_+/a)^2/(16384a^3)$ and $|E_0|/N = 25\pi^2\hbar^2|\delta a_+/a|^3/(49152ma^2)$ [46, 68], we then find

$$\begin{aligned} \frac{E}{|E_0|} = -3\left(\frac{n}{n^{(0)}}\right) + \frac{1}{2\sqrt{2}}\left(\frac{n}{n^{(0)}}\right)^{3/2} \sum_{\pm}\left(\frac{\delta a_{\pm}}{a}\right)^{5/2} - \frac{R\sigma^2}{48\xi^2}\left|\frac{\delta a_+}{a}\right| \\ \times \sum_{\pm} \ln\left(1 \mp \frac{2\xi^2}{\sigma^2|\delta a_{\pm}/a|\,(n/n^{(0)})}\right), \end{aligned} \tag{4.27}$$

where $R = U_R^2/(|E_0|/N)^2$ is the dimensionless disorder strength, and $\xi = \hbar/\sqrt{mgn^{(0)}}$ is the droplet healing length.

In figure 4.5 we show the ground-state energy for different values of the disorder parameters and interspecies interactions. One can clearly identify two regions: In the low density regime where $n \leq n_{\text{eq}}$, we see that for fixed values of R and σ/ξ and as $|a_{12}/a|$ gets larger, the energy decreases with the interspecies interactions $|a_{12}/a|$ and hence the local minimum of the energy starts to disappear revealing the evaporation of the self-bound droplet (see figure 4.5.(a)). This can be attributed to

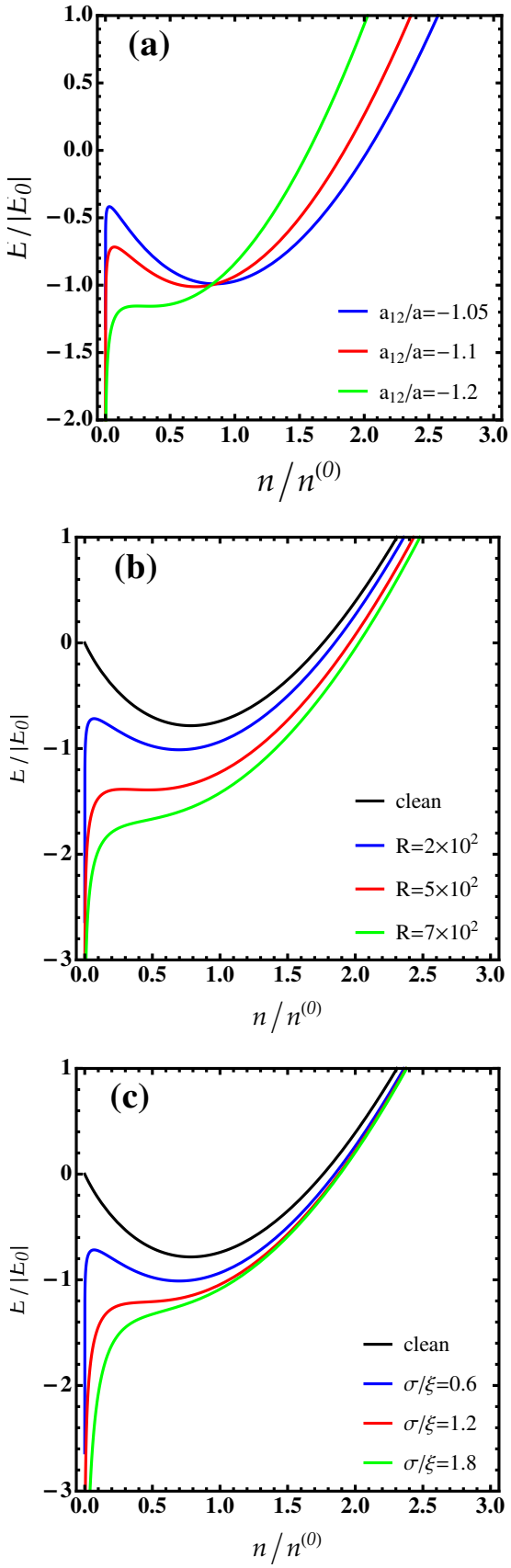

Figure 4.5: (a) Ground-state energy from Eq.(4.27) as a function of the density n for various values of the interspecies interactions, a_{12}/a, and for $R = 200$ and $\sigma/\xi = 0.6$. (b) Ground-state energy as a function of the density n for various values of the disorder strength R and for $a_{12}/a = -1.1$ and $\sigma/\xi = 0.6$. (c) Ground-state energy as a function of the density n for various values of the disorder correlation length σ/ξ and for $a_{12}/a = -1.1$ and $R = 200$.

peculiar competition between the disorder, interaction and quantum fluctuations. The situation is inverted for $n \geq n_{\rm eq}$ where the energy increases with $|a_{12}/a|$ in agreement with the case of a clean droplet [68]. Figures 4.5.(b) and (c) show that for large σ/ξ and R, the self-bound state solutions become unstable. In such a situation, the atoms leave the droplet and localize in the respective minima of the speckle For $R > R_c \simeq 500$ and $\sigma > \sigma_c \simeq 1.2$, the energy decreases and thus, the droplet becomes unstable and destroys ultimately.

Glassy fraction

Introducing the function (4.26) into equation (4.17) and performing the integration over the momentum form 0 to $2/\sigma$, we obtain for the glassy fraction inside the droplet

$$\frac{n_{R\pm}}{n} = \frac{R\sigma^2}{288\xi^2}\left(\frac{\delta a_+}{a}\right)^2\left[|\delta a_\pm/a|\frac{n}{n^{(0)}}\left((\sigma^2/\xi^2)|\delta a_\pm/a|\frac{n}{n^{(0)}} \mp 2\right)\right]^{-1}, \tag{4.28}$$

its behavior is displayed in figure 4.6. We see that n_R increases with the disorder parameters (the strength and the correlation length) indicating that the atoms are strongly localized in such a regime. Surprisingly, the glassy fraction n_R increases as the correlation length gets larger even for $\sigma > \xi$ which is in stark contrast to ordinary disordered BECs where the glassy fraction lowers with the correlation length [54, 76]. This can be interpreted as the fact that the disorder potential dominates both the LHY quantum corrections and the interactions.

4.5 Gaussian-correlated disorder

We now consider a disorder potential with Gaussian auto-correlation function which is very popular in ultracold atom experiments. This simple model is useful in three respects. Firstly, it can be realized either with speckle potentials or with Gaussian impurity disorders [90]. Secondly, it is analytically tractable, and therefore provides

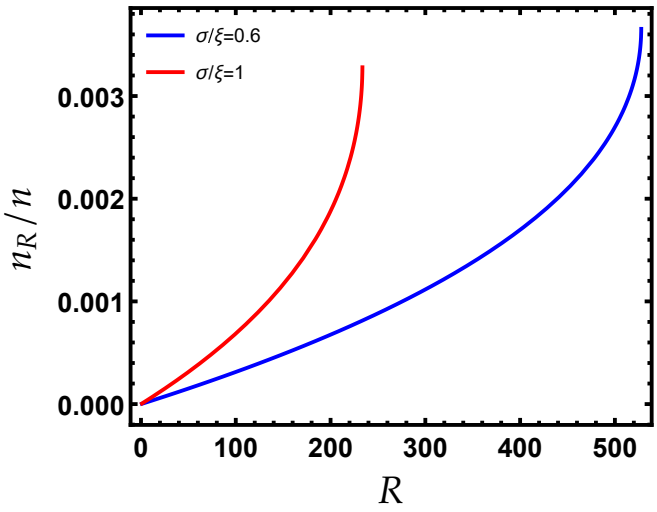

Figure 4.6: Disorder fraction in the droplet n_R/n_{eq} as a function of the disorder strength R for two values of σ/ξ and $a_{12}/a = -1.1$.

a test for the numerical simulation. Thirdly, the energy shift due to the Gaussian-correlated disorder does not require any regularization (i.e. safe from ultraviolet divergence), unlike the δ-correlated random potential made of a random series of δ peaks.

We recall that the Fourier transform of its autocorrelation function has the form [100, 179]:

$$R_k = R_0\, e^{-\sigma^2 k^2/2}, \tag{4.29}$$

where R_0 with dimension (energy) ^{2} $\times$ (length)^3 and σ characterize respectively, the strength and the correlation length of the disorder.

Energy and stability

Substituting equation (4.29) into equation (4.14) and integrating over k we obtain the ground state energy. Normalizing the resulting energy and the density to their equilibrium values $n^{(0)}$ and E_0 we then find:

$$\begin{aligned}\frac{E}{|E_0|} = -3\left(\frac{n}{n^{(0)}}\right) + \frac{1}{2\sqrt{2}}\left(\frac{n}{n^{(0)}}\right)^{3/2}\sum_{\pm}\left(\frac{\delta a_{\pm}}{a}\right)^{5/2} \\ - \sum_{\pm}\frac{R|(\delta a_+/a)|}{24\sqrt{2}\pi(\sigma/\xi)}\left[\frac{1}{\sqrt{\pi}} - \frac{\sigma}{\xi_{\pm}}e^{\sigma^2/\xi_{\pm}^2}\mathrm{erfc}\left(\frac{\sigma}{\xi_{\pm}}\right)\right],\end{aligned} \tag{4.30}$$

where erfc(x) is the complementary error function, $R = R_0 N^2/(\xi^3 E_0^2)$, and $\xi_\pm = \xi/\sqrt{(n/n^{(0)})(\delta a_\pm/a)}$. For $\sigma/\xi \to 0$, the energy correction due to the disorder contribution reduces to the result of δ-correlated disorder potential namely: $R\big(|(\delta a_+/a)|/24\sqrt{2}\pi\big)\sqrt{(\delta a_\pm/a)n/n^{(0)}}$.

In order to prove the relevance of our model for current experiments, we consider the ^{39}K mixture droplets [47]. The intraspecies scattering length is chosen to $a = 71a_0$ with a_0 being the Bohr radius. Note that a_{12} which can be adjusted via the Feshbach resonances is selected in such a way that the droplet phase is reached. The disorder strength R_0 used in the experiment ranges from $\sim 1.26.10^{-82}$ J^2.m^3 to $\sim 1.52.10^{-80}$J^2.m^3 (or equivalently R from 75.34 to 9116.77), and the correlation length is $\sigma \simeq 0.13\,\mu$m [180].

In figure 4.7 we show the ground-state energy using different values for the disorder parameters and interspecies interactions. Similarly to the speckle disorder case, one can distinct two regions: In the low density regime where $n \leq n^{(0)}$, we see that for fixed values of R and σ/ξ, the energy decreases with the interspecies interactions $|a_{12}/a|$ and then the local minimum of the energy starts to disappear revealing the evaporation of the self-bound droplet (see figure 4.7.(a)). This can be attributed to the peculiar competition between the disorder, interaction and quantum fluctuations. The situation is inverted for $n \geq n^{(0)}$ where the energy increases with $|a_{12}/a|$ in agreement with the case of a clean droplet [64, 68].

Figures 4.7.(b) and (c) show that for small correlation length σ/ξ and large disorder strength R, the energy decreases without any special structure giving rise to unstable self-bound state solutions. In such a situation, the droplet could segregate into multiple mini droplets similarly to the two-dimensional case [107]. For $\sigma > \xi$, the energy simplifies to that of clean droplets indicating that the disorder effects are not important in this regime (see figure.4.7.(b)). Once the disorder parameters exceed their critical values (i.e. $R > R_c \simeq 2.5 \times 10^3$ and $\sigma/\xi > \sigma_c/\xi \simeq 1.2$), the atoms leave the droplet and accumulate in the depleted region. Therefore, the

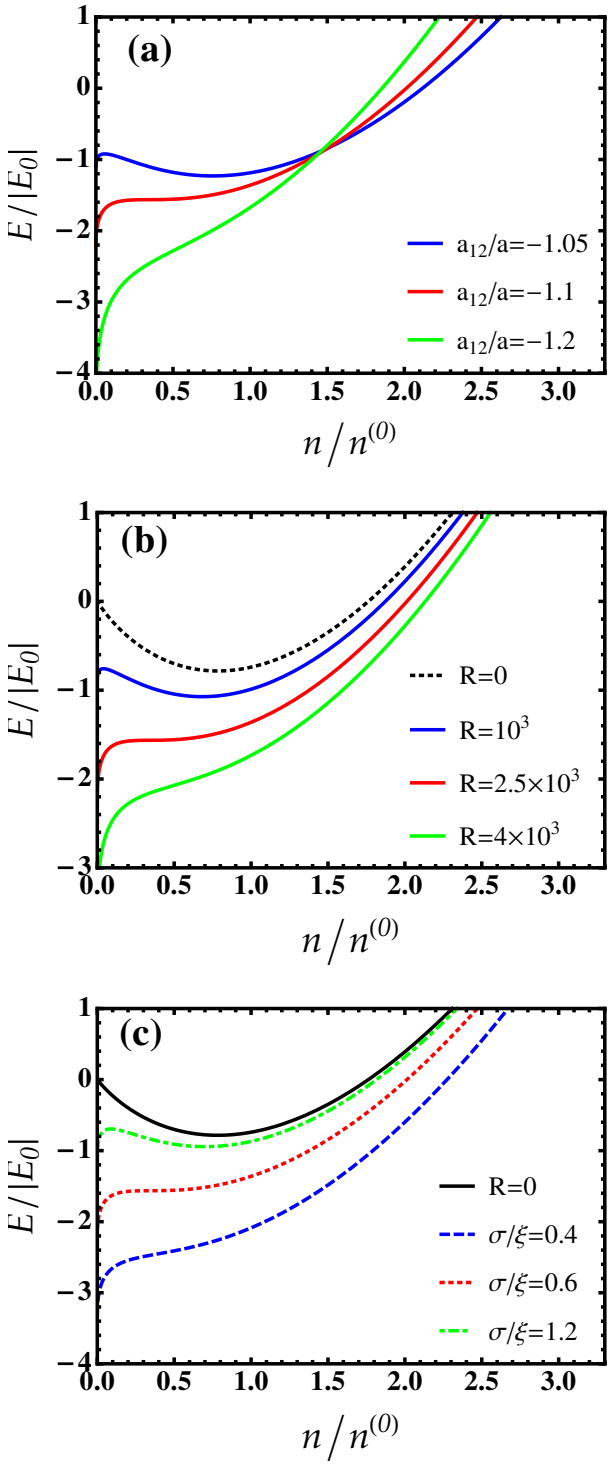

Figure 4.7: (a) Ground-state energy from equation (4.30) as a function of the density n for various values of the interction strength a_{12}/a, and for $R = 10^3$ and $\sigma/\xi = 0.63$. (b) Ground-state energy as a function of the density n for various values the disorder strength R, and for $a_{12}/a = -1.1$ and $\sigma/\xi = 0.63$. (c) Ground-state energy as a function of the density n for various values the disorder correlation length σ/ξ, and for $a_{12}/a = -1.1$ and $R = 2.5 \times 10^3$.

self-bound state loses its intriguing self-evaporation phenomenon and completely destroys eventually.

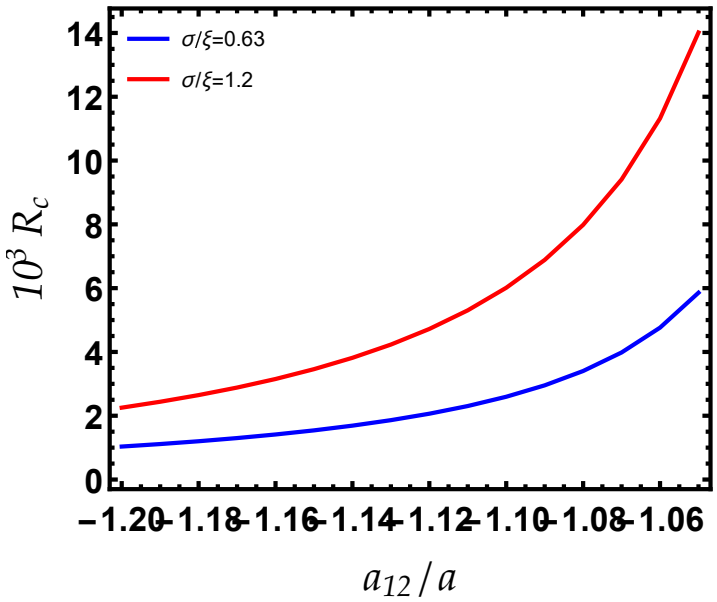

Figure 4.8: Critical disorder strength as a function of a_{12}/a for two different values of σ/ξ.

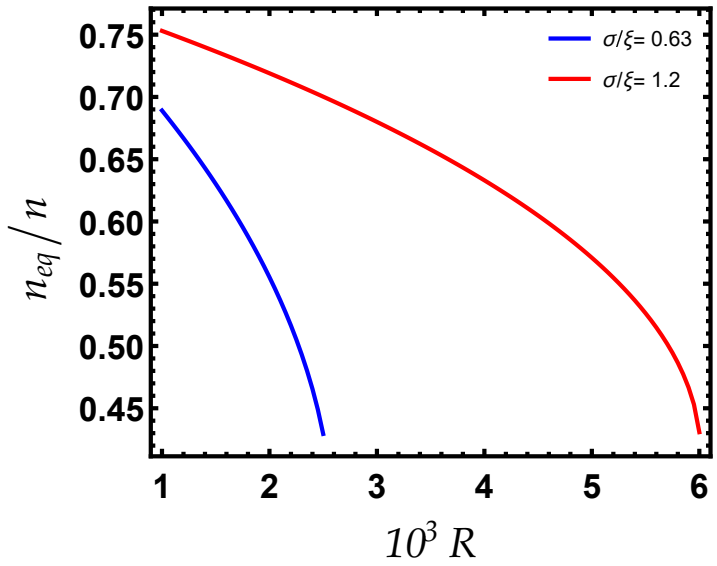

Figure 4.9: Equilibrium density of a dirty droplet $n_{\rm eq}$ with respect to $n^{(0)}$ as a function of the disorder strength for various values of a_{12}/a and σ/ξ.

The critical disorder strength R_c corresponds to the local minimum of the energy in terms of the interspecies interactions a_{12}/a for two different values of σ/ξ is captured in figure 4.8. We see that R_c increases with a_{12}/a and decays with σ/ξ.

The equilibrium density of the dirty droplet $n_{\rm eq}$ is obtained numerically by mini-

mizing the ground-state (4.30) with respect to the density. Its behavior as a function of the disorder strength for various values of a_{12}/a and σ/ξ is depicted in figure 4.9. Remarkably, the equilibrium density decreases with increasing the disorder strength regardless of the values a_{12}/a and σ/ξ leading to destabilize the droplet and eventually destroy it.

Glassy fraction

Introducing the function (4.29) into equation (4.17) and performing the integration over the momentum, we obtain for the disorder fraction inside the droplet

$$\frac{n_R}{n} = \frac{\sqrt{2}R(\delta a_+/a)^2}{144\pi\sqrt{\left(\frac{n}{n^{(0)}}\right)\left(\frac{\delta a_-}{a}\right)}}\left[-\frac{\sigma}{\sqrt{\pi}\xi_-} + \left(\frac{1}{2} + \left(\frac{\sigma}{\xi_-}\right)^2\right) e^{\sigma^2/\xi_-^2}\mathrm{erfc}\left(\frac{\sigma}{\xi_-}\right)\right]. \quad (4.31)$$

For $\sigma \to 0$, equation (4.31) reduces to $n_R/n = (\delta a_+/a)^2 R/\left[144\pi\sqrt{2n/n^{(0)}}\sqrt{(\delta a_-/a)}\right]$ which corresponds to the results of the white-noise disorder potential. For $\sigma \to 0$ and $a_{12} = 0$, one recovers the seminal HM results for a single dirty Bose gas [140]. We see from figure 4.10.(a) that in the region $\sigma \to 0$ and for small a_{12}/a, the total glassy fraction n_R/n is significant. By increasing the disorder strength or reducing the interspecies interaction, the macroscopic occupation of the ground-state decreases more and more, hence the fragmented droplets in the small wells of the random potential increase even at zero temperature due to the randomness. Lifting further the disorder strength one can expect that the droplet becomes completely depleted giving rise to completely destroy the coherence. For relatively large a_{12}/a and $\sigma \gg \xi$, n_R becomes negligibly small indicating that the atoms are less localized in such a regime leading to the formation of an extended droplet. This delocalization can be interpreted as the fact that the disorder potential is screened by both the LHY quantum corrections and the interactions. This behavior holds true also in the case of a dirty ordinary BEC (see e.g.[76, 100, 180]). For ^{39}K atoms we have $a = 71a_0$ [47] and for $a_{12}/a = -1.05$,

$R_0 \sim 1.52.10^{-80}\mathrm{J}^2.\mathrm{m}^3$ and $\sigma = 0.13\,\mu$m [180], the disorder fraction inside the droplet is about $n_R/n_{\mathrm{eq}} = 6 \times 10^{-4}$ ensuring the sufficient criterion for the weak disorder regime.

Quantum depletion and anomalous density of the droplet

The noncondensed $\tilde{n}_\pm$ and anomalous $\tilde{m}_\pm$ densities at zero temperature, in the presence of a disordered potential can be calculated through expressions (4.18) and (4.19). Performing the integration over the momentum and adding the formula of n_R (4.31), we obtain

$$\frac{\tilde{n}_\pm}{n} = \frac{5}{96\sqrt{2}}\sqrt{\frac{n}{n^{(0)}}}\left|\frac{\delta a_+}{a}\right|\left(\frac{\delta a_\pm}{a}\right)^{3/2} + \frac{\sqrt{2}R(\delta a_+/a)^2}{144\pi\sqrt{\left(\frac{n}{n^{(0)}}\right)\left(\frac{\delta a_-}{a}\right)}} \times\left[-\frac{\sigma}{\sqrt{\pi}\xi_-} + \left(\frac{1}{2} + \left(\frac{\sigma}{\xi_-}\right)^2\right) e^{\sigma^2/\xi_-^2}\mathrm{erfc}\left(\frac{\sigma}{\xi_-}\right)\right], \tag{4.32}$$

and

$$\frac{\tilde{m}_\pm}{n} = \frac{15}{96\sqrt{2}}\sqrt{\frac{n}{n^{(0)}}}\left|\frac{\delta a_+}{a}\right|\left(\frac{\delta a_\pm}{a}\right)^{3/2} + \frac{\sqrt{2}R(\delta a_+/a)^2}{144\pi\sqrt{\left(\frac{n}{n^{(0)}}\right)\left(\frac{\delta a_-}{a}\right)}} \times\left[-\frac{\sigma}{\sqrt{\pi}\xi_-} + \left(\frac{1}{2} + \left(\frac{\sigma}{\xi_-}\right)^2\right) e^{\sigma^2/\xi_-^2}\mathrm{erfc}\left(\frac{\sigma}{\xi_-}\right)\right]. \tag{4.33}$$

The profiles of the total depletion $\tilde{n} = \sum_\pm \tilde{n}_\pm$ and anomalous density $\tilde{m} = \sum_\pm \tilde{m}_\pm$ are shown in figures 4.10 (b) and (c). We observe that the depletion and the anomalous correlation of the droplet decrease with a_{12}/a and σ/ξ. The anomalous density is somehow insensitive to the disorder correlation length (slightly decays with σ/ξ, see figure.4.10.(c)).

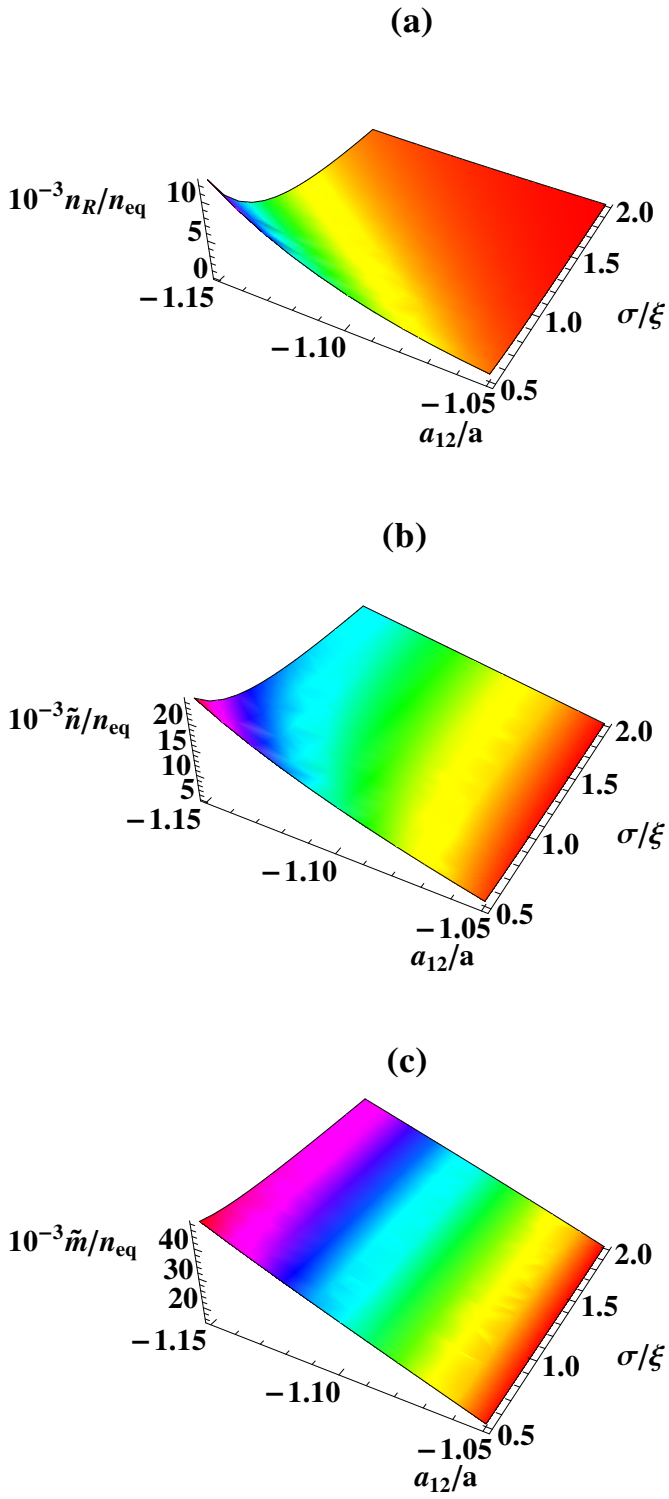

Figure 4.10: (a) Glassy fraction n_R, (b) the total depletion $\tilde{n}$, (c) the anomalous density of the droplet $\tilde{m}$ as a function of a_{12}/a and σ/ξ for $R = 1000$.

Finite temperature effects

At finite temperature the properties of the droplet can be analyzed by minimizing the free energy (1.55). In terms of the equilibrium density it turns out to be given by

$$\frac{F}{|E_0|} = \frac{E}{|E_0|} - \sum_{\pm} \frac{\sqrt{2}\pi^4(\delta a_+/a)^4(n/n^{(0)})^{-5/2}}{124416(\delta a_\pm/a)^{3/2}} \left(\frac{T}{|E_0|/N}\right)^4, \tag{4.34}$$

which is divergent when the density tends to zero. Its behavior is depicted in figure 4.11.

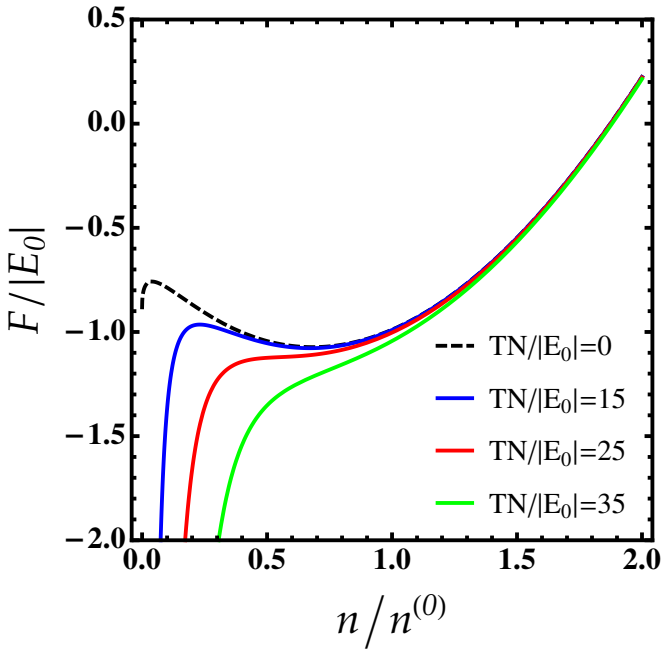

Figure 4.11: Free energy F from equation (4.34) as a function of the density n for $a_{12}/a = -1.1$ and $\sigma/\xi = 0.63$, and $R = 1000$.

Figure 4.11 shows that at temperatures $T = T_c \geq 25E_0$ and for $R = 10^3$, the local minimum of the free energy start to disappear signaling the destabilization of the self-bound droplet. Rising further the temperature $T > T_c$, the droplet is fully evaporated due to the thermal fluctuations. For larger R, the droplet evaporates even at very low temperatures. This tendency can be interpreted as natural that as temperature increases, effect of the interplay between disorder and thermal fluctuations becomes prominent making the atomic motion increasingly significant. In such a situation, the droplet may fail to maintain its zero-pressure state and thus,

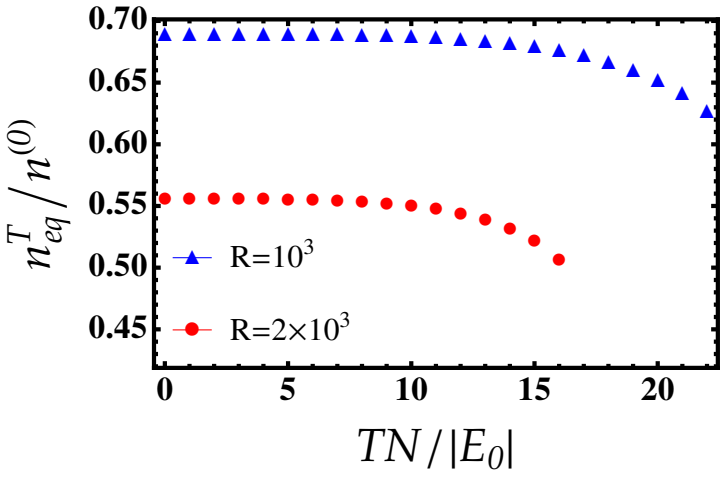

Figure 4.12: Thermal equilibrium density $n^T_{\rm eq}/n^{(0)}$ as a function of the temperature for different values of the disorder strength and $a_{12}/a = -1.1$ and $\sigma/\xi = 0.63$.

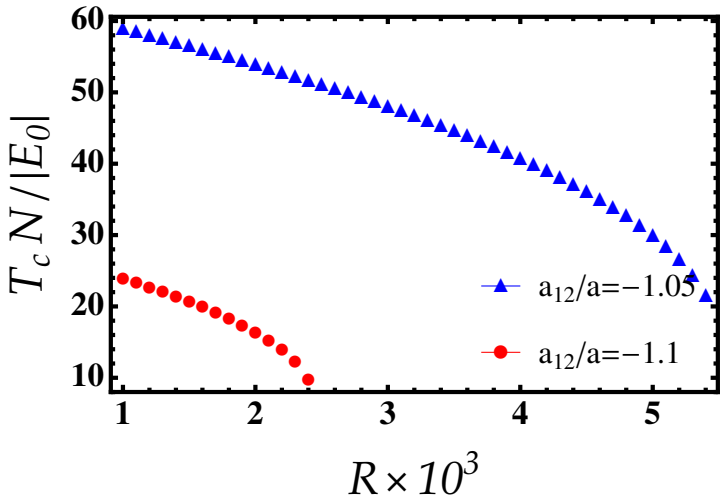

Figure 4.13: Critical temperature as a function of the disorder strength R for different values of a_{12}/a and $\sigma/\xi = 0.63$.

evaporates [69].

The temperature dependence of the equilibrium density and the critical temperature of the droplet can be determined by setting $\partial F/\partial n = 0$, and $\delta a_+/a \ll 1$ [46, 62]. Figure 4.12 shows that the thermal equilibrium density $n_{\rm eq}^T$ exhibits very weak temperature dependence at $T \leq 13|E_0|/N$, while it reduces for higher temperatures. We see also that it sorely diminishes with the disorder strength, indicating that the droplet becomes strongly depleted.

Effects of the disorder strength on the critical temperature is displayed in figure 4.13. We see that T_c decreases with increasing R and with decaying $|a_{12}/a|$.

4.6 Generalized Gross-Pitaevskii equation

To better understand effects of disorder on the droplet state, we will derive in this section the generalized disorder GPE and solve it numerically. By solving such an equation, various observables and properties of the self-bound droplet, including density profiles, excitation spectrum, and collective modes, can be calculated. Moreover, theoretical solutions of the developed generalized GPE serve as a guide for designing and optimizing experiments for quantum droplets.

In the miscible phase and close to the collapse point, we can describe the system with an effective low-energy theory, an effective single component GPE, where we neglect the internal dynamics between the respective components, and we consider identical spatial modes for the two components:

$$\psi_j(\mathbf{r}, t) = \sqrt{n_j}\phi(\mathbf{r}, t), \tag{4.35}$$

where $\phi(\mathbf{r}, t)$ is a scalar wave-function common to both species, which implies that the density ratio is locked to the condition [46]

$$\frac{n_1}{n_2} = \sqrt{\frac{g_2}{g_1}}. \tag{4.36}$$

We then will introduce two assumptions: (i) The condensate, the thermal cloud and the anomalous correlation must vary slowly at the scale of the extended healing length [62, 64]. (ii) The disorder potential changes smoothly in space on a length scale comparable to the healing length [181]. For the sake of simplicity, we neglect the fluctuations induced by the disorder potential. The functional energy associated to the equation of state (4.30) which describes a self-bound droplet subjected to an external disorder can be written in the following dimensionless form:

$$\mathcal{E}(\phi,\phi^*) = \frac{1}{2}|\nabla\phi|^2 - \frac{3}{2}|\phi|^4 + \sqrt{\frac{n_{\rm eq}}{n^{(0)}}}|\phi|^5 + \tilde{U}|\phi|^2, \tag{4.37}$$

where $\tilde{U} = U\tau/\hbar$, and $\tau = 6\hbar/n_{\rm eq}g|(\delta a/a)_+|$. The corresponding GPE can be derived using $i\partial\phi/\partial\tilde{t} = \partial\mathcal{E}/\partial\phi^*$. This yields

$$i\frac{\partial\phi(\tilde{\mathbf{r}},\tilde{t})}{\partial\tilde{t}} = \left(-\frac{1}{2}\nabla^2_{\tilde{\mathbf{r}}} + \tilde{U}(\tilde{\mathbf{r}}) - 3|\phi|^2 + \frac{5}{2}\sqrt{\frac{n_{\rm eq}}{n^{(0)}}}|\phi|^3\right)\phi(\tilde{\mathbf{r}},\tilde{t}), \tag{4.38}$$

where we introduced the rescaled coordinate $\tilde{r} = r\sqrt{m/\hbar\tau}$ and the rescaled time $\tilde{t} = t/\tau$. Equation (4.38) can be thought of as describing self-consistently the LHY and disorder effects.

Stationary solutions of the generalized GPE (4.38) are looked for as $\phi(\tilde{\mathbf{r}},\tilde{t}) = \phi(\tilde{\mathbf{r}})\exp(-i\tilde{\mu}\tilde{t})$, where $\phi(\tilde{\mathbf{r}})$ obeys the static generalized GPE

$$\tilde{\mu}\phi(\tilde{\mathbf{r}}) = \left(-\frac{1}{2}\nabla^2_{\tilde{\mathbf{r}}} + \tilde{U}(\tilde{\mathbf{r}}) - 3|\phi|^2 + \frac{5}{2}\sqrt{\frac{n_{\rm eq}}{n^{(0)}}}|\phi|^3\right)\phi(\tilde{\mathbf{r}}), \tag{4.39}$$

which enables us to analyze the droplet density profiles for different regimes.

We consider now a Gaussian correlated disorder potential defined as [182]:

$$\tilde{U}(\mathbf{r}) = \tilde{U}_0\sum_{j=1}^{M} f(\tilde{\mathbf{r}} - \mathbf{r}_j), \tag{4.40}$$

where M is the number of impurities, U_0 is the amplitude, and r_j are the uncorrelated

random positions, and f is a real-valued function of width σ and has Gaussian-shaped impurities $f(\tilde{\mathbf{r}}) = e^{-\tilde{\mathbf{r}}^2/\tilde{\sigma}^2}$, such that $0 \leq f(r) \leq 1$, with $\tilde{\sigma} = \sigma\sqrt{m/\hbar\tau}$ being the dimensionless the characteristic length of the disorder.

4.6.1 Density profiles

Now we address different aspects that can be emerged in a disordered stationary droplet by numerically solving equation (4.39) using the split-step method which bases on the fast Fourier transforms [49]. To generate the Gaussian potential we use a set of random numbers which are then mapped into the interval $[0, L]$ by a linear transformation. We choose $M = 300$, $L = 30$, and a small width [182].

In figure 4.14 we plot the density profiles as a function of the radial distance. Two fascinating properties are observed here. First, the density in the plateau region increases and varies fastly with the disorder strength and the correlation length. Second, the situation is completely different near the edge of the droplet, the atomic density varies slowly even for large disorder parameters since the LHY and interaction energies dominate over the disorder effects.

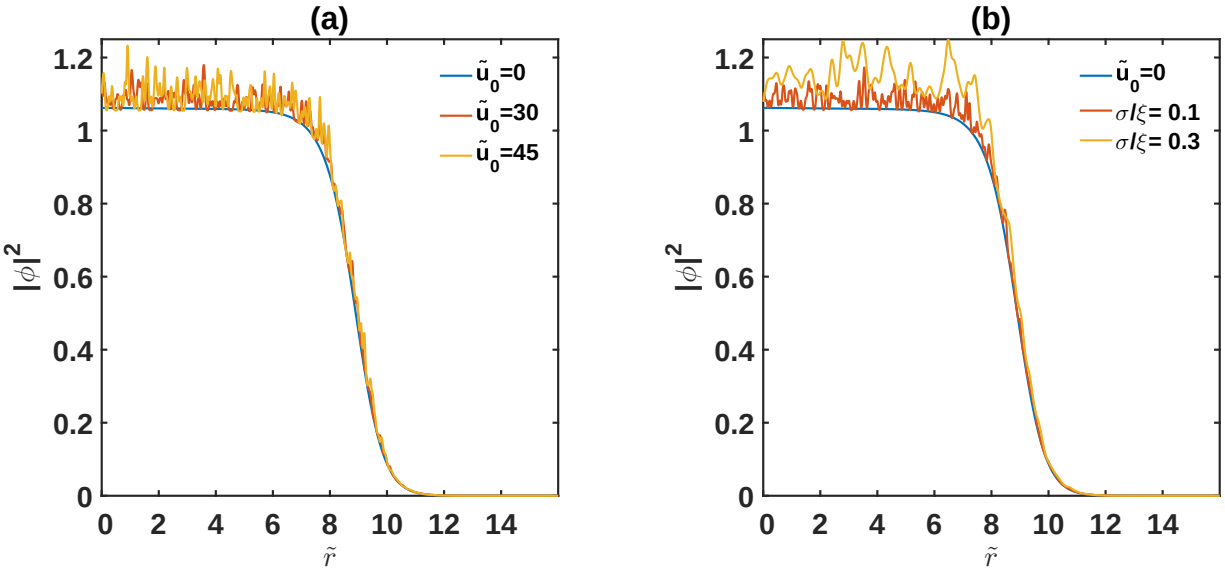

Figure 4.14: (a) Density profiles of the droplet for different values of the disorder strength for $\tilde{N} = 3000$, $\tilde{\sigma} = 0.1$, and $a_{12}/a = -1.05$. (b) Density profiles of the droplet for different values of the disorder correlation length for $\tilde{N} = 3000$, $\tilde{U} = 30$, and $a_{12}/a = -1.05$.

4.6.2 Collective modes

A useful way to qualitatively or even quantitatively analyze the collective modes of disordered droplets is to use a variational method. The Gaussian variational approach gives a useful and important approximate description of the quantum droplet. We then consider a simplified Gaussian variational ansatz:

$$\phi(\tilde{\mathbf{r}},\tilde{t}) = \sqrt{\frac{\tilde{N}}{\pi^{3/2}q(\tilde{t})^3}}\exp\left[\frac{-\tilde{\mathbf{r}}^2}{2q(\tilde{t})^2} + i\gamma(\tilde{t})\tilde{\mathbf{r}}^2\right], \tag{4.41}$$

where the variational parameters are the droplet width q, and the phase γ. The normalization factor ensures the conservation of the condition: $\int d\tilde{\mathbf{r}}\phi(\tilde{\mathbf{r}},\tilde{t}) = \tilde{N}$, where $\tilde{N} = (m/\hbar\tau)^{3/2}\,N/n_{\rm eq}$ with N being the total number of particles in the droplet. We replace the ansatz (4.41) in the density Lagrangian

$$\mathcal{L} = \frac{i}{2}\int_0^\infty d\mathbf{r}\left[\phi\frac{d\phi^*}{dt} - \phi^*\frac{d\phi}{dt}\right] + \mathcal{E}, \tag{4.42}$$

obtain the Lagrangian

$$L = \int d\mathbf{r}\mathcal{L}. \tag{4.43}$$

Performing integration over r-space, we get

$$\begin{aligned}\frac{L}{\tilde{N}} = {}& \frac{3}{2}\dot{\gamma}q^2 + 3\gamma^2q^2 + \frac{3}{4q^2} - \frac{3\tilde{N}}{2^{5/2}\pi^{3/2}q^3} + \sqrt{\frac{n_{\rm eq}}{n^{(0)}}}\frac{2^{3/2}\tilde{N}^{3/2}}{\pi^{9/4}5^{3/2}q^{9/2}} \\ & + \sum_{j=1}^{M}\tilde{U}_0\frac{\tilde{\sigma}^3}{(q^2+\tilde{\sigma}^2)^{3/2}}\exp\left[\frac{-\tilde{r}_j^2}{\tilde{\sigma}^2}\left(1-\frac{q^2}{q^2+\tilde{\sigma}^2}\right)\right].\end{aligned} \tag{4.44}$$

The corresponding Euler-Lagrange equations of motion read:

$$\gamma = \frac{1}{2q}\frac{dq}{dt}, \tag{4.45}$$

and

$$\frac{d^2q}{dt^2} = -\frac{dU_{\rm eff}(q)}{dq}, \tag{4.46}$$

where we have introduced the effective potential for oscillations of the droplet width

$$U_{\text{eff}}(q) = \frac{1}{2q^2} - \frac{\tilde{N}}{2^{3/2}\pi^{3/2}q^3} + \sqrt{\frac{n_{eq}}{n^{(0)}}}\frac{2^{5/2}\tilde{N}^{3/2}}{3\pi^{9/4}5^{3/2}q^{9/2}} + \frac{2}{3}\sum_{j=1}^{M}\tilde{U}_0\frac{\tilde{\sigma}^3}{(q^2+\tilde{\sigma}^2)^{3/2}}\exp\left[\frac{-\tilde{r}_j^2}{\tilde{\sigma}^2}\left(1-\frac{q^2}{q^2+\tilde{\sigma}^2}\right)\right]. \tag{4.47}$$

The droplet width can be obtained by numerically solving the variational differential equation (4.46). In figure (4.15) we plot the results of the simulation for system parameters used above. Figure 4.15. (a) shows that the droplet width q increases with the particle number while it decreases with the disorder strength notably for large $\tilde{N}$. It exhibits periodic oscillations during its time evolution as shown in figure 4.15 (b). We see also that the temporal width is periodically broadening for relatively strong strength.

The low-lying excitations around the equilibrium solutions q_0 (droplet minimum) can be computed by using the linearization $q(t) = q_0 + \delta q(t)$, where $\delta q(t) \ll q_0$, and $\delta q(t) = \delta q e^{i\omega t}$. Therefore, this gives for the frequencies of the breathing modes:

$$\omega^2 = \frac{d^2U_{\text{eff}}(q)}{dq^2}\Big|_{q=q_0}. \tag{4.48}$$

In figure 4.16 we plot the resulting oscillation frequencies as predicted by equation (4.48). It is interesting to observe that the frequencies of the breathing modes of the droplet are increasing with the disorder strength in the whole range of atoms number.

This chapter has focused on how weak 3D random potentials (with correlated and uncorrelated functions) influence the properties of self-bound droplets. All in all we found that the interplay of interspecies interactions, the repulsive LHY corrections and the disorder plays a pivotal role in the formation, the stability, the structure, and the breathing modes of the quantum liquid droplet. We showed in particular that when the disorder parameters (the strength and the correlation length) and the

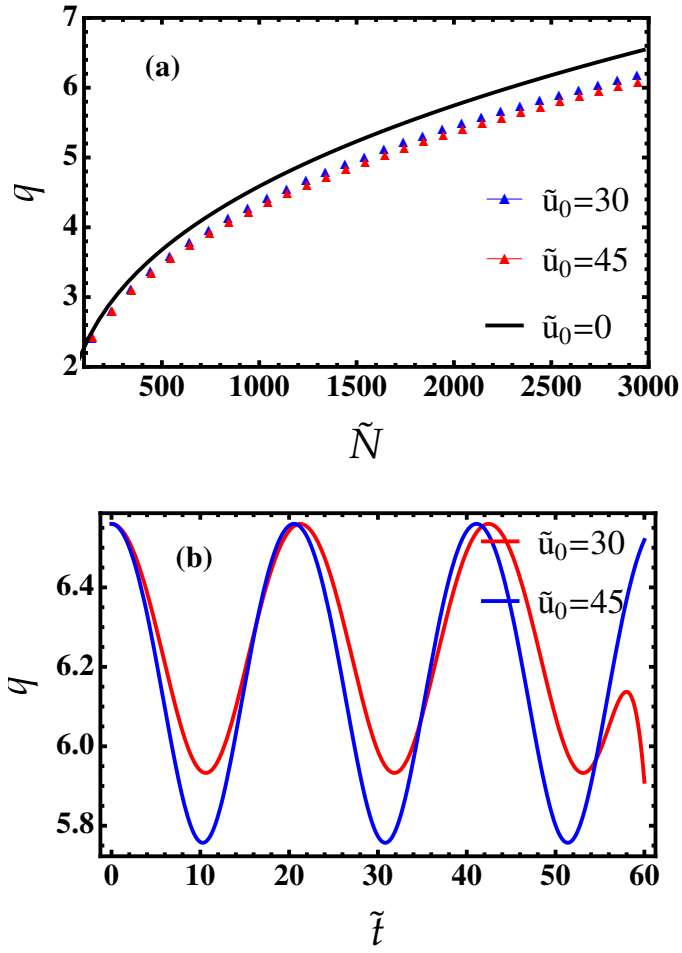

Figure 4.15: (a) Droplet width as a function of the particle number for several values of $\tilde{U}_0$. (b) Time evolution of the droplet width for several values of $\tilde{U}_0$. Parameters are $a_{12}/a = -1.05$ and $\tilde{\sigma} = 0.1$.

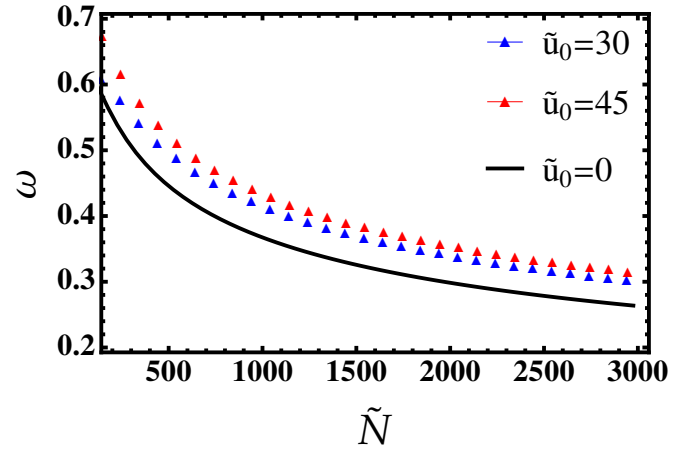

Figure 4.16: Excitation frequencies in units of $1/\tau$ as a function of the particle number for several values of $\tilde{U}_0$.

temperature exceed a certain critical value, the droplet evaporates and eventually entirely destroys.

In the next chapter we are going to examine the role of a 1D random speckle potential on the equilibrium and dynamical properties of self-bound droplets in binary BECs.

Chapter 5

Self-bound liquid droplets in one-dimensional speckle potentials

As we have seen in previous chapters, the self-bound droplet stabilizes due to the delicate balance between mean-field attraction and beyond mean-field repulsion provided by the LHY corrections. This exquisite stabilization relies critically on the dimensionality of the system; the LHY fluctuations are repulsive in higher dimensions while being attractive in 1D. A major advantage of 1D problem which reflected in a suppression of three-body losses [8], is that a stable droplet can survive even in a strongly-interacting regime due to the boosted role played by quantum fluctuations [29, 71]. In addition, 1D quantum droplets typically exhibit intriguing properties, such as solitonic behavior and robust stability against collapse [125]. In 1D configuration, such self-bound droplets can exist in two different regimes namely: Gaussian-like shape for small number of particles and flat-top shape in the case of large number of atoms [61, 183].

Early studies in 1D quantum droplets focused on stability, structure and on the dynamics [61, 183]. More recently, several aspects of 1D quantum liquids have been explored including collective excitations [184], quantum Monte-Carlo simulations [71], the impact of discreteness in the form of discrete droplets [185, 186], thermal

effects and evaporation [20, 188, 187], effects of higher-order corrections [44, 68, 69, 189, 190], phase diagram in 1D optical lattices [191], universality classes [192], and droplet molecules [193].

However, to the best of our knowledge, the physics of 1D disordered ultradilute quantum liquids has never been explored before. The aim of this chapter is then to investigate the impacts of 1D weakly random potential created by optical speckles on a self-bound droplet of Bose mixtures. Major features of such optical speckles are: i) long-ranged, ii) non-Gaussian potentials, iii) their amplitude, geometry and correlation length can be readily adjusted. These features allow us to explore quantum droplets with a high degree of control.

We shed light in particular on how quantum and speckle disorder fluctuations affect the stability and equilibrium properties of the self-bound droplets. Using the HM [140] theory developed in Chapter 4, we derive useful analytical expressions for the equation of state, the equilibrium density, and the glassy fraction in terms of the disorder parameters (strength and correlation length) at both zero and finite temperatures. We investigate in addition the equilibrium and the dynamics of such a disordered droplet in both Gaussian-like and flat-top regimes. To this end, we solve numerically the generalized disorder-dependent GPE.

5.1 Bulk properties

Throughout this chapter we consider a weakly interacting symmetric Bose mixture with equal masses $m_1 = m_2 = m$, equal densities $n_1 = n_2 = n/2$, equal intraspecies and interspecies coupling constants $g_1 = g_2 = g$, $g_{12} = g_{21}$, subjected to a weak disorder potential U. We recall that the disorder potential is assumed to have vanishing ensemble averages $\langle U(\mathbf{r})\rangle = 0$ and a finite correlation of the form $\langle U(\mathbf{r})U(\mathbf{r}')\rangle = R(\mathbf{r}-\mathbf{r}')$.

Assuming the weak-coupling regime where the correlation length is much larger

than the mean interparticle separation [194]. The Bogoliubov theory can be then safely used in low-dimensional systems at both zero and finite temperatures. Let us then consider a self-bound droplet subjected to a 1D weak speckle disorder which is often used with ultracold atoms experiments [80, 81, 83, 177, 133]. Experimentally, effective 1D speckle disorder can be created when coherent light is diffracted by a ground glass diffuser with a quasi-1D slit and focused by a convergent lens [80, 81, 83, 177, 133]. The speckle disorder is characterized by the following real-space correlation function : $R(x) = U_R^2 \mathrm{sinc}^2(x/\sigma)$, where U_R is the disorder strength and σ is the disorder correlation length. In Fourier space, it can be written as [178, 145]:

$$R(k) = \pi\sigma U_R^2 \left(1 - \frac{k\sigma}{2}\right) \Theta\left(1 - \frac{k\sigma}{2}\right), \tag{5.1}$$

where Θ denotes the Heaviside function. Indeed the function $R(k)$ has a sharp high-momentum cutoff at $k = 2/\sigma$.

5.1.1 Energy and stability

Inserting equation (5.1) into equation (4.14), one obtains for the ground-state energy:

$$\frac{2E}{N|\varepsilon_B|} = \frac{32(g/g_{12})^2}{9\pi^2(\delta g_+/g)} \left(\frac{n}{n^{(0)}}\right) - \frac{16\sqrt{2}(g/g_{12})^2}{9\pi^2(\delta g_+/g)} \sqrt{\frac{n}{n^{(0)}}} \sum_{\pm} \left(\frac{\delta g_\pm}{g}\right)^{3/2} - \frac{9\pi^2(g_{12}/g)^2(\delta g_+/g)^2 R^2\sigma^2}{256\xi^2} \tag{5.2}$$

$$\times \sum_{\pm} \left\{ \frac{2\sqrt{2}\cot^{-1}\left[\frac{\sigma}{\sqrt{2}\xi}\sqrt{(n/n^{(0)})(\delta g_\pm/g)}\right]}{(\sigma^2/\xi^2)(n/n^{(0)})(\delta g_\pm/g)} + \ln\left[\frac{(n/n^{(0)})(\delta g_\pm/g)}{2\xi^2/\sigma^2 + (n/n^{(0)})(\delta g_\pm/g)}\right] \right\},$$

where $n^{(0)} = 16gm/\left(9\pi^2\hbar^2(\delta g_+/g)^2\right)$ is the 1D equilibrium density [61], $R = U_R/|\varepsilon_B|$, and $|\varepsilon_B| = \hbar^2/ma_{12}^2$ is the binding energy of dimers composed from atoms from different component. For $R = 0$, the energy (5.2) reduces to the result of a clean droplet [61, 189].

Figure 5.1 shows that by increasing R and decreasing σ/ξ, the minimum and

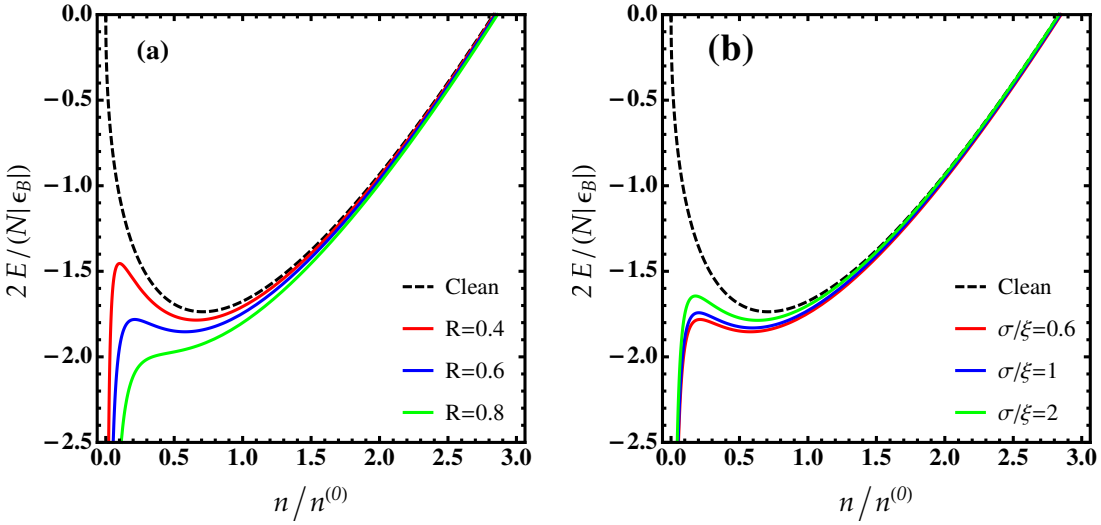

Figure 5.1: (a) Ground-state energy of a 1D liquid from equation (5.2) as a function of the density n for various values of the disorder strength for $g_{12/g} = -0.7$ and $\sigma/\xi = 0.6$. (b) Ground-state energy of a 1D liquid as a function of the density n for various values of the correlation length for $g_{12}/g = -0.7$ and $R = 0.6$.

maximum start to disappear, indicating that the liquid phase becomes unstable. Note that the liquid droplet evaporates even for very small R. This can be understood from the intrinsic strong correlation between particles arising from the geometric confinement in 1D. Remarkably, the 1D droplet remains robust even for relatively small correlation length, σ/ξ, on contrary to the 3D droplet which evaporates for small σ/ξ (disappearance of the local minimum in the ground-state energy) [195]. Our results suggest also that the disorder correlation length has a minor effect at higher densities ($n/n^{(0)} \geq 1$) as shown in figure 5.1. (b), which is not the case in 3D disordered droplets.

The glassy fraction $n_R/n = \sum_{\pm} n_{R\pm}/n$ can be computed via equation (4.17)

$$\frac{n_R}{n} = \frac{9\pi^2 (g_{12}/g)^2 (\delta g_+/g)^2 R^2 \sigma}{256\sqrt{2}\xi} \sum_{\pm} \frac{\cot^{-1}\left[\frac{\sigma}{\xi\sqrt{2}}\sqrt{(n/n^{(0)})(\delta g_\pm/g)}\right]}{(n/n^{(0)})^{3/2}(\delta g_\pm/g)^{3/2}}, \tag{5.3}$$

its behavior in terms of the disorder strength R is depicted in figure 5.2. We see that n_R increases monotonically with R signaling that the atoms occupy the localized state giving rise to the transition to a new quantum phase. Consequently, the presence of a small amount of disorder may significantly alter the stability and the

formation of the droplet.

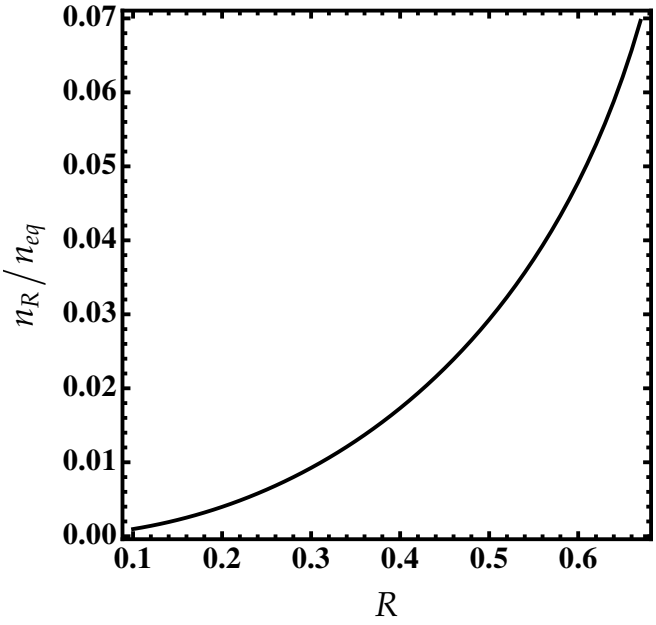

Figure 5.2: Glassy fraction $n_R = \sum_{\pm} n_{R\pm}$ inside the droplet as a function of the disorder srength R for $\sigma/\xi = 0.6$ and $g_{12}/g = -0.7$.

The validity criterion of the present approach requires the condition $n_R/n \ll 1$. For instance, in the case of $g_{12}/g = -0.7$ and $\sigma/\xi = 0.6$, one has $n_{\rm eq}/n^{(0)} = 0.7$, and hence the critical disorder strength below which the droplet is stable must be $R \ll 3.183$.

In figure 5.3 we present the equilibrium density $n_{\rm eq}/n^0$ of a 1D dirty quantum liquid, found from the minimum of the ground-state energy (5.2). As expected, the equilibrium density decreases in the limit of small disorder correlation length. In such a regime the disorder effects dominate both the LHY and the mean-field forces.

5.1.2 Thermal effects

It is well known that ignoring entirely thermal fluctuation effects is a difficult task in current experiments. Therefore, it is instructive to analyze the role of low but finite temperatures on the equation of state and on the stability of the quantum

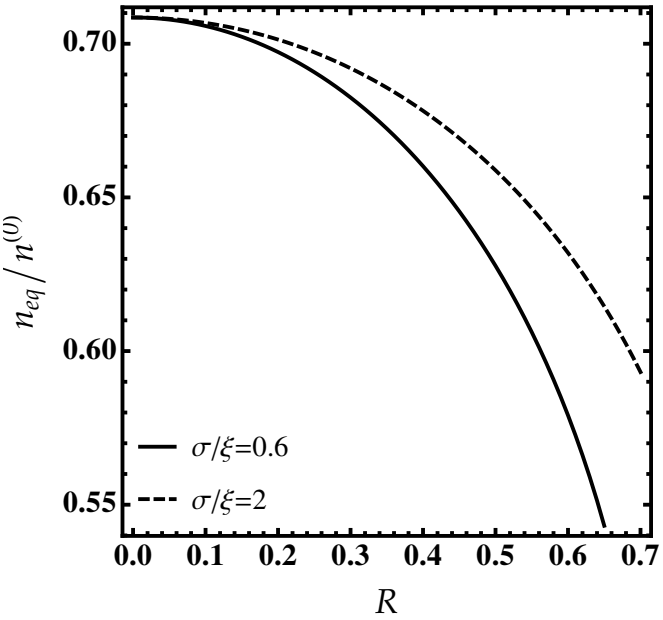

Figure 5.3: Equilibrium density $n_{\rm eq}/n^{(0)}$ of a of a 1D dirty quantum liquid as a function of the disorder strength R for various values of σ/ξ.

droplet. At finite temperature the free energy is given by [62, 63]:

$$F = E + T\int \frac{dk}{2\pi}\sum_{\pm}\ln\left(\frac{2}{\coth\left(\varepsilon_{k\pm}/2T\right)+1}\right). \tag{5.4}$$

By integrating this expression over momentum we arrive

$$\frac{F}{L} = \frac{E}{L} - \frac{\pi\sqrt{m}T^2}{12\hbar}\left[\left(n\frac{\delta g_+}{g}\right)^{-1/2} + \left(n\frac{\delta g_-}{g}\right)^{-1/2}\right], \tag{5.5}$$

which takes the following dimensionless form:

$$\frac{2F}{N|\varepsilon_B|} = \frac{2E}{N|\varepsilon_B|} - \frac{\pi(g/g_{12})^2}{6}\left(\frac{32(n/n^{(0)})}{9\pi^2(\delta g_+/g)^2}\right)^{-3/2}\times\left(\frac{T}{|\varepsilon_B|}\right)^2\sum_{\pm}\left(\frac{\delta g_\pm}{g}\right)^{-1/2}, \tag{5.6}$$

where E is given in equation (5.2) and the subleading term accounts for thermal fluctuation corrections.

Figure 5.4 shows that the free energy exhibits first a maximum in the limit of small densities. After this maximum is exceeded, the droplet spreads spontaneously

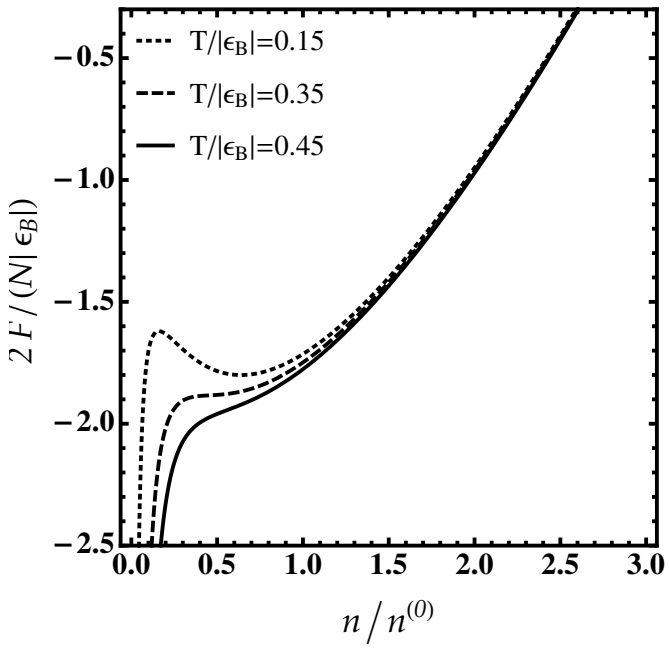

Figure 5.4: Free energy from Eq.(5.6) for different values of temperatures $T/|\varepsilon_B|$. Parameters are: $\sigma = 0.6$, $R = 0.4$, and $\delta g_+/g = -0.7$.

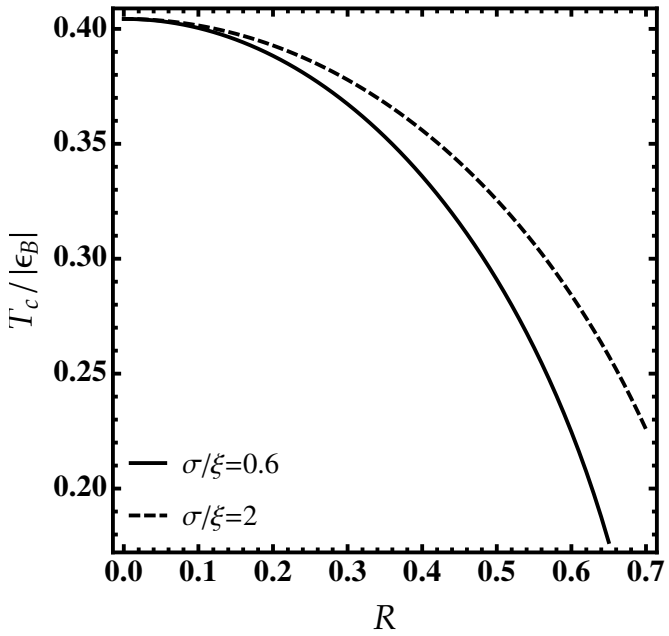

Figure 5.5: Critical temperature T_c of a 1D droplet as a function of the disorder strength R for different values of the disorder correlation length σ. Parameters are: $\sigma = 0.6$, and $\delta g_+/g = -0.7$.

until it reaches the minimum free energy value. The state corresponding to this minimum is a stable quantum droplet phase, while the maximum corresponds to an unstable state. The two solutions start to disappear at a critical temperature $T \simeq 0.35|\varepsilon_B|$. For $T > 0.35|\varepsilon_B|$, the quantum droplet becomes unstable and eventually evaporates.

In Figure 5.5 we plot the critical temperature T_c associated with the free energy minimum as a function of the disorder strength for different values of the disorder correlation length. We see that T_c decreases with R while it increases with σ notably for large R due to the interply of the disorder and LHY effects.

5.2 Static and dynamical properties

To gain a deeper understanding of the formation, profiles, and characteristics of 1D quantum droplets, the generalized GPE must be solved.

Following the same procedure provided in Chapter 4 and assume that the condensate ϕ varies smoothly at the scale of the extended healing length. As a consequence, we can include corrections due to quantum, thermal and disorder fluctuations locally as nonlinear terms in the GPE and treat them classically. The functional energy reads:

$$\mathcal{E}(\phi,\phi^*) = \frac{\hbar^2}{2m}|\nabla\phi|^2 + \frac{\delta g_+}{4g}|\phi|^4 + U|\phi|^2 - \frac{\sqrt{m}}{3\sqrt{2}\pi\hbar}g^{3/2}|\phi|^3\sum_{\pm}\left(\frac{\delta g_\pm}{g}\right)^{3/2}. \quad (5.7)$$

It is convenient to introduce characteristic units of length $\tilde{x} = x/\xi$, time $\tilde{t} = \hbar t/(m\xi^2)$, and energy $E_0 = \hbar^2/(m\xi^2)$, where $\xi = (\pi\hbar^2/\sqrt{2}mg)\sqrt{\delta g_+/g}$ is the extended healing length. This gives for the wavefunction

$$\tilde{\phi} = \sqrt{\frac{\pi\xi}{2}}\left(\frac{\delta g_+}{g}\right)^{3/4}\phi. \quad (5.8)$$

The regime of interest consists of setting $\delta g_+/g \sim 0$ and $\delta g_-/g \approx 2$ [61], thus the

dimensionless functional energy turns out to be given

$$\tilde{\mathcal{E}}(\tilde{\phi},\tilde{\phi}^*)=\frac{1}{2}|\nabla\tilde{\psi}|^2+\frac{1}{2}|\tilde{\phi}|^4+\tilde{U}|\tilde{\phi}|^2-\frac{1}{3\sqrt{2}}|\tilde{\phi}|^3\sum_{\pm}\left(\frac{\delta g_{\pm}}{g}\right)^{3/2}, \tag{5.9}$$

where $\tilde{U}=U/E_0$.

The droplet wavefunction is then given by the solution of the 1D disorder-dependent GPE which can be derived using $i\partial\tilde{\phi}/\partial t=\partial\tilde{\mathcal{E}}/\partial\tilde{\phi}^*$:

$$i\frac{\partial\tilde{\phi}(\tilde{x},\tilde{t})}{\partial\tilde{t}}=\Big[-\frac{1}{2}\frac{\partial^2}{\partial\tilde{x}^2}+\tilde{U}(\tilde{x})+|\tilde{\phi}|^2-\frac{1}{2^{3/2}}\sum_{\pm}\left(\frac{\delta g_{\pm}}{g}\right)^{3/2}|\tilde{\phi}|\Big]\tilde{\phi}(\tilde{x},\tilde{t}). \tag{5.10}$$

In the absence of the disorder potential, equation (5.10) reduces to that derived in the literature [61].

We choose for the disorder potential a Gaussian spikes defined as [182]:

$$\tilde{U}(\tilde{x})=\tilde{U}_0\sum_{i=1}^{M}e^{-(\tilde{x}-\tilde{x}_i)^2/\sigma^2}, \tag{5.11}$$

where M is the number of impurities, $\tilde{U}_0$ is the strength of the spike, and σ is a dimensionless width. This speckle potential is generated using a set of random numbers which are then mapped into the interval $[-L,L]$ by a linear transformation. For $M=300$, $L=30$, and a small width [182, 195], the behavior of the potential (5.11) is displyaed in figure 5.6.

5.2.1 Flat-top droplet

In order to obtain the stationary localized states, we perform the numerical integration of the static generalized GPE by adopting the split-step Fourier spectral method. Stationary states with chemical potential, μ, can be computed using $\phi(\tilde{x},\tilde{t})=\phi(\tilde{x})\exp(-i\mu\tilde{t})$, where $\phi(\tilde{x})$ is an equilibrium solution. The results are shown in figure 5.7.

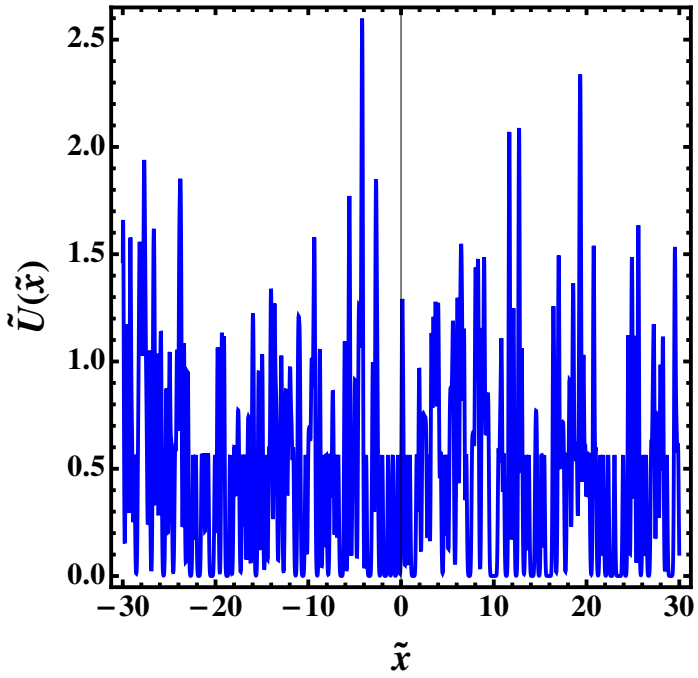

Figure 5.6: Typical disordered speckle potential from equation (5.11) for $M = 300$, $L = 30$, $\tilde{U}_0 = 1$, and $\sigma = 0.1$.

We see from figure 5.7. (a) and (b) that in the absence of disorder, the droplet reaches its flat top shape without any special structure. However, modulations in the density of the self-bound droplet are observed at finite disorder (even as small as $\tilde{U}_0 = 0.02$) in the plateau region. These modulations manifest themselves as a deformation of the quantum liquid droplet. As the strength, $\tilde{U}_0$, and the correlation length, σ, of the disorder are increased, the density fluctuations become larger leading to the emergence of a localized fraction. The same behavior holds true in the 3D case. When $\tilde{U}_0$ becomes sufficiently strong one can expect that the droplet fragments into multiple mini droplets.

An important remark is that the disorder effects are practically suppressed near the edge of the droplet whatever the values of the disorder strength and the temperature, most likely due to the surface effects which are striking enough to eliminate the influence of the disorder potential in this region. Similar behavior holds true in the 3D case as we have shown in Chapter 4.

Having obtained the stationary solution, we evolve it in time by solving the full time-dependent generalized GPE (5.10). In figure 5.8 we plot the spatiotemporal

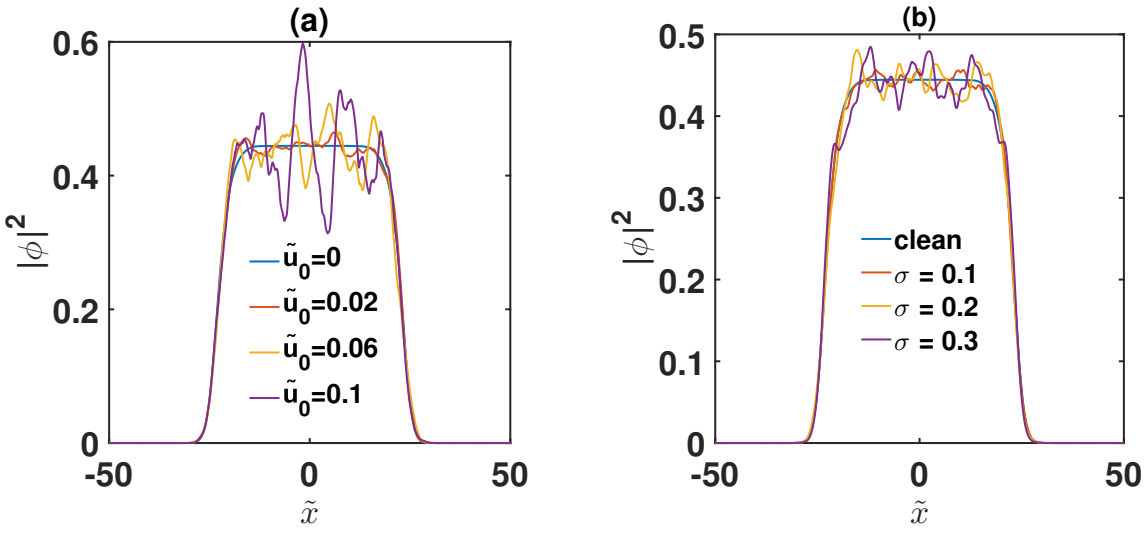

Figure 5.7: (a) Density profiles of a 1D droplet for different values of the disorder strength, $\tilde{U}_0$, and $\sigma = 0.1$. (b) The same but for different values of the disorder correlation length, σ, and $\tilde{U}_0 = 0.06$. Parameters are: $\tilde{N} = 20$, and $\delta g_+/g = 0.1$.

density of the evolution of a disordered droplet for several values of the disorder strength. It is clearly visible that the droplet is significantly sensitive to disorder and fragments into several localized modes (mini droplets) even for small disorder strength (see figure 5.8.(a)). Note that the number of the droplets depends on the disorder parameters. Increasing further the disorder strength, the long-range order is destroyed and thus, the droplet completely evaporates (see Fig. 5.8.b).

To better understand the time evolution of the droplet, we investigate its mean width, q. It can be calculated from the disorder-dependent GPE (5.10) using $q = \sqrt{\int_{-\infty}^{+\infty} d\tilde{x}\, \tilde{x}^2 |\phi(\tilde{x},\tilde{t})|^2}/2\tilde{N}$. We present the numerical results in figure 5.9. For weak disorder strength, the droplet width increases and then saturates. It exhibits slight oscillations in the long time limit. We also see that the presence of a weak disorder leads to shift the width from its clean counterpart at larger times, $t \geq 100$ (see red and orange curves).

5.2.2 Small droplet

In the case of a small droplet ($\tilde{N} \ll 1$), our simulations depict smooth density profiles (see figures 5.10. (a) and (b)) indicating that the disorder slightly deforms

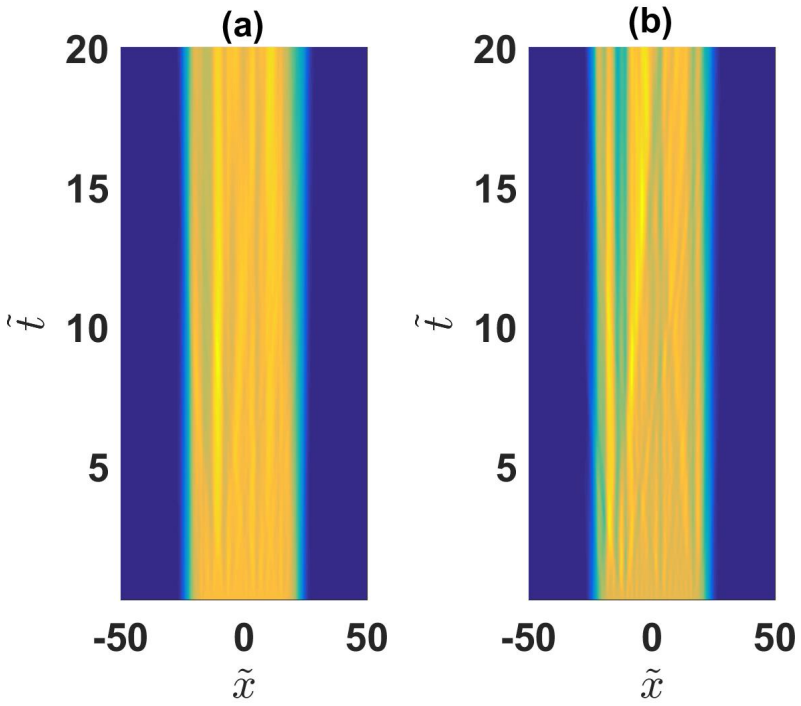

Figure 5.8: Spatiotemporal density plot of the evolution of a disordered 1D droplet for $\tilde{U}_0 = 0.06$ (a) and $\tilde{U}_0 = 0.1$ (b).

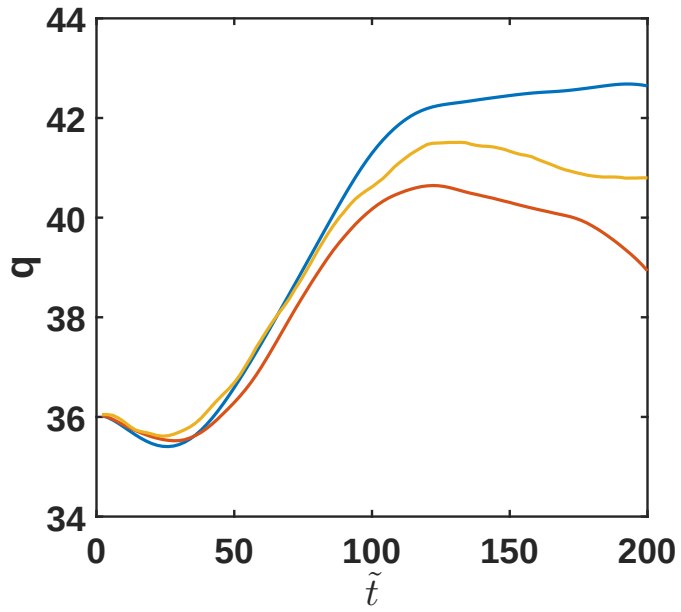

Figure 5.9: Time evolution of the 1D droplet width for several values of disorder strength. Blue line: $\tilde{U}_0 = 0$. Red line: $\tilde{U}_0 = 0.02$. Orange line: $\tilde{U}_0 = 0.06$. Parameters are: $\sigma = 0.1$, $\tilde{N} = 20$, and $\delta g_+/g = 0.1$.

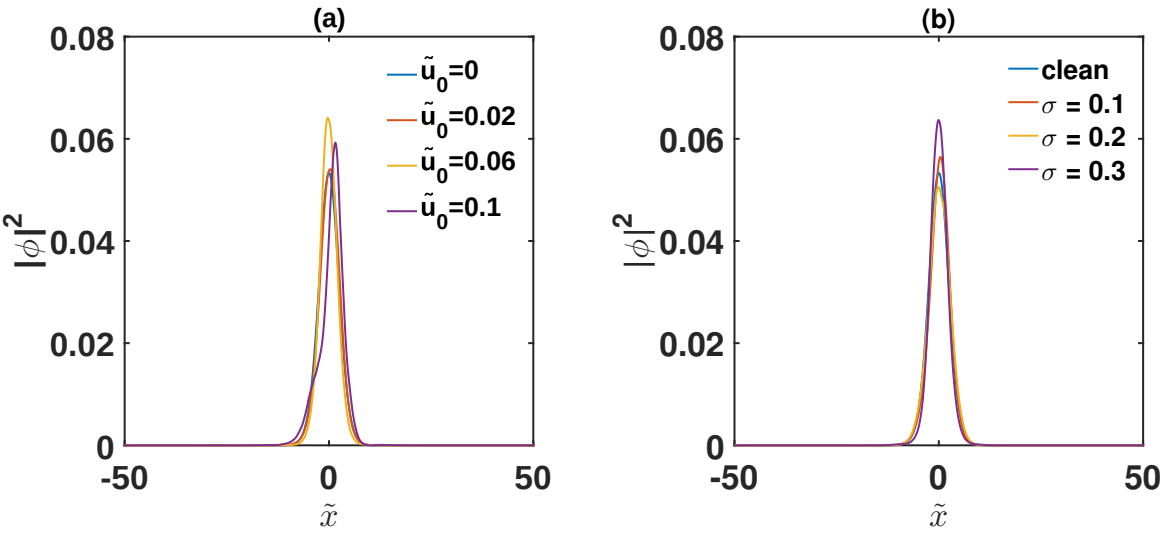

Figure 5.10: (a) Density profiles of a 1D droplet for different values of the disorder strength, $\tilde{U}_0$, and $\sigma = 0.1$. (b) The same but for different values of the disorder correlation length, σ, and $\tilde{U}_0 = 0.06$. Parameters are: $\tilde{N} = 0.2$, and $\delta g_+/g = 0.1$.

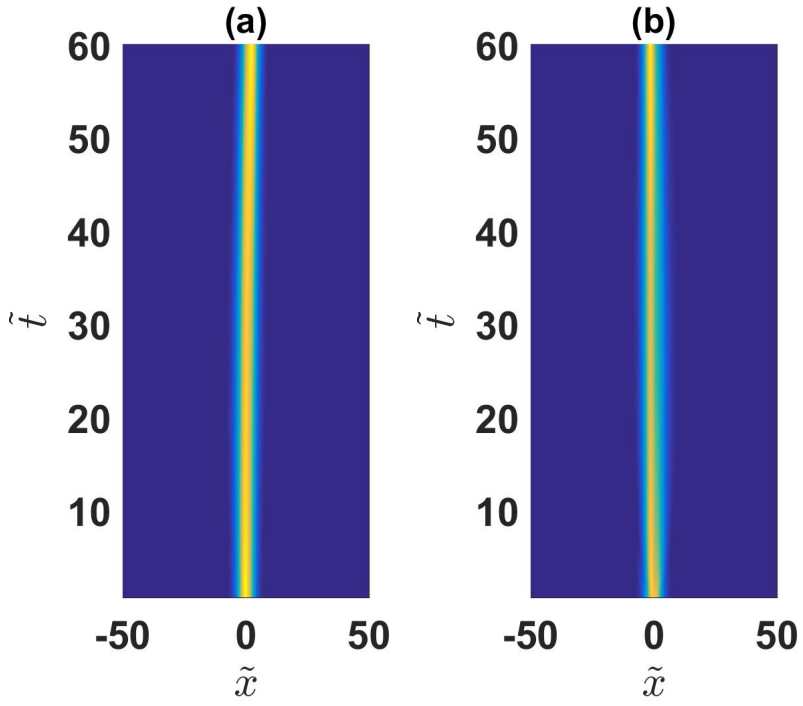

Figure 5.11: Spatiotemporal density plot of the evolution of a disordered 1D droplet for $\tilde{U}_0 = 0.06$ (a) and $\tilde{U}_0 = 0.1$ (b). Parameters are: $\sigma = 0.1$, $\tilde{N} = 0.2$, and $\delta g_+/g = 0.1$.

the small droplet compared to the flat top case. Notably, we observe that the droplet size shrinks as the disorder strength is increased and the amplitude reduces as the disorder correlation length gets larger. This can be attributed to the fact that the disorder is not strong enough to balance the LHY forces.

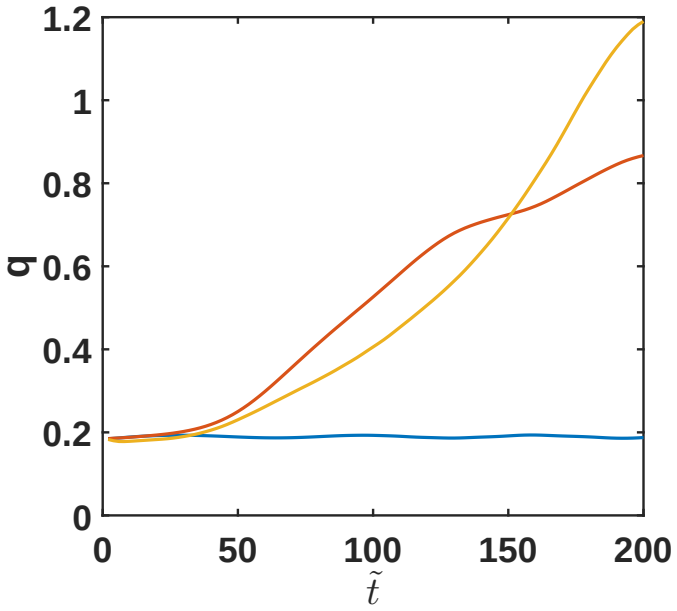

Figure 5.12: Time evolution of the 1D droplet width for several values of disorder strength. Blue line: $\tilde{U}_0 = 0$. Red line: $\tilde{U}_0 = 0.02$. Orange line: $\tilde{U}_0 = 0.06$. Parameters are: $\sigma = 0.1$, $\tilde{N} = 0.2$, and $\delta g_+/g = 0.1$.

Let us now discuss the time evolution of a small droplet. Figure 5.11. (a) shows that for a very weak disorder, the small droplet remains almost stable during its time evolution. The disordered droplet becomes narrower and develops small density modulations near the center as the disorder strength increases signaling that the action of the disorder is effective as shown in figure 5.11. (b). In such a situation many atoms, spewing more energy due to the disorder, leave the droplet and spread out thus dispersing over time.

Figure 5.12 shows that in the presence of a weak disorder, the width increases with time revealing that the droplet expands rapidly.

We infer that the ground-state properties of 1D droplets strongly depend on the speckle disorder parameters. It is revealed that stability of the droplet requires small disorder strength and large disorder correlation length (i.e. exceeds the healing

length of the condensate). Practically the same behavior persists for delta- and Gaussian-correlated disorder potentials (see Appendix A). The numerical simulation of the generalized GPE points out that the disorder tends to significantly affect the droplet profiles and its width. Noteworthy, the frequency of the breathing modes can be computed following the same variational method discussed in Chapter 4.

General conclusion

This chapter is intended to give a concluding overview of the achievements of this thesis, and to present an outlook for further studies.

Summary

The main theme of this thesis has been the study of the impact of weak disorder potentials on the properties of self-bound quantum droplets of a Bose-Bose mixture at both zero and finite temperatures.

The first part of this thesis was dedicated to the investigation of the equilibrium and nonequilibrium behaviors of homogeneous 3D binary BECs at zero temperature using the perturbative theory. We derived analytical expressions for the physical quantities of interest such as the glassy fraction, the EoS, the compressibility, and the superfluid density. Our results revealed that the intriguing interplay of the disorder and intra- and interspecies coupling may strongly influence both the quantum fluctuations and the superfluidity yielding a variety of interesting situations for relevant experimental parameters. We showed in addition that the localization of one component does not necessarily trigger the localization of the other species. Interestingly, we found that the disorder potential leads to a dramatic phase separation between the two species, changing the miscibility criterion of the mixture.

Additionally, we explored the non-equilibrium dynamics of binary BECs subjected to a Gaussian disorder potentials with time-periodic driving employing the time-dependent perturbative theory. We showed that the disorder fluctuations grow

with time and exhibit an oscillating character, its magnitude strongly depends on the system parameters. Among the main results emerging from our study is that even though the disorder is naively weak, it could have spectacular effects on the localization of atoms during the time evolution of the system. To date, there is no experimental work confirming this oscillating character of the condensate deformation.

Our predictions open up new perspectives for an experimental demonstration of the peculiar interplay between the disorder and interspecies interaction in the equilibrium and non-equilibrium regimes. They provide also deep insights for understanding phase separation of Bose-Bose mixtures.

In the second part of this thesis, we theoretically studied the properties of self-bound droplets in symmetric Bose mixtures, examining both 3D and 1D configurations. Our main objective is to understand the peculiar interplay among interspecies interactions, the LHY quantum fluctuations, and the disorder potential, and how these ingredients collectively affect the formation and the stability of these quantum objects. Initially, we conducted an analysis of disordered droplets, considering uncorrelated disorder (white-noise). We delve further into the impacts of correlated disorders on the droplet state, employing the two common models namely: Gaussian-correlated disorder and speckle potential, at both zero and finite temperatures. Throughout our investigation, we place particular emphasis on the fundamental properties exhibited by these droplets on a bulk level. By means of the extended HM theory that we developed in this thesis, we calculated the ground-state energy, the equilibrium density, the glassy fraction, the depletion, the anomalous density, the free energy, and the critical temperature of the droplet in terms of the disorder parameters.

At zero temperature, our analysis has uncovered the crucial role of disorder correlation in the stability of the droplet state. Specifically, we observed that the presence of white-noise disorder contributes positively to the ground-state energy.

Consequently, as the strength of the disorder increases, the ground-state energy rises and thus the mixture can be brought to a metastable state. Conversely, correlated disorders exhibit a negative effect on the ground-state energy. In this scenario, increasing the disorder strength tends to a decrease in the energy, causing the complete disappearance of the local minimum, resulting in the destruction of the liquid state once the disorder strength reaches its critical value. This latter strongly depends on the inherent system characteristics such as the interspecies interaction and the disorder correlation length. The stability of the droplet is influenced also by the type of disorder. For instance, in the case of a Gaussian disorder potential, a large correlation length may enhance the stability of the droplet, while the opposite situation holds for speckle potentials (i.e the droplet becomes less robust for large correlation length). Furthermore, we showed that the disorder may enhance the depletion and the anomalous density of the droplet. This can be explained by the fact that as the disorder strength gets larger, the atoms gradually leave the droplet and localize in the depleted region. As a result, the equilibrium density decays and thus, the self-bound state loses its fascinating self-evaporation phenomenon and eventually undergoes complete destruction. At finite temperatures, we computed the thermal density equilibrium and accurately determined the critical temperature above which the BEC-droplet phase transition emerges. Our findings indicate that the interplay of the disorder and thermal fluctuations may destabilize the self-bound droplet and eventually dissolve it.

To study the finite-size quantum liquid droplets in detailed and refined manner, we have carried out the simulation of the density profiles in the framework of the generalized disorder-dependent GPE which we derived self-consistently. It was further demonstrated that the density follows the modulations of the disorder in bulk. Such modulations become important for large disorder strength. We also examined the influence of the disorder on the width and on the breathing modes of the droplet utilizing a Gaussian variational ansatz.

On the other hand, we constructed the Bogoliubov-HM theory for disordered droplets in a 1D configuration and successfully described several observables of interest, such as the equilibrium density, the glassy fraction, and the density profiles at both zero and finite temperatures. Our results reveal that even small amounts of disorder may substantially deform the atomic density and modify the ground-state properties of the droplet. We also found that the equilibrium density and the glassy fraction are less sensitive to the disorder correlation in contrast to the 3D case. Moreover, we showed that the droplet fragments into many small droplets during its spatiotemporal evolution for relatively large disorder strength even at low temperatures.

It is clear that the results we predict in this work are achievable in current experimental setups and provide deep insights for understanding the profound properties of quantum droplets in weak disorder potentials. Our study not only bridges the gap between ultradilute droplets and disorder but also elucidates the localization phenomenon of droplets in binary BECs. We believe that the findings of this work add extra richness to the diversity of disordered ultracold atoms.

Outlook

Let us now discuss some possible directions for future work.

First our study is based on the Bogoliubov approach and the generalized GPE with the local density approximation and are therefore not valid to describe droplets with very strong disorder, where the system most likely undergoes a phase transition to new quantum states. The exploration of such a regime would need either a non-perturbative approach or Quantum Monte Carlo simulations.

Also of interest is the question concerning the existence of Anderson localization in ultradilute quantum droplets. Understanding the interplay between disorder, quantum fluctuations and interactions is key to elucidating such a peculiar phe-

nomenon on the expansion of a quantum droplet, released from a harmonic trap, in a random potential. In principle this can be achieved in a systematic way by numerically solving the underlying generalized Gross-Pitaevskii equation.

Other open questions concern the structure and the dynamics of a mixed-bubble state [196] in the presence of random potentials. This new mixed-bubble phase where bubbles of the mixed phase coexist with a pure phase of one of the components (i.e has a finite mixing ratio), occurs for unequal intraspecies interactions or unequal masses due to the beyond-mean-field effect [196].

Finally, an important extension of this work would be to analyze effects of a disordered potential in a mixture droplet state with strong dipole-dipole interactions. The competition between dipolar interaction , the LHY quantum corrections and the disorder potential would provide unique opportunities for quantitatively exploring phase diagrams that feature a variety of exotic supersolid and superglass states.

Appendix A

Quantum droplets in 1D delta- and Gaussian-correlated disorder potentials

In this Appendix we shed some light on the bulk properties of self-bound droplet in the presence of 1D delta-correlated and Gaussian-correlated disorder potentials.

Let us then first consider a symmetric self-bound droplet subjected to a 1D weak 1D delta-correlated (point-like) and Gaussian-correlated disorder potentials. Its correlations function is defined in equation (2.8). Unlike the 3D case, the disorder contribution to the ground-state energy does not require any regularization scheme. Using equation (4.14), we thus obtain for the total ground-state energy

$$\frac{2E}{NE_0} = n|a|\left(\frac{\delta g_+}{g}\right) - \frac{4}{3\pi}\sqrt{n|a|}\sum_{\pm}\left(\frac{\delta g_\pm}{g}\right)^{3/2} - \frac{R}{2\sqrt{n|a|}}\sum_{\pm}\left(\frac{\delta g_\pm}{g}\right)^{-1/2}, \quad \text{(A.1)}$$

where $E_0 = \hbar^2/(ma^2)$; and $R = R_0/(E_0^2|a|)$. Its behavior is displayed in figure A.1. As expected, we see that by increasing R, the local minimum starts to disappear indicating that the liquid phase becomes unstable.

Now we focus ourselves to analyze the effects of a 1D disorder potential with

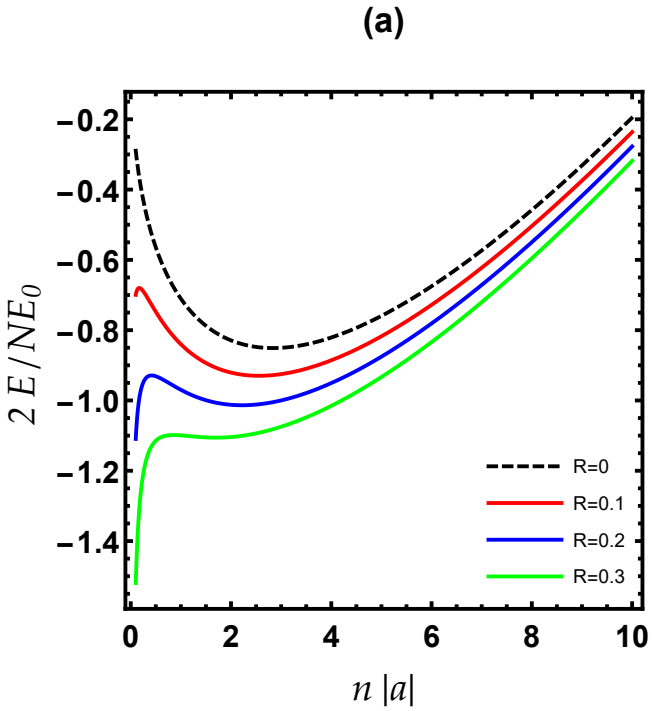

Figure A.1: Ground-state energy of a self-bound droplet with 1D δ-correlated disorder as a function of the density for $g_{12}/g = -0.7$.

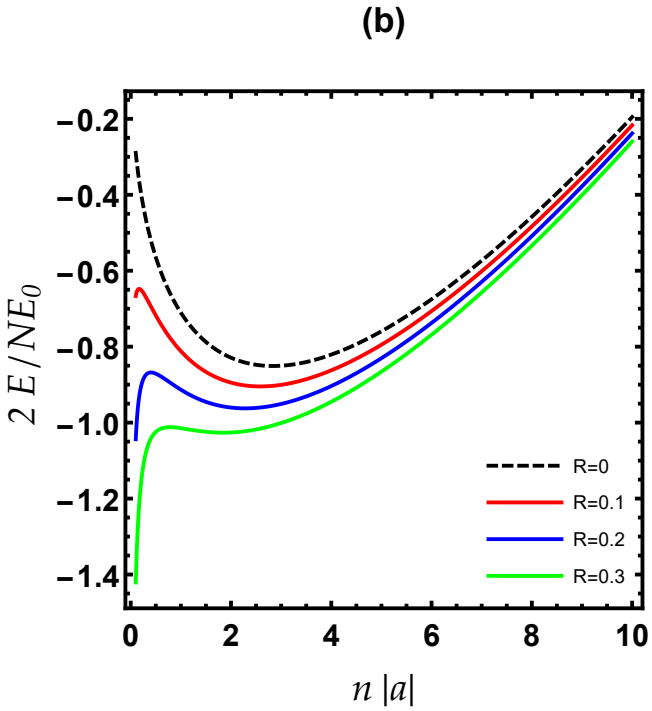

Figure A.2: Ground-state energy of a self-bound droplet with 1D Gaussian-correlated disorder as a function of the density for $g_{12}/g = -0.7$, and $\sigma/\xi = 0.63$.

Gaussian autocorrelation function on a quntum droplet. Its autocorrelation function is given by equation (2.10). The ground-state energy can be obtained from equation (4.14):

$$\frac{2E}{NE_0} = n|a|\left(\frac{\delta g_+}{g}\right) - \frac{4}{3\pi}\sqrt{n|a|}\sum_{\pm}\left(\frac{\delta g_\pm}{g}\right)^{3/2} - \frac{R}{2\sqrt{n|a|}}\sum_{\pm}\frac{e^{b_\pm}\mathrm{erfc}[\sqrt{b_\pm}]}{\left(\frac{\delta g_\pm}{g}\right)^{1/2}}, \quad \text{(A.2)}$$

where

$$b_\pm = \frac{9\pi^2}{32}\left(\frac{\delta g_+}{g}\right)^2\left(\frac{\delta g_\pm}{g}\right)\left(\frac{\sigma}{\xi}\right)^2 n|a|.$$

As shown in figure A.2, the behavior of the ground-state energy (A.2) is almost similar to that found for a 1D δ-correlated disorder.

The equilibrium and dynamical properties of self-bound droplets with delta and Gaussian disorder potentials can be examined within the generalized disorder-dependent GPE (5.10).

References

[1] *M. H. Anderson, J. R. Ensher, M. R. Matthews, C. E. Wieman and E. A. Cornell*, Observation of Bose-Einstein Condensation in a Dilute Atomic Vapor, **Science. 269**, 5221 (1995).

[2] *K. B. Davis, M. O. Mewes , M. R. Andrews, N. J. van Druten, D. S. Durfee, D. M. Kurn and W. Ketterle*,Bose-Einstein Condensation in a Gas of Sodium Atoms, **Phys. Rev. Lett. 75**, 3969 (1995).

[3] *B. DeMarco and D. S. Jin*, Onset of Fermi Degeneracy in a Trapped Atomic Gas, **Science. 285**, 1703 (1999).

[4] *F. Dalfovo, S. Giorgini, L. P. Pitaevskii, and S. Stringari*, Theory of Bose-Einstein condensation in trapped gases, **Rev.Mod. Phys. 71**, 463 (1999).

[5] *L. Pitaevskii and S. Stringari*, Bose-Einstein Condensation, **Oxford University Press**, (2016).

[6] *C. J. Pethick and H. Smith*, second edition, **Cambridge University Press**, (2008).

[7] *C. J. Myatt, E. A. Burt, R. W. Ghrist, E. A. Cornell, and C. E. Wieman*, Production of Two Overlapping Bose-Einstein Condensates by Sympathetic Cooling, **Phys. Rev. Lett. 78**, 586 (1997).

[8] *D. S. Hall, M. R. Matthews, J. R. Ensher, C. E. Wieman, and E. A. Cornell*, Dynamics of Component Separation in a Binary Mixture of Bose-Einstein Condensates, **Phys. Rev. Lett. 81**, 1539 (1998).

[9] *D. M. Stamper-Kurn, M. R. Andrews, A. P. Chikkatur, S. Inouye, H.-J. Miesner, J. Stenger, and W. Ketterle*, Optical Confinement of a Bose-Einstein Condensate, **Phys. Rev. Lett. 80**, 2027 (1998).

[10] *J. Stenger, S. Inouye, D. M. Stamper-Kurn, H.-J. Miesner, A. P. Chikkatur, and W. Ketterle*, Spin domains in ground state spinor Bose-Einstein condensates, **Nature (London). 396**, 345 (1998).

[11] *P. Maddaloni, M. Modugno, C. Fort, F. Minardi, and M. Inguscio*, Collective Oscillations of Two Colliding Bose-Einstein Condensates, **Phys. Rev. Lett. 85**, 2413 (2000).

[12] *L. E. Sadler, J. M. Higbie, S. R. Leslie, M. Vengalattore, and D. M. Stamper-Kurn*, Spontaneous symmetry breaking in a quenched ferromagnetic spinor Bose-Einstein condensate, **Nature (London) 443**, 312 (2006).

[13] *S. B. Papp, J. M. Pino, and C. E.Wieman*, Tunable Miscibility in a Dual-Species Bose-Einstein Condensate, **Phys. Rev. Lett. 101**, 040402 (2008).

[14] *S. Sugawa, R. Yamazaki, S. Taie, and Y. Takahashi*, Bose-Einstein condensate in gases of rare atomic species, **Phys. Rev. A 84**, 011610 (2011).

[15] *G. Modugno, M. Modugno, F. Riboli, G. Roati, and M. Inguscio*, Two atomic species superfluid, **Phys. Rev. Lett. 89**, 190404 (2002);

[16] *D. J. McCarron, H.W. Cho, D. L. Jenkin, M. P. Köppinger, and S. L. Cornish*, Dual-species Bose-Einstein condensate of ^{87}Rb and ^{133}Cs, **Phys. Rev. A 84**, 011603 (2011).

[17] *A. D. Lercher, T. Takekoshi, M. Debatin, B. Schuster, R.Rameshan, F. Ferlaino, R. Grimm, and H.-C. Nägerl*, Production of a dual-species Bose-Einstein condensate of Rb and Cs atoms, **Eur. Phys. J. D 65**, 3 (2011).

[18] *B. Pasquiou, A. Bayerle, S. M. Tzanova, S. Stellmer, J. Szczepkowski, M. Parigger, R. Grimm, and F. Schreck*, Quantum degenerate mixtures of strontium and rubidium atoms, **Phys. Rev. A 88**, 023601 (2013).

[19] *L. Wacker, N. B. Jorgensen, D. Birkmose, R. Horchani, W.Ertmer, C. Klempt, N. Winter, J. Sherson, and J. J. Arlt*, Tunable dual-species Bose-Einstein condensates of ^{39}K and ^{87}Rb, **Phys. Rev. A 92**, 053602 (2015).

[20] *F. Wang, X. Li, D. Xiong, and D. Wang*, A double species ^{23}Na and $_{87}Rb$ Bose–Einstein condensate with tunable miscibility via an interspecies Feshbach resonance, **J. Phys. B 49**, 015302 (2016).

[21] *P. Ilzhöfer, G. Durastante, A. Patscheider, A. Trautmann, M. J. Mark, and F. Ferlaino*, Two-species five-beam magneto-optical trap for erbium and dysprosium, **Phys. Rev. A 97**, 023633 (2018).

[22] *Y. Kawaguchi, and M. Ueda*, Spinor Bose–Einstein condensates, **Phys. Rep. 520**, 253 (2012).

[23] *D. M. Stamper-Kurn, and M. Ueda*, Spinor Bose gases: Symmetries, magnetism, and quantum dynamics, **Rev. Mod. Phys. 85**, 1191-1244 (2013).

[24] *Tin-Lun Ho and V. B. Shenoy*, Binary mixtures of Bose condensates of alkali atoms, **Phys. Rev. Lett. 77**, 3276 (1996).

[25] *H. Pu and N. P. Bigelow*, Properties of two-species Bose condensates, **Phys. Rev. Lett. 80**, 1130 (1998).

[26] *K-L. Lee, N. B. Jorgensen, I-K. Liu, L. Wacker, J. Arlt, and N. P. Proukakis*, Phase separation and dynamics of two-component Bose-Einstein condensates, **Phys. Rev. A 94**, 013602 (2016).

[27] *S. Lellouch, L-K Lim, and L. Sanchez-Palencia*, Propagation of collective pair excitations in disordered Bose superfluids, **Phys. Rev. A 92**, 043611 (2015).

[28] *A. Roy and D. Angom*, Thermal suppression of phase separation in condensate mixtures, **Phys. Rev. A 92**, 011601(R) (2015).

[29] *A. Boudjemâa*, Quantum and thermal fluctuations in two-component Bose gases, **Phys. Rev. A 97**, 033627 (2018).

[30] *M. Ota, S. Giorgini, S. Stringari*, Magnetic phase transition in a mixture of two interacting superfluid Bose gases at finite temperature, **Phys. Rev. Lett. 123**, 075301 (2019).

[31] *P. G. Kevrekidis, H. E. Nistazakis, D. J. Frantzeskakis, B. A. Malomed and R. Carretero-González*, Families of matter-waves in two-component Bose-Einstein condensates, **Eur. Phys. J. D 28**, 181 (2004).

[32] *M. R. Matthews, B. P. Anderson, P. C. Haljan, D. S. Hall, C. E. Wieman, and E. A. Cornell*, Vortices in a Bose-Einstein condensate, **Phys. Rev. Lett. 83**, 2498 (1999).

[33] *A. F. Andreev and E. P. Bashkin*, Three-velocity hydrodynamics of superfluid solutions, **Sov. Phys.-JETP 42**, 164 (1976).

[34] *D.V. Fil and S.I. Shevchenko*, Nondissipative drag of superflow in a two-component Bose gas, **Phys. Rev. A 72**, 013616 (2005).

[35] *L. Chen, C. Zhu, Y. Zhang, H. Pu*, Spin-exchange-induced spin-orbit coupling in a superfluid mixture, **Phys. Rev. A 97**, 031601 (2018).

[36] *I. M. Khalatnikov*, Hydrodynamics of solutions of 2 superfluid liquids, **Sov. Phys. JETP 5**, 542 (1957).

[37] *W. H. Bassichis*, Generalization of the Boguliubov Method Applied to Mixtures of Bose-Einstein Particles, **Phys. Rev. A 134**, 543 (1964).

[38] *Y. A. Nepomnyashchii, Zh. Eksp.* **Teor. Fiz. 70**, 1070 (1976), [**Sov. Phys. - JETP 43**, 559 (1976)]; **Teor. Mat. Fiz. 20**, 399 (1974).

[39] *W. B. Colson and A. L. Fetter*, Mixtures of Bose liquids at finite temperature, **J. Low. Temp. Phys. 33**, 231 (1978).

[40] *E. Fava, T. Bienaimé, C. Mordini, G. Colzi, C. Qu, S. Stringari, G. Lamporesi*, G. Ferrari, Observation of spin superfluidity in a Bose gas mixture, **Phys. Rev. Lett. 120**, 170401 (2018).

[41] *A. Boudjemâa*, Superfluidity and coherence in uniform dipolar binary Bose mixtures, **J. Phys. A: Math. Theor. 53**, 435001(2020).

[42] *B. Cherifi and A. Boudjemâa*, Moving Bose mixtures with dipole–dipole interactions, **Eur. Phys. J. D 76**, 226 (2022).

[43] *A. Boudjemâa and K. Abbas*, Bose-Bose mixtures in a weak-disorder potential: Fluctuations and superfluidity, **Phys. Rev. A, 102**, 023325 (2020).

[44] *A. Boudjemâa* , Moving binary Bose-Einstein condensates in a weak random potential, **Phys. Lett. A 424**, 127867 (2022).

[45] *K. Abbas and A. Boudjemâa*, Binary Bose–Einstein condensates in a disordered time-dependent potential, **J. Phys.: Condens. Matter, 34**, 125102 (2022).

[46] *D. S. Petrov*, Quantum mechanical stabilization of a collapsing Bose-Bose mixture, **Phys. Rev. Lett. 115**, 155302 (2015).

[47] *C. R. Cabrera, L. Tanzi, J. Sanz, B. Naylor, P. Thomas, P. Cheiney, L. Tarruell*, Quantum liquid droplets in a mixture of Bose-Einstein condensates, **Science 359**, 301 (2018).

[48] *P. Cheiney, C. R. Cabrera, J. Sanz, B. Naylor, L. Tanzi, and L. Tarruell*, Bright soliton to quantum droplet transition in a mixture of Bose-Einstein condensates, **Phys. Rev. Lett. 120**, 135301 (2018).

[49] *G. Semeghini, G. Ferioli, L. Masi, C. Mazzinghi, L. Wolswijk, F.Minardi, M. Modugno, G. Modugno, M. Inguscio, and M. Fattori*, Self-bound quantum droplets of atomic mixtures in free space, **Phys. Rev. Lett. 120**, 235301 (2018).

[50] *C. D'Errico, A. Burchianti, M. Prevedelli, L. Salasnich, F. Ancilotto, M. Modugno, F. Minardi, and C. Fort*, Observation of quantum droplets in a heteronuclear bosonic mixture, **Phys. Rev. Research 1**, 033155 (2019).

[51] *A. Boudjemâa*, Fluctuations and quantum self-bound droplets in a dipolar Bose-Bose mixture, **Phys. Rev. A 98**, 033612 (2018).

[52] *A. R. P. Lima and A. Pelster*, Quantum fluctuations in dipolar Bose gases, **Phys. Rev. A 84**, 041604 (R) (2011).

[53] *A. Boudjemâa*, Theory of excitations of dipolar Bose–Einstein condensate at finite temperature, **J. Phys. B: At. Mol. Opt. Phys. 48**, 035302 (2015).

[54] *A. Boudjemâa*, Properties of dipolar bosonic quantum gases at finite temperatures, **J. Phys. A: Math. Theor. 49**, 285005 (2016).

[55] *H. Kadau, M. Schmitt, M. Wenzel, C. Wink, T. Maier, I. Ferrier-Barbut and T. Pfau*, Observing the Rosensweig instability of a quantum ferrofluid, **Nature 530** ,194 (2016).

[56] *M.Schmitt, M. Wenzel, F.Böttcher, I. Ferrier-Barbut and T. Pfau*, Self-bound droplets of a dilute magnetic quantum liquid, **Nature 539**, 259 (2016).

[57] *L. Chomaz, S. Baier, D. Petter, M. J. Mark, F. Wächtler, L. Santos and F. Ferlaino*, Quantum-fluctuation-driven crossover from a dilute Bose-Einstein condensate to a macrodroplet in a dipolar quantum fluid, **Phys. Rev. X 6**, 041039 (2016).

[58] *T. D. Lee, K. Huang and C. N. Yang*, Eigenvalues and eigenfunctions of a Bose system of hard spheres and its low-temperature properties, **Phys. Rev 106**, 1135 (1957).

[59] *D. Rakshit, T. Karpiuk, M. Brewczyk and M. Gajda*, Quantum Bose-Fermi droplets , **SciPost Phys. 6**, 079 (2019).

[60] *I. Ferrier-Barbut, H. Kadau, M. Schmitt, M. Wenzel and T. Pfau*, Observation of quantum droplets in a strongly dipolar Bose gas, **Phys. Rev. Lett. 116**, 215301 (2016).

[61] *D. S. Petrov and G. E. Astrakharchik*, Ultradilute low-dimensional liquids, **Phys. Rev. Lett. 117**, 100401 (2016).

[62] *N. Guebli and A. Boudjemâa*, Quantum self-bound droplets in Bose-Bose mixtures: Effects of higher-order quantum and thermal fluctuations, **Phys. Rev. A 104**, 023310 (2021).

[63] *A. Boudjemâa*, Many-body and temperature effects in two-dimensional quantum droplets in Bose–Bose mixtures, **Sci. Rep. 11**, 21765 (2021).

[64] *A. Boudjemâa, K. Abbas, and N. Guebli*, Ultradilute Quantum Droplets in the Presence of Higher-Order Quantum Fluctuations, **Atoms, 10**, 64 (2022).

[65] *A. Boudjemâa and N. Guebli*, Effects of higher-order fluctuations on the bulk and surface properties of quantum droplets in a heteronuclear Bose-Bose mixture, **Phys. Rev. A 108**, 013305 (2023).

[66] *N. Guebli*, Quantum droplets in Bose-Bose mixtures, **Ph.D. thesis**, Hassiba Benbouali University of Chlef (2022).

[67] *Q. Gu and L. Yin*, Phonon stability and sound velocity of quantum droplets in a boson mixture, **Phys. Rev. B 102**, 220503 (R) (2020).

[68] *M. Ota, and G. E. Astrakharchik*, Beyond Lee-Huang-Yang description of self-bound Bose mixtures, **SciPost Phys. 9**, 020 (2020).

[69] *H. Hu and X-J. Liu*, Consistent theory of self-bound quantum droplets with bosonic pairing, **Phys. Rev. Lett. 125**, 195302 (2020).

[70] *V. Cikojevic, L. V. Markic, G. E. Astrakharchik and J. Boronat*, Universality in ultradilute liquid Bose-Bose mixtures, **Phys. Rev. A 99**, 023618 (2019).

[71] *L. Parisi, G. E. Astrakharchik and S. Giorgini*, Liquid state of one-dimensional Bose mixtures: a quantum Monte Carlo study, **Phys. Rev. Lett. 122**, 105302 (2019).

[72] *V. Cikojević, E. Poli, F. Ancilotto, L. Vranješ-Markić, and J. Boronat*, Dilute quantum liquid in a $K - Rb$ Bose mixture, **Phys. Rev. A 104**, 033319 (2021).

[73] *P. W. Anderson*, Absence of diffusion in certain random lattices, **Phys. Rev. 109**, 1492 (1958).

[74] *P. Lugan and L. Sanchez-Palencia*, Localization of Bogoliubov quasiparticles in interacting Bose gases with correlated disorder, **Phys. Rev. A 84**, 013612 (2011).

[75] *C. Gaul and C. A. Müller*, Bogoliubov excitations of disordered Bose-Einstein condensates, **Phys. Rev. A 83**, 063629 (2011).

[76] *C. Krumnow and A. Pelster*, Dipolar Bose-Einstein condensates with weak disorder, **Phys. Rev. A 84**, 021608(R) (2011).

[77] *B. Nikolic, A. Balaz, and A. Pelster*, Dipolar Bose-Einstein condensates in weak anisotropic disorder, **Phys. Rev. A 88**, 013624 (2013).

[78] *A. Boudjemâa*, Effects of the Lee-Huang-Yang quantum corrections on a disordered dipolar Bose gas, **Eur. Phys. J. B 92**, 145 (2019).

[79] *L. Sanchez-Palencia*, Smoothing effect and delocalization of interacting Bose-Einstein condensates in random potentials, **Phys. Rev. A. 74**, 053625 (2006).

[80] *J. E. Lye, L. Fallani, M. Modugno, D. S. Wiersma, C. Fort, and M. Inguscio*, Bose-Einstein condensate in a random potential, **Phys. Rev. Lett. 95**, 070401 (2005).

[81] *J. Billy, V. Josse, Z. Zuo, A. Bernard, B. Hambrecht, P. Lugan, D. Clément, L. Sanchez-Palencia, P. Bouyer, and A. Aspect*, Direct observation of Anderson localization of matter waves in a controlled disorder, **Nature 453**, 891 (2008).

[82] *B. Damski, J. Zakrzewski, L. Santos, P. Zoller, and M. Lewenstein*, Atomic Bose and Anderson glasses in optical lattices, **Phys. Rev. Lett. 91**, 080403 (2003).

[83] *G. Roati, C. D'Errico, L. Fallani, M. Fattori, C. Fort, M. Zaccanti, G. Modugno, M. Modugno, and M. Inguscio*, Anderson localization of a non-interacting Bose–Einstein condensate, **Nature 453**, 895 (2008).

[84] *M. Ma, B. I. Halperin, and P. A. Lee*, Strongly disordered superfluids: Quantum fluctuations and critical behavior, **Phys. Rev. B 34**, 3136 (1986).

[85] *T. Giamarchi and H. J. Schulz*, Localization and interaction in one-dimensional quantum fluids, **Europhys. Lett. 3**, 1287 (1987).

[86] *M. P. A. Fisher, P. B.Weichman, G. Grinstein, and D. S. Fisher*, Boson localization and the superfluid-insulator transition, **Phys. Rev. B 40**, 546 (1989).

[87] *R. T. Scalettar, G. G. Batrouni, and G. T. Zimanyi*, Localization in interacting, disordered, Bose systems, **Phys. Rev. Lett. 66**, 3144 (1991).

[88] *W. Krauth, N. Trivedi, and D. Ceperley*, Superfluid-insulator transition in disordered boson systems, **Phys. Rev. Lett. 67**, 2307 (1991).

[89] *T. Schulte, S. Drenkelforth, J. Kruse, W. Ertmer, J. Arlt, K. Sacha, J. Zakrzewski, and M. Lewenstein*, Routes towards Anderson-like localization of Bose-Einstein condensates in disordered optical lattices, **Phys. Rev. Lett. 95**, 170411 (2005).

[90] *L. Sanchez-Palencia, D. Clément, P. Lugan, P. Bouyer, G. V. Shlyapnikov, and A. Aspect*, Anderson localization of expanding Bose-Einstein condensates in random potentials, **Phys. Rev. Lett. 98**, 210401 (2007).

[91] *P. Lugan, D. Clément, P. Bouyer, A. Aspect, and L. Sanchez-Palencia*, Anderson localization of Bogolyubov quasiparticles in interacting Bose-Einstein condensates, **Phys. Rev. Lett. 99**, 180402 (2007).

[92] *S. E. Skipetrov, A. Minguzzi, B. A. van Tiggelen, and B. Shapiro*, Anderson localization of a Bose-Einstein condensate in a 3D random potential, **Phys. Rev. Lett. 100**, 165301 (2008).

[93] *M. White, M. Pasienski, D. McKay, S. Q. Zhou, D. Ceperley, and B. DeMarco*, Strongly interacting bosons in a disordered optical lattice, **Phys. Rev. Lett. 102**, 055301 (2009).

[94] *M. Pasienski, D. McKay, M. White, and B. DeMarco*, A disordered insulator in an optical lattice, **Nature Phys. 6**, 677 (2010).

[95] *B. Deissler, M. Zaccanti, G. Roati, C. D'Errico, M. Fattori, M. Modugno, G. Modugno, and M. Inguscio*, Delocalization of a disordered bosonic system by repulsive interactions, **Nature Phys. 6**, 354 (2010).

[96] *I. L. Aleiner, B. L. Altshuler, and G. V. Shlyapnikov*, Finite temperature phase transition for disordered weakly interacting bosons in one dimension, **Nature, Phys. 6**, 900 (2010).

[97] *V. Ahufinger, L. Sanchez-Palencia, A. Kantian, A. Sanpera, and M. Lewenstein*, Disordered ultracold atomic gases in optical lattices: A case study of Fermi-Bose mixtures, **Phys. Rev. A 72**, 063616 (2005).

[98] *F. Crépin, G. Zaránd, P. Simon*, Disordered One-Dimensional Bose-Fermi Mixtures: The Bose-Fermi Glass, **Phys. Rev. Lett. 105**, 115301 (2010).

[99] *M. Ghabour and A. Pelster*, Bogoliubov theory of dipolar Bose gas in a weak random potential, **Phys. Rev. A 90**, 063636 (2014).

[100] *A. Boudjemâa*, Superfluidity and Bose–Einstein condensation in a dipolar Bose gas with weak disorder, **Low Temp. Phys. 180**, 377 (2015).

[101] *A. Boudjemâa*, Two-dimensional dipolar bosons with weak disorder, **Phys. Lett. A 379**, 2484 (2015).

[102] *A. Boudjemâa*, Thermodynamics of a two-dimensional dipolar Bose gas with correlated disorder in the roton regime, **J. Phys. B: At. Mol. Opt. Phys. 49**, 105301 (2016).

[103] *J. Wehr, A. Niederberger, L. Sanchez-Palencia, and M. Lewenstein*, Disorder versus the Mermin-Wagner-Hohenberg effect: From classical spin systems to ultracold atomic gases, **Phys. Rev. B 74**, 224448 (2006).

[104] *A. Niederberger, T. Schulte, J. Wehr, M. Lewenstein, L. Sanchez-Palencia, and K. Sacha*, Disorder-induced order in two-component Bose-Einstein condensates, **Phys. Rev. Lett. 100**, 030403 (2008).

[105] *K-T. Xi, J. Li and D-N. Shi*, Localization of a two-component Bose–Einstein condensate in a one-dimensional random potential, **Physica B: Condensed Matter, 459**, 6 (2015).

[106] *Sh. Mardonov, M. Modugno, and E. Ya. Sherman*, Dynamics of spin-orbit coupled Bose-Einstein condensates in a random potentia, **Phys. Rev. Lett. 115**, 180402 (2015).

[107] *S. Sahu and D. Majumder*, Two-dimensional interacting Bose–Bose droplet in random repulsive potential, **Eur. Phys. J. Plus 137**, 1020 (2022).

[108] *Z.-H. Luo, W. Pang, B. Liu, Y.-Y. Li, and B. A. Malomed*, A new form of liquid matter: Quantum droplet, **Frontiers of Physics 16**, 32201 (2021).

[109] *F. Boëttcher, J.-N. Schmidt, J. Hertkorn, K. Ng, Graham, M. Guo, T. Langen, and T. Pfau*, New states of matter with fine-tuned interactions: quantum droplets and dipolar supersolids, **Reports on Progress in Physics 84**, 012403 (2021).

[110] *M. Guo and T. Pfau*, A new state of matter of quantum droplets, **Frontiers of Physics 16**, 32202 (2021).

[111] *E.P. Gross*, Structure of a quantized vortex in boson systems, **Nuovo Cimento 20**, 454 (1961).

[112] *L. Pitaevskii*, Vortex lines in an imperfect Bose gas, **Sov. Phys. JETP 13**, 451 (1961).

[113] *G. Thalhammer, G. Barontini, L. De Sarlo, J. Catani, F.Minardi, and M. Inguscio*, Double species Bose-Einstein condensate with tunable interspecies interactions, **Phys. Rev. Lett. 100**, 210402 (2008).

[114] *E. Timmermans*, Phase separation of Bose-Einstein condensates, **Phys. Rev. Lett. 81**, 5718 (1998).

[115] *P. Ao and S. T. Chui*, Binary Bose-Einstein condensate mixtures in weakly and strongly segregated phases, **Phys. Rev. A. 58**, 4836 (1998).

[116] *C. R. Cabrera*, Quantum liquid droplets in a mixture of Bose-Einstein condensates, **Ph.D. Thesis**, The Institute of Photonic Sciences Universidad Politécnica de Cataluna (2018).

[117] *M.Trippenbach*, Structure of binary Bose-Einstein condensates, **J. Phys. B: At. Mol. Opt. Phys. 33**, 4017. (2000).

[118] *P.Tommasini, E. J. V. de Passos, A. F. R. de T. Piza, and M. S. Hussein*, Bogoliubov theory for mutually coherent condensates, **Phys. Rev. A 67**, 023619 (2003).

[119] *D. M. Larsen*, Binary mixtures of dilute bose gases with repulsive interactions at low temperature, **Ann. Phys. 24**, 89(1963).

[120] *A. Boudjemâa*, Degenerate Bose Gas at Finite Temperatures, **LAP LAMBERT Academic Publishing** (2017).

[121] *A. Boudjemâa*, Dynamics of ultracold gases, **Ph.D. thesis**, Hassiba Benbouali University of Chlef (2013).

[122] *N. N. Bogoliubov*, On the theory of superfluidity, **J. Phys. (USSR) 11**, 23 (1947).

[123] *R. Lopes, C. Eigen, N. Navon, D. Clément, R. P. Smith, and Z. Hadzibabic*, Quantum depletion of a homogeneous Bose-Einstein condensate, **Phys. Rev. Lett. 119**, 190404 (2017).

[124] *G. E. Astrakharchik and B. A. Malomed*, Dynamics of one-dimensional quantum droplets, **Phys. Rev. A 98**, 013631 (2018).

[125] *M. Tylutki, G. E. Astrakharchik, B. A. Malomed, and D. S. Petrov*, Collective excitations of a one-dimensional quantum droplet, **Phys. Rev. A 101**, 051601(R) (2020).

[126] *A. Boudjemâa*, Quantum dilute droplets of dipolar bosons at finite temperature, **Annals of Physics. 381**, 68 (2017).

[127] *A. Burchianti, C. D'Errico, M. Prevedelli, L. Salasnich, F. Ancilotto, M. Modugno, F. Minardi and C. Fort*, A dual-species Bose-Einstein condensate with attractive interspecies interactions, **Condensed Matter. 5**, 1 (2020).

[128] *V. N. Popov*, To the theory of superfluidity of the twodimensional and one-dimensional Bose systems, **Teor. Mat. Fiz. 11**, 354 (1971).

[129] *J. Wang, X-J Liu and H. Hu, Chin*, Ultradilute self-bound quantum droplets in Bose–Bose mixtures at finite temperature, **Chinese Phys. B 30**, 010306 (2021).

[130] *S. S. Kondov, W. R. McGehee, J. J. Zirbel, B. DeMarco*, Three-dimensional Anderson localization of ultracold matter, **Science 334**, 66 (2011).

[131] *D. Clément*, Proprietes stastiques et dynamique d'un condensat de Bose-Einstein dans un potentiel aleatoire, **Ph.D thesis**, (2008).

[132] *S. Lellouch*, Collective localization transitions in interacting disordered and quasiperiodic Bose superfluids, **Ph.D thesis**, (2014).

[133] *D. Clément, A. F. Varon, J. A. Retter, L. Sanchez-Palencia, A. Aspect, and P. Bouyer*, Experimental study of the transport of coherent interacting matter-waves in a 1D random potential induced by laser speckle, **New J. Phys. 8**, 165, (2006).

[134] *L. Sanchez-Palencia and M. Lewenstein*, Disordered quantum gases under control, **Nature Phys, 6** , 87–95, (2010).

[135] *L. Fallani, C. Fort, and M. Inguscio, Adv. At. Mol*, Bose–Einstein condensates in disordered potentials, **Opt. Phys. 56**, 119, (2008).

[136] *R. Touzi and al*, A review of polarimetry in the context of synthetic aperture radar: concepts and information extraction, **Can.J. Rem, Sens. 30**, 380 (2004).

[137] *S. Sudha, G. R. Suresh, and R. Sukanesh*, Speckle noise reduction in ultrasound images using context-based adaptive wavelet thresholding, **IETE J. Res. 55**, 135 (2009).

[138] *B. Ayerdi and M. G. Romay*, Hyperspectral image analysis by spectral–spatial processing and anticipative hybrid extreme rotation forest classification, **Geo. Rem. Sens, IEEE Trans. 54**, 2627 (2016).

[139] *H. L. Frisch and S. P. Lloyd*, Electron levels in a one-dimensional random lattice, **Phys. Rev. 120**, 1175 (1960).

[140] *K. Huang and H.-F. Meng*, Hard-sphere Bose gas in random external potentials, **Phys. Rev. Lett. 69**, 644 (1992).

[141] *S. Giorgini, L. Pitaevskii, and S. Stringari*, Effects of disorder in a dilute Bose gas, **Phys. Rev. B. 49**, 12938 (1994).

[142] *M. Kobayashi and M. Tsubota*, Bose-Einstein condensation and superfluidity of a dilute Bose gas in a random potential, **Phys. Rev.B 66**, 174516 (2002).

[143] *P .Laugan*, Ultracold Bose gases in random potentials: collective excitations and localization effects. **Ph.D thesis**, (2010).

[144] *A. Aspect, and M. Inguscio*, Anderson localization of ultracold atoms, **Physics Today. 62**, 30–35 (2009).

[145] *P. Lugan, D. Clément, P. Bouyer, A. Aspect, M. Lewenstein, and L. Sanchez-Palencia*, Ultracold Bose gases in 1D disorder: From Lifshits glass to Bose-Einstein condensate, **Phys. Rev. Lett. 98**, 170403 (2007).

[146] *K. Redaouia and A. Boudjemâa*, Dipolar Bose gas with three-body interactions in weak disorder, **Eur. Phys. J. D . 73**, 115 (2019).

[147] *M. Holthaus*, Floquet engineering with quasienergy bands of periodically driven optical lattices, **J. Phys. B: At. Mol. Opt. Phys. 49**, 013001 (2016).

[148] *O. R. Diermann and M. Holthaus*, Floquet-state cooling, **Sci. Rep. 9**, 17614 (2019).

[149] *S. Mukherjee and M. C. Rechtsman*, Observation of Floquet solitons in a topological bandgap, **Science 368**, 856 (2020).

[150] *V. V. Konotop and M. Salerno*, Modulational instability in Bose-Einstein condensates in optical lattices, **Phys. Rev. A 65**, 021602(R) (2002).

[151] *A. Eckardt, M. Holthaus, H. Lignier, A. Zenesini,D. Ciampini, O. Morsch, and E. Arimondo*, Exploring dynamic localization with a Bose-Einstein condensate, **Phys. Rev. A 79**, 013611 (2009).

[152] *M. Lopez, J. F. Clément, P. Szriftgiser, J. C. Garreau, and D. Delande*, Experimental test of universality of the Anderson transition, **Phys. Rev. Lett. 108**, 095701 (2012)

[153] *G. Jotzu, M. Messer, R. Desbuquois, M. Lebrat, T. Uehlinger, D. Greif, and T. Esslinger*, Experimental realization of the topological Haldane model with ultracold fermions, **Nature (London) 515**, 237 (2014).

[154] *M. Aidelsburger, M. Lohse, C. Schweizer, M. Atala, J. Barreiro, S. Nascimbene, N. R. Cooper, I. Bloch, and N. Goldman*, Measuring the Chern number of Hofstadter bands with ultracold bosonic atoms, **Nat. Phys. 11**, 162 (2015).

[155] *C. J. Kennedy, W. C. Burton, W. C. Chung, and W. Ketterle*, Observation of Bose–Einstein condensation in a strong synthetic magnetic field, **Nat. Phys. 11**, 859 (2015).

[156] *N. Goldman, J.C. Budich, and P. Zoller*, Topological quantum matter with ultracold gases in optical lattices, **Nat. Phys. 12**, 639 (2016).

[157] *S. F. Edwards and P. W. Anderson*, Theory of spin glasses, **J. Phys. F. 5**, 965 (1975).

[158] *V. I. Yukalov and R. Graham*, Bose-Einstein-condensed systems in random potentials, **Phys. Rev. A. 75**, 023619 (2007).

[159] *M. Egorov, B. Opanchuk, P. Drummond, B. V. Hall, P. Hannaford, and A. I. Sidorov*, Measurement of s-wave scattering lengths in a two-component Bose-Einstein condensate, **Phys. Rev. A. 87**, 053614 (2013).

[160] *G. M. Falco, A. Pelster, and R. Graham*, Thermodynamics of a Bose-Einstein condensate with weak disorder, **Phys. Rev. A. 75**, 063619 (2007).

[161] *C. J. Pethick and H. Smith*, Bose-Einstein Condensation in Dilute Gases, **2nd ed. (Cambridge University Press)**. 2008.

[162] *M. Radonjić, A. Pelster*, Non-equilibrium evolution of Bose-Einstein condensate deformation in temporally controlled weak disorder, **SciPost Phys. 10**, 008 (2021).

[163] *T. Nattermann and V. L. Pokrovsky*, Bose-Einstein condensates in strongly disordered traps, **Phys. Rev. Lett. 100**, 060402 (2008).

[164] *A. Boudjemâa*, Dipolar Bose gas in a weak isotropic speckle disorder, **Phys. Rev. A 91**, 053619 (2015).

[165] *M. Kobayashi and M. Tsubota*, Bose-Einstein condensation and superfluidity of a dilute Bose gas in a random potential, **Phys. Rev.B 66**, 174516 (2002).

[166] *S. Krinner, D. Stadler, J. Meineke, J. P. Brantut and T. Esslinger*, Superfluidity with disorder in a thin film of quantum gas, **Phys. Rev. Lett. 110**, 100601 (2013).

[167] *C. Meldgin, U. Ray, P. Russ, D. Chen, D. M. Ceperley, and B. De Marco*, Probing the Bose glass–superfluid transition using quantum quenches of disorder, **Nat. Phys. 12**, 646 (2016).

[168] *L. Chen, Z. Liang, Y. Hu, and Z. Zhang*, Non-equilibrium disordered Bose gases: condensation, superfluidity and dynamical Bose glass, **J. Phys. B: At. Mol Opt. Phys. 49**, 025303 (2016).

[169] *B. Nagler, S. Hiebel, S. Barbosa, J. Koch, and A. Widera*, Ultracold Bose gases in disorder potentials with spatiotemporal dynamics, **arXiv:2007**. 11523 (2020).

[170] *S. Lellouch, M. Bukov, E. Demler, and N. Goldman*, Parametric instabilities in resonantly-driven Bose–Einstein condensates, **Phys. Rev. X 7**, 021015 (2017).

[171] *M. Holthaus*, Floquet engineering with quasienergy bands of periodically driven optical lattices, **J. Phys. B: At. Mol. Opt. Phys. 49**, 013001 (2016).

[172] *O. R. Diermann and M. Holthaus*, Periodic thermodynamics of a two spin Rabi model, **Sci. Rep.9**, 17614 (2019).

[173] *M. Modugno*, Collective dynamics and expansion of a Bose-Einstein condensate in a random potential, **Phys. Rev. A 73**, 013606 (2006).

[174] *L. Sanchez-Palencia, D. Clément, P. Lugan, P. Bouyer, G. V. Shlyapnikov, and A. Aspect*, Anderson localization of expanding Bose-Einstein condensates in random potentials, **Phys. Rev. Lett. 98**, 210401 (2008).

[175] *E. Akkermans and G. Montambaux*, Mesoscopic physics of electrons and photons, **Cambridge University Press**, Cambridge, (2007).

[176] *G. E. Astrakharchik, J. Boronat, J. Casulleras, and S.Giorgin*, Superfluidity versus Bose-Einstein condensation in a Bose gas with disorder, **Phys. Rev. A, 66**, 023603 (2002).

[177] *D. Clément, A. F. Varon, M. Hugbart, J. A. Retter, P. Bouyer, L. Sanchez-Palencia, D. M. Gangardt, G. V. Shlyapnikov, and A. Aspect*, Suppression of transport of an interacting elongated Bose-Einstein condensate in a random potential, **Phys. Rev. Lett. 95**, 170409 (2005).

[178] *R. C Kuhn, O. Sigwarth, C. Miniatura, D. Delande and C. A. Muller*, Coherent matter wave transport in speckle potentials, **New J. Phys. 9**, 161 (2007).

[179] *M. Kobayashi and M. Tsubota*, Bose-Einstein condensation and superfluidity of a dilute Bose gas in a random potential, **Phys. Rev.B 66**, 174516 (2002).

[180] *F. Jendrzejewski, A. Bernard, K. Müller, P. Cheinet, V. Josse, M. Piraud, L. Pezzé, L. Sanchez-Palencia, A. Aspect, and P. Bouyer*, Three-dimensional localization of ultracold atoms in an optical disordered potential, **Nat. Phys. 8**, 398 (2012).

[181] *B. Nagler, M. Radonjić, S. Barbosa, J. Koch, A. Pelster, A. Widera*, Cloud shape of a molecular Bose–Einstein condensate in a disordered trap: a case study of the dirty boson problem, **New. J. Phys. 22**, 033021 (2020).

[182] *Y. Cheng and S. K. Adhikari*, Matter-wave localization in a random potential, **Phys. Rev. A 82**, 013631 (2010).

[183] *G.E. Astrakharchik, B.A. Malomed*, Dynamics of one-dimensional quantum droplets, **Phys Rev A 98**, 013631 (2018).

[184] *M. Tylutki, G.E. Astrakharchik, B. A. Malomed, D.S. Petrov*, Collective excitations of a one-dimensional quantum droplet, **Phys Rev A 101**, 051601 (2020).

[185] *X. Zhang, X. Xu, Y. Zheng, Z. Chen, B. Liu, C. Huang, B. A. Malomed, and Y. Li*, Semidiscrete quantum droplets and vortices, **Phys. Rev. Lett. 123**, 133901 (2019).

[186] *A. Boudjemâa and K. Mohammed Elhadj*, Discrete quantum droplets in one-dimensional binary Bose–Einstein condensates, **Chaos, Solitons and Fractals, 176**, 114133 (2023).

[187] *G. De Rosi, G. E. Astrakharchik, and P. Massignan*, Thermal instability, evaporation, and thermodynamics of one-dimensional liquids in weakly interacting Bose-Bose mixtures, **Phys. Rev. A 103**, 043316 (2021).

[188] *T. Mithun, S. I. Mistakidis, P. Schmelcher, P. G. Kevrekidis*, Statistical mechanics of one-dimensional quantum droplets, **Phys. Rev. A 104**, 033316 (2021).

[189] *A. Boudjemâa*, Moving binary Bose-Einstein condensates in a weak random potential, **Phys. Lett. A 424**, 127867 (2022).

[190] *A. Boudjemâa, and K. Abbas*, Quantum droplets in one-dimensional Bose-Bose mixtures: beyond the Lee-Huang-Yang description, **New J. Phys. 25**, 093052 (2023).

[191] *I. Morera, G. E. Astrakharchik, A. Polls, and B. Julia-Dıaz*, Universal dimerized quantum droplets in a one-dimensional lattice, **Phys.Rev.Lett.126**, 023001 (2021).

[192] *I. Morera, B. Juliá-Díaz, and M. Valiente*, Universality of quantum liquids and droplets in one dimension, **Phys. Rev. Research 4**, L042024 (2022).

[193] Quantum droplet molecules in Bose-Bose mixtures, K. Mohammed Elhadj, L. Al Sakkaf, A. Boudjemâa and U. Al Khawaja, **Phys. Lett. A 494**, 129274 (2023).

[194] *D.S. Petrov, D.M. Gangardt, and G.V. Shlyapnikov*, Low-dimensional trapped gases, **J. Phys. IV (France) 116**, 5 (2004).

[195] *K. Abbas and A. Boudjemâa*, Quantum liquid droplets in Bose mixtures with weak disorder, **Phys. Rev. A. 107**, 033306 (2023).

[196] *P. Naidon and D. S. Petrov*, Mixed Bubbles in Bose-Bose Mixtures, **Phys. Rev. Lett. 126**, 115301 (2021).